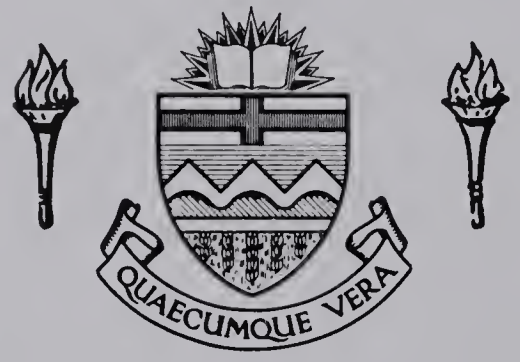

THE UNIVERSITY OF ALBERTA

RELEASE FORM

NAME OF AUTHOR Barbara J. Tilley

TITLE OF THESIS "Sedimentology and Clay Mineralogy of the Glauconitic Sandstone, Suffield Heavy Oil Sands, Southeastern Alberta"

DEGREE FOR WHICH THESIS WAS PRESENTED Master of Science

YEAR THIS DEGREE GRANTED Fall, 1982

THE UNIVERSITY OF ALBERTA

"Sedimentology and Clay Mineralogy of the Glauconitic Sandstone, Suffield Heavy Oil Sands, Southeastern Alberta"

by

© Barbara J. Tilley

A THESIS

SUBMITTED TO THE FACULTY OF GRADUATE STUDIES AND RESEARCH

IN PARTIAL FULFILMENT OF THE REQUIREMENTS FOR THE DEGREE

OF Master of Science

Department of Geology

EDMONTON, ALBERTA

Fall, 1982

THE UNIVERSITY OF ALBERTA

FACULTY OF GRADUATE STUDIES AND RESEARCH

The undersigned certify that they have read, and recommend to the Faculty of Graduate Studies and Research, for acceptance, a thesis entitled "Sedimentology and Clay Mineralogy of the Glauconitic Sandstone, Suffield Heavy Oil Sands, Southeastern Alberta" submitted by Barbara J. Tilley in partial fulfilment of the requirements for the degree of Master of Science.

Abstract

Heavy gravity oil occurs in the Glauconitic Sandstone of the Lower Cretaceous Mannville Group in the Suffield area, southeastern Alberta. The Glauconitic Sandstone ranges in thickness from zero to over 45 metres and has a pay zone averaging 20 metres thick. The thickest sandstones occur in a northwest to southeast trending broad arch which represents an ancient shoreline position with the sea to the east. Facies present in the sandstone include, in ascending order; coarsening–upward sandstone, medium– to coarse–grained sandstone, laminated sandstone, argillaceous sandstone, carbonaceous sandstone and shale, and very fine grained sandstone, siltstone, and shale. These facies represent,in order; the lower–middle shoreface, middle shoreface, upper shoreface–foreshore, backshore, marsh and lagoonal or continental zones of a progradational beach system. The environment is microtidal with the sandstone belt, including the reservoir, dissected by few tidal inlets and channels.

The thickness of the pay zone depends upon the amount of structural movement on local basement faults during subsequent deposition, as well as the facies distribution. Movement on basement faults may also have resulted in the continuous, abnormally thick, progradational beach sequence.

The Glauconitic Sandstone is a litharenite, composed of quartz, chert, other sedimentary rock fragments, and trace amounts of feldspar. Kaolinite is the dominant clay mineral present in all sandstones. Depotassified, chloritized illite and interstratified illite–smectite occur in minor amounts, and smectite abundance varies from a trace in the oil–saturated sandstones to 10% in some sandstones below the oil/water interface. Chlorite is present in trace amounts. The paragenetic sequence is: (1) first stage calcite cementation and pyrite crystallization; (2) quartz cementation and kaolinite growth; (3) second stage calcite cementation, feldspar leaching, minor kaolinite/illite crystallization and still later precipitation of calcite crystals; and (4) smectite/chlorite growth and hydrocarbon emplacement.

The abundance of detrital kaolinite present in the sandstone is the main control on its reservoir quality. The laminated facies has the best reservoir qualities: high porosity, low clay content and good lateral continuity. Authigenic phases, such as kaolinite, quartz, and deformed rock fragments, cause only minor reduction in porosity and permeability.

The argillaceous or bioturbated facies, characterized by irregular argillaceous zones, has poor reservoir qualities.

The main concern related to fluid sensitivity is the dispersion of fine kaolinite. Pyrite and Fe-chlorite are sensitive to acidization, but occur in minor amounts. An increase in temperature of the reservoir during combustion may cause a reduction in permeability as a result of formation of smectite, and the dissolution and reprecipitation of silica.

Acknowledgements

This study is based on core from the Suffield Heavy Oil Pilot project operated by Alberta Energy Company with AOSTRA, Dome Petroleum, and Westcoast Petroleum as partners. I would like to thank each of these companies for their permission to examine and freely sample the confidential project core and for access to other confidential geological information. Without this access and permission to publish the findings, this thesis would not have been possible. Brian Wells, Allan Olhauser and Bill Male were very helpful in providing materials and information in relation to the SHOP project and their comments at various stages helped guide the direction of study. I also acknowledge the various suggestions made by members of the SHOP project technical committee during monthly meetings.

Fred Longstaffe, at the University of Alberta, supervised the project with particular emphasis on the mineralogy section, and provided constructive criticism of various drafts of the manuscript. Fran Hein suggested improvements on an early draft of the thesis. John Kramers supervised the project at the Alberta Geological Survey. Daryl Wightman, Doug Cant, Peter Flach, Ray Rahmani, Brian Rottenfusser, Rand Harrison, and Grant Mossop all offered advise and criticism at various stages throughout the study.

Numerous people provided technical support, both at the Research Council and at the University of Alberta. Thin sections, SEM mounts, oil extractions, and grain size analyses were done by Tim Berezniuk, Max Baaske, Lavorka Swenson and Campbell Kidston. A survey of the clay mineralogy was provided by XRD analyses run by Susan Putz. Diane Caird at the University of Alberta carefully and efficiently processed and ran samples for detailed X-ray diffraction and powder camera analyses. Palynological data was processed by Bruno Untergasser and interpreted by Chaitanya Singh. Most diagrams were drafted by the Research Council drafting department and photographic plates were printed by Leslie Lorinczi. Sandra Walliser and Ilona Dugan provided varied technical assistance and Joan Checholik, Linda Jones, Kathi Skogg, and Sheila Binda typed the tables and figure captions. I wish to express my appreciation to all of these people and to all others who helped in any way.

Table of Contents

Tables

Figures

Plates

I. INTRODUCTION

Heavy gravity oil (13^0 API) occurs in the Glauconitic Sandstone of the Lower Cretaceous Mannville Group, in southeastern Alberta. This study is based largely on cores from the Suffield Heavy Oil Pilot (SHOP) project. The pilot, which taps the Glauconitic Sandstone, is located north of Medicine Hat on the northwestern corner of a Special Oil Production Area, within the Suffield Military Range (Fig. 1). The experimental aspect of the SHOP project is the application of *in situ* wet combustion in a reservoir where the oil zone is underlain by water. The project consists of an inverted five spot pattern (Fig. 2) with the production wells enclosing an area of 2.02 hectares (5 acres). The pilot is operated by Alberta Energy Company with Alberta Oil Sands Technology and Research Authority, Dome Petroleum, and Westcoast Petroleum as partners.

A. Purpose of this Study

Cores from each of the SHOP project wells were taken during the drilling phase of the project. Three of these cores include the entire Glauconitic Sandstone interval, whereas the rest only go down into the producing zone. The purpose of this study was to extract all geological information available from these cores as a step towards the development of a comprehensive understanding of the Glauconitic Sandstone reservoir in the SHOP project. Specific objectives of this study were to:

1. Determine the depositional environment and facies distribution. This information provides a basis for predicting inhomogeneities and lateral facies changes within the rock formation which may affect the flow path of the combustion front and migration of fluids during the recovery process. Also, an understanding of the depositional environment may help in the planning of the location for future pilot or production sites.
2. Determine the bulk mineralogy, clay mineralogy, diagenetic history, and pore morphology within each facies in order to determine the reservoir quality and fluid sensitivity. Fine-grained minerals have the highest potential for reaction with fluids in the pores. Knowledge of the nature and distribution of clay minerals in the

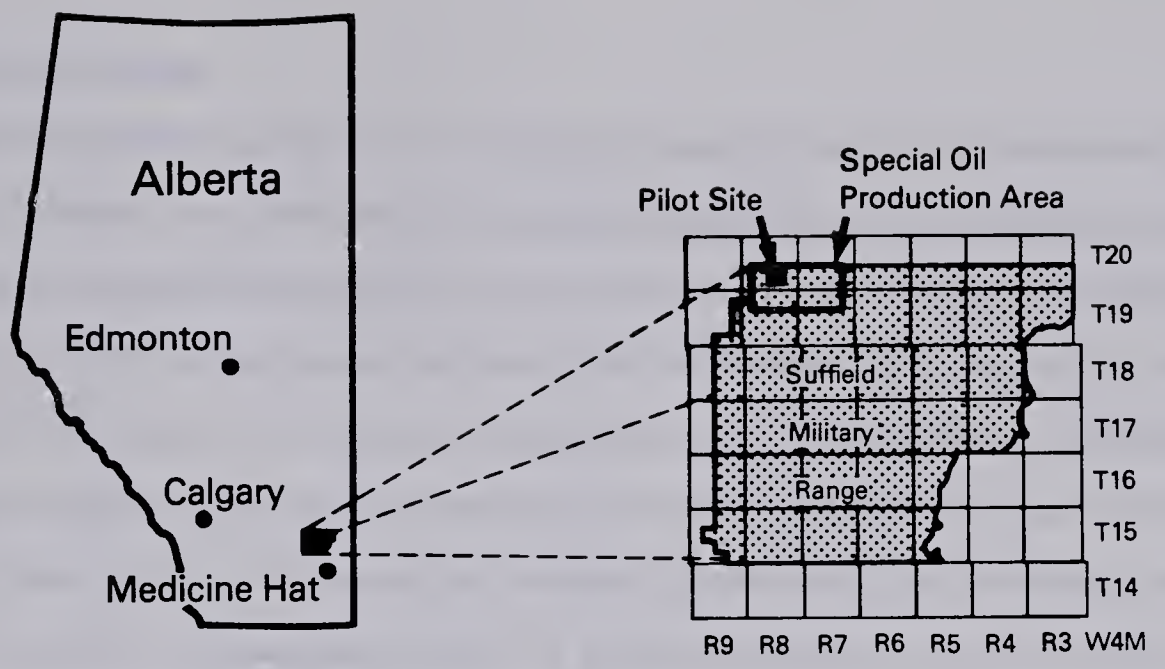

FIGURE 1. Location of the Suffield Heavy Oil Pilot project.

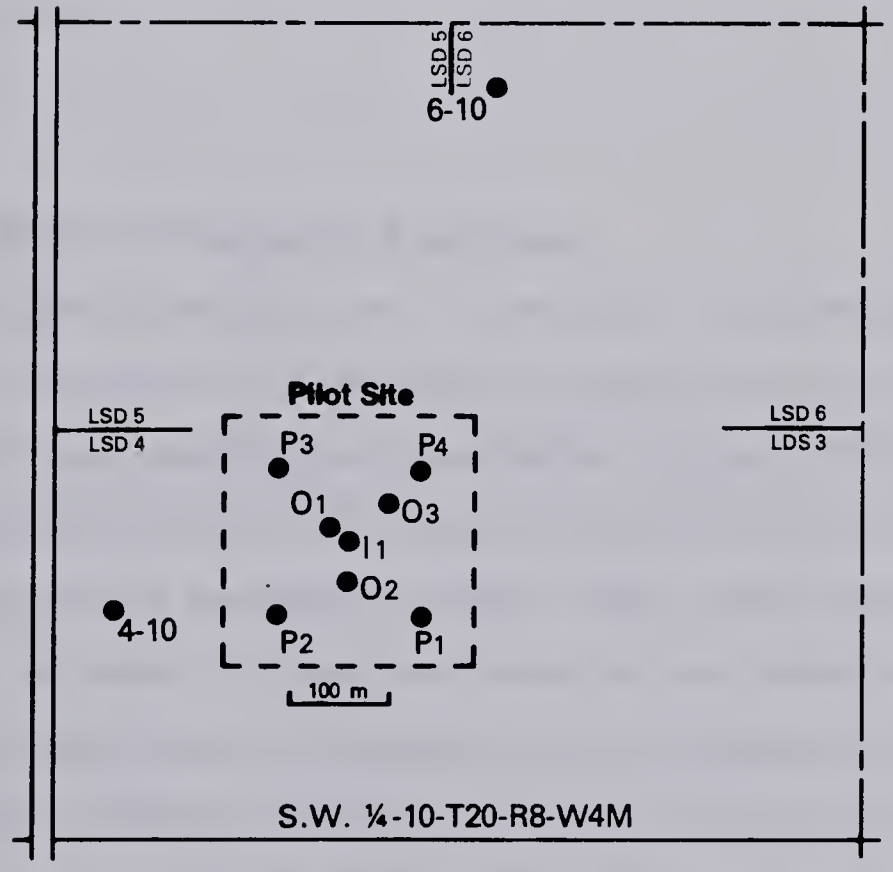

FIGURE 2. Map of the SHOP project site showing the location of the Production (P), injection (I) and observation (O) wells.

reservoir is essential, especially where large volumes of fluids are pumped through a formation at high temperatures, as in the wet combustion recovery process.

B. Geological Setting

The Glauconitic Sandstone occurs at the base of the Lower Cretaceous, Upper Mannville Formation. It is underlain by calcareous sediments of the "ostracode zone" [1] and overlain by a continental sequence of sand, silt, shale and coal in south and central Alberta (Fig. 3). In the SHOP project area, the Glauconitic Sandstone is 45 metres thick with an average pay thickness of 20 metres. Thick sandstone (>15m) occurs in a broad arch extending to the northwest and southeast of the pilot site (Map 1, in pocket). This belt of sandstone, which is 5 to 10 kilometres wide and a minimum of 35 kilometres long, is the focus of this study. A less extensive belt of thinner sandstone occurs four miles to the east of the major sandstone belt but was not studied in detail. The stratigraphic equivalent of the Glauconitic Sandstone to the west of the thick sandstone belt is an indistinct sequence of thin sandstone, siltstone, shale and coal, and to the east the sandstone loses its distinctive character.

C. History of the Term "Glauconitic Sandstone"

The Glauconitic Sand Series was first described in the Edmonton – Stettler area by Layer (1949) who divided the Mannville Group sediments into the Coaly Series, Glauconitic Sand Series, and the Quartz Sand Series. Loranger (1951) began the division of the Glauconitic Sand Series into the Glauconitic Sand above and the Ostracode Zone below (Alberta Society of Petroleum Geologists, 1960). Other workers studying the Mannville Group correlated this "glauconitic" sand unit over a large part of Alberta. It has been correlated with the Bluesky Formation in northwest Alberta, the Wabiskaw Member of the Clearwater Formation in northeast Alberta, and the upper part of the Cummings Member in east-central Alberta (Fig. 3; Rudkin, 1964). In local areas throughout Alberta, the "Glauconitic Sandstone" has been called the Bluesky, Wabiskaw, Glauconitic, Home,

---

[1]The "ostracode zone" was originally described by Loranger (1951) as a biostratigraphic zone. Years of incorrect usage of the term "ostracode zone" has resulted in its common recognition as a lithostratigraphic unit, correlative to the Calcareous Member of the southern Foothills (Rudkin, 1964).

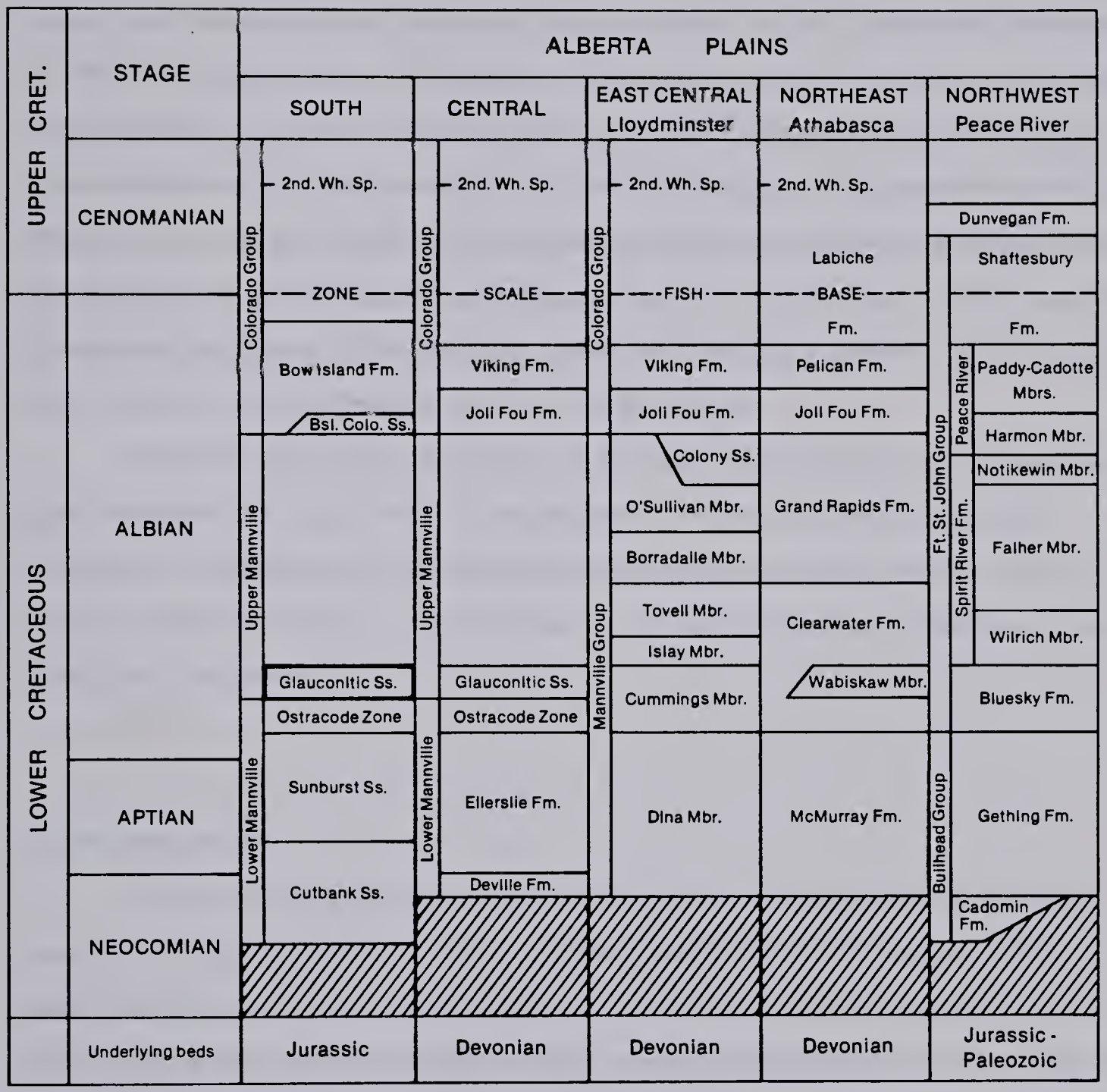

FIGURE 3. Stratigraphic correlation chart (modified from Rudkin, 1964)

Islay, and Kerkhoff.

"Glauconitic Sandstone" is not an approved geological name for a formation. In 1959, Workman proposed the term Bluesky Formation be re-defined and extended from the Peace River region to designate the sandstone previously called the Glauconite Sandstone. He advocated an approved geological name for the "Glauconitic Sandstone" for the following reasons: (1) the unique stratigraphic position of the Glauconitic Sand; (2) its widespread occurrence; (3) its importance to the oil and gas industry; (4) because glauconite can not always be detected in it; and (5) there are other glauconite sands in the Blairmore[2]; (Workman, 1959). . His proposal was largely ignored by later workers who perpetuated the terms: Glauconitic Sandstone (Rudkin, 1964; Herbaly, 1974); Glauconite Sandstone (Conybeare, 1976); and Glauconite Sand (Holmes and Rivard, 1976). As can be seen, there is no consistent title used for this sandstone.

Since the "Glauconitic" Sandstone in the study area contains only trace amounts of glauconite, the term "glauconitic" is a misnomer. However, the name "Glauconitic Sandstone" is recognized by the operators in the area and various other workers in southern Alberta. In order to avoid confusion, the term Glauconitic Sandstone will be continued in this thesis.

D. Previous Work

The Glauconitic Sandstone in the Suffield area of southeastern Alberta was examined briefly by Herbaly (1974) and Holmes and Rivard (1977). Herbaly (1974) described the sandstone (>100 ft thick) as an almost dune-like development cut by silt-filled channels. Holmes and Rivard (1977) studied cores from two pools in the Jenner field (Twps. 20 & 21, Rge. 8 W4) and interpreted the sandstone as a barrier-island deposit, representing the last marine deposition of the Upper Mannville section. They also described the petrology of the sandstone.

Regional studies indicate that the percentage of glauconite in the Glauconitic Sandstone decreases east of the 5th meridian and south of Edmonton (Glaister, 1959 and Conybeare, 1976). The sandstone is predominantly marine in the Edmonton area and

---

[2]Blairmore is the Mannville equivalent in the southern Foothills.

becomes more nonmarine towards the south. The thickness of the sandstone ranges from an average of 6 to 9 metres to greater than 30 metres, and changes markedly over a distance of a few kilometres (Conybeare, 1976; Workman, 1958)

Individual field studies provide some understanding of the regional variation in depositional environment. The Glauconitic Sandstone in southernmost Alberta (Twps. 1-15, Rges. 16-20, W4) has been interpreted as representing floodplain and channel deposits (Herbaly, 1974 and Brown, 1976). Herbaly (1974) also postulated channel deposition in the Countess field area (Twps. 18-20, Rges. 15-17, W4). In the Little Bow area (Twps. 14 & 15, Rge. 20 W4), Hermanson et. al. (1982) described subtidal marine bars, locally cut by channels; in the Carbon field (Twp. 29, Rge. 22), the Glauconitic Sandstone has been interpreted as a tidal channel (Conybeare, 1976).

E. Methods

The eight cores from the SHOP project which form the basis of this study were examined, described in detail, and sedimentary facies were defined. Core logs for each well are included in Appendix A. A total of 42 samples, representing units of varying lithology, grain size, sedimentary structures or oil saturation within each well, were analyzed for grain-size properties and examined in thin section and by scanning electron microscopy (SEM) for mineralogy, texture, pore morphology and diagenesis. A survey of the clay minerals present in the <2 micrometre size-fraction of the SHOP project sandstones was obtained from X-ray diffraction analyses performed by Alberta Research Council.

In order to obtain a regional perspective on the sedimentary environment represented by the Glauconitic Sandstone, and to observe any regional mineralogical variations, cores from a total of 77 wells surrounding the pilot site were also examined. Unfortunately, many of these cores are only 10 to 20 metres long and include only the mid-portion of the Glauconitic Sandstone. Therefore, the sequence of facies could only be defined from the SHOP project cores and correlated to regional wells wherever there was sufficient core. Thirty-five samples representing 15 regional wells were examined in thin section and by SEM. A detailed clay mineralogical study involved XRD of these

samples as well as re-examination of sandstone samples from well 02. XRD procedures for these analyses are described in Appendix B.

A sandstone thickness map for the Glauconitic Sandstone (Map 1) was computer-generated from a data base of 758 wells. The sand thickness for each well was determined based on the 70 per cent sand/shale line on the gamma-ray logs.

Twelve shale or silty-shale samples from below, within, and above the Glauconitic Sandstone were selected for palynological analysis. The samples were examined for palymorphs and dinoflagellates by C.Singh.

II. FACIES ANALYSIS

A. Facies Descriptions

The Glauconitic Sandstone consists of six lithological facies [3]. In ascending order these include: coarsening-upward sandstone, medium- to coarse-grained sandstone, laminated sandstone, argillaceous sandstone, carbonaceous sandstone and shale, and fine-grained sandstone, siltstone, and shale. Although these facies have been defined entirely on the basis of the eight cores from the SHOP project, they are generally applicable within the regional framework. Three cores (wells O1, O2, and O3) from the SHOP project include almost the entire Glauconitic Sandstone interval, whereas cores from wells in the regional setting generally include only small portions of the interval. The most important variations within facies are described as subfacies. These subfacies apply to local phenomena which are of limited lateral extent.

The grain mineralogy of the Glauconitic Sandstone is fairly monotonous (Table 1) consisting of quartz, approximately equal proportions of chert and other sedimentary rock fragments, and trace amounts of feldspar. Only mineralogical anomalies are discussed in the facies descriptions. The distribution of facies within the SHOP project wells relative to geophysical logs is shown in figures 4 and 5. A summary of grain size analyses for samples representing each facies is given in Table 2. Table 3 is a summary of porosities for each facies.

Facies 6. Coarsening-upward sandstone.

Facies 6 is the lowermost unit of the Glauconitic Sandstone and lies gradationally above the "ostracode zone". It consists of a siltstone or very fine grained sandstone which gradually coarsens upwards to a fine-grained sandstone. The sandstone is medium well sorted and contains 2.5 to 5.5 per cent clay. Subfacies 6b (comprising about 70% of the total thickness for facies 6) is characterized by a light grey to light brown, very fine to fine-grained sandstone which has well-defined laminations (Plate 1-1). Carbonaceous debris commonly outlines laminations, especially in the lower portion of facies 6. Sedimentary structures include horizontal, planar laminations, cross-laminations, wave

---

[3]Facies are defined on the basis of observed lithologic variations within the Glauconitic Sandstone, and the descriptions include all the characteristics that make an environmental interpretation possible. See Krumbein and Sloss (1963) for a detailed discussion of the definition of facies.

Table 1. Grain Percentages Based on Thin Section Point Counts[1] for Well 01

Facies	Sample	Log Depth	Quartz	Chert	Rock Fragments	Feldspar	Opaques
3a	147	911.3	57	32	6	4	0
3ci	148	912.3	60	19	21	0	0
3d	149	915.3	62	24	15	0	0
4	151	929.0	61	16	23	tr	0
5	152	940.5	30	54	16	0	0
6a	153	944.2	70	17	8	1	3
6b	155	953.4	68	11	15	4	3
6c	154	952.6	73	10	6	8	2

[1] 300 points were counted for each section

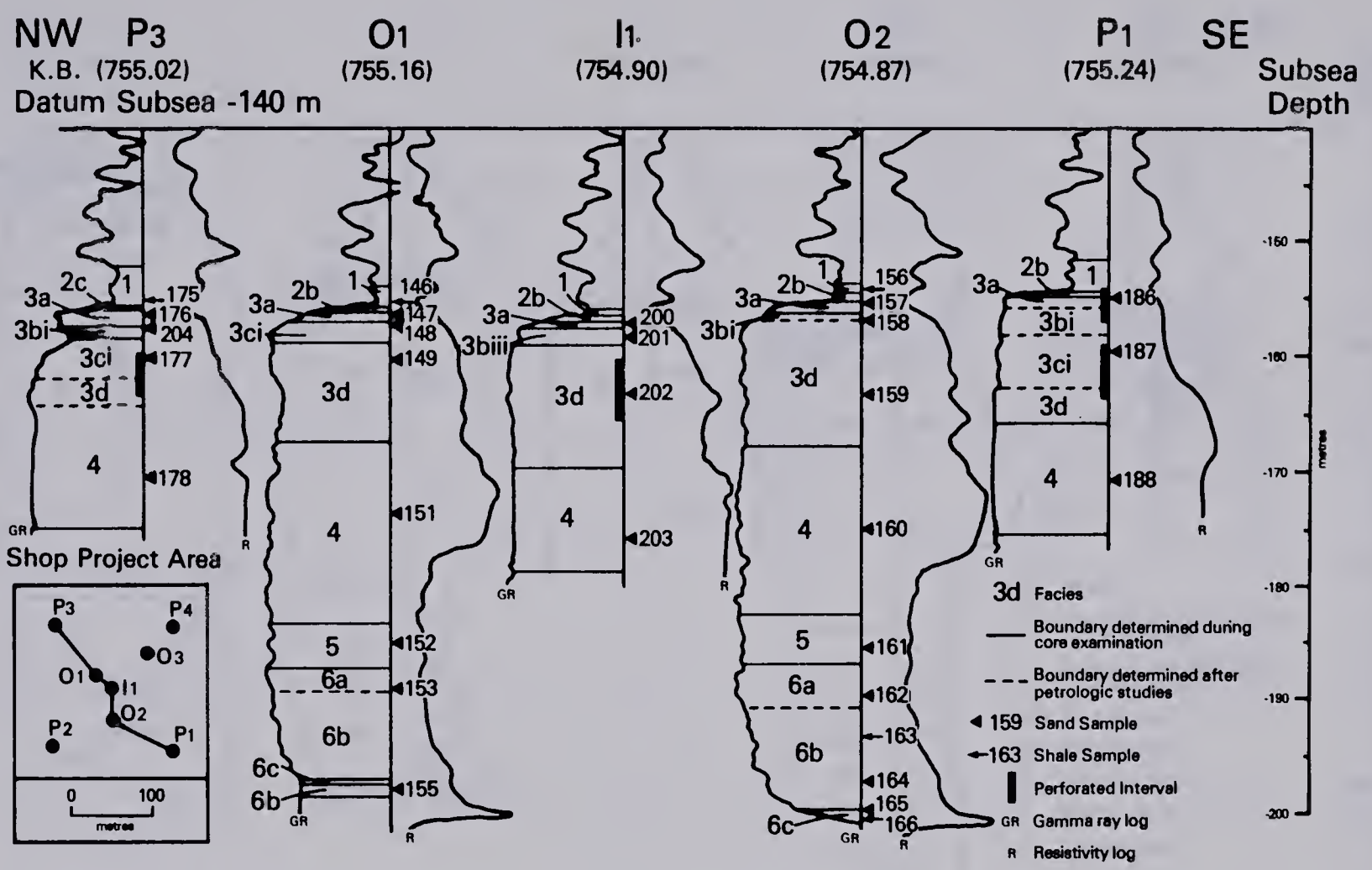

FIGURE 4. Northwest-southeast structural cross-section through the SHOP project area, showing the distribution of facies and samples in each well relative to the geophysical logs.

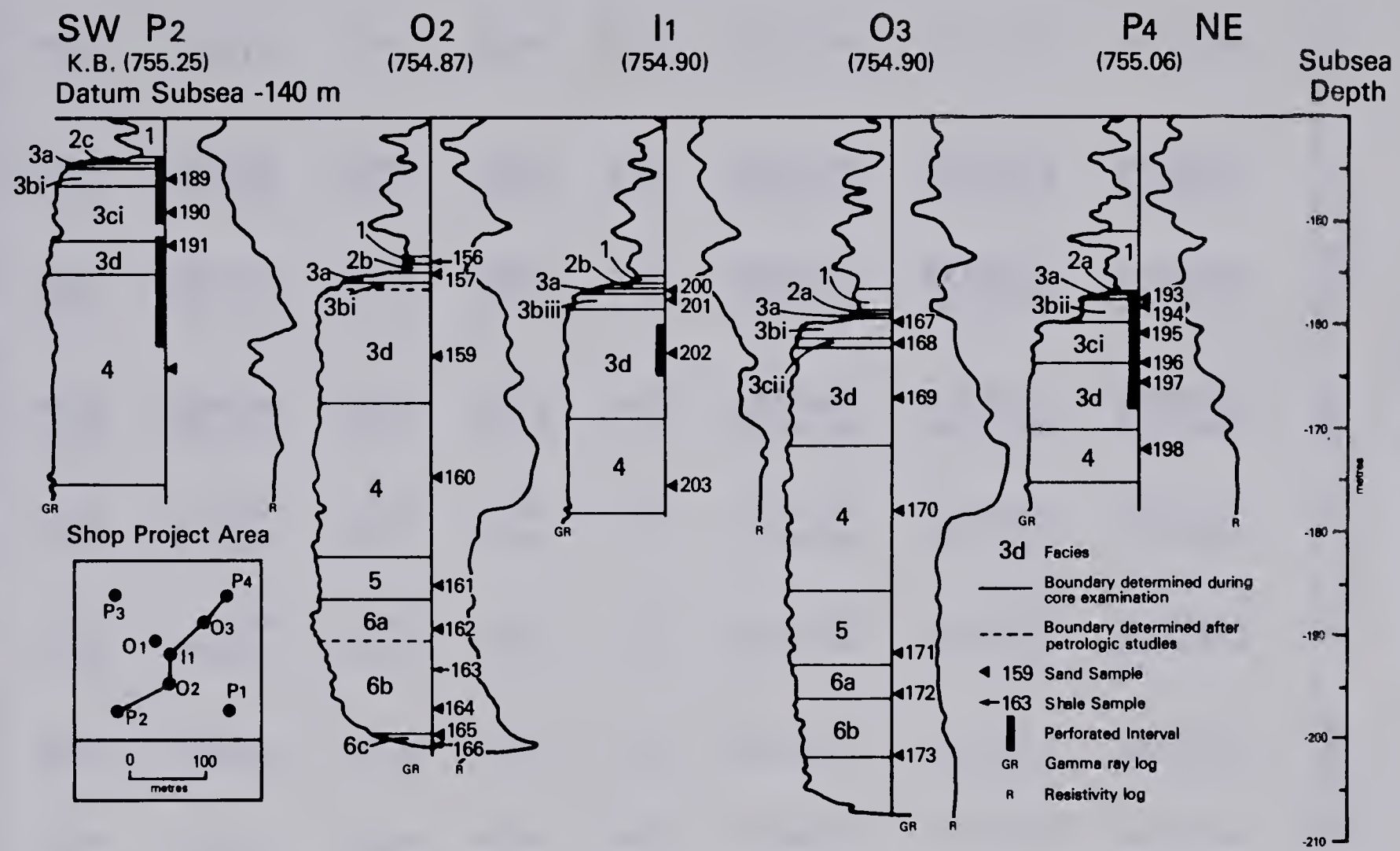

FIGURE 5. Southwest-northeast structural cross-section through the SHOP project area, showing the distribution of facies and samples in each well relative to the geophysical logs.

Table 2. Summary of Grain Size Analyses

Sample [1]	Facies	Depth (m) [2] Log	Depth (m) [2] Drilling	Composition (Wt %) Sand	Silt	Clay	Grain Size (µm) Median	Mean	Largest	Standard Deviation
Well 01										
147	3a	911.3	911.4	73.06	17.20	9.74	146	75	350	3.05
148	3ci	912.3	912.4	83.83	6.56	9.61	144	85	710	2.85
149	3d	915.3	915.3	87.28	6.78	5.94	143	90	710	2.29
151	4	929.0	929.1	86.68	11.29	2.12	143	102	350	1.55
152	5	940.5	940.6	92.17	4.28	3.55	153	125	710	1.86
153	6a	944.2	944.3	86.46	9.19	4.35	107	81	250	1.94
155	6b	953.4	953.5	65.22	32.18	2.60	80	78	250	1.95
Well 02										
157	3a	910.0	910.4	69.54	16.77	13.69	136	46	1000	3.10
158	3bi	911.6	912.4	84.28	7.68	8.04	145	81	1000	2.56
159	3d	918.1	919.3	89.11	8.17	2.72	144	105	1000	1.67
160	4	929.9	930.0	88.04	9.17	2.79	144	104	500	1.70
161	5	940.2	940.2	90.94	5.94	3.12	165	156	1400	2.02
162	6a	944.6	944.5	97.51	7.88	4.61	105	75	500	1.94
164	6b	952.8	951.8	56.79	38.79	4.42	70	51	177	1.94
Well 03										
167	3bi	914.7	913.3	54.55	25.91	19.54	92	24	1400	3.39
168	3cii	916.8	916.3	75.73	9.80	14.47	145	56	710	3.12
169	3d	922.0	921.9	85.70	8.88	5.42	144	87	500	2.16
170	4b	932.9	932.9	87.84	9.09	3.07	144	99	500	1.73
171	5	941.7	941.3	93.45	3.19	3.36	224	180	1000	1.92
172	6a	950.7	950.1	85.40	8.54	6.07	105	67	350	2.11
173	6b	956.6	955.8	62.93	31.57	5.50	78	54	250	2.14
Well P1										
186	3a	910.4	910.3	58.79	21.71	19.50	111	28	710	3.53
187	3ci	915.0	914.8	82.42	6.16	11.42	148	69	1400	3.00
188	4b	926.3	926.0	86.33	10.58	3.09	138	93	500	1.78
Well P2										
189	3bi	901.6	902.0	67.42	16.70	15.89	139	51	710	3.61
190	3ci	904.6	905.2	73.12	18.42	8.46	142	61	1000	2.62
191	3d	907.7	908.2	84.92	11.81	3.26	151	103	1000	1.92
192	4a	919.6	920.2	86.43	9.81	3.75	141	90	350	1.89
Well P3										
176	3a	911.5	909.4	62.03	16.17	21.80	128	31	500	3.80
204	3bi	912.7	912.7	76.26	14.15	9.59	149	72	1000	2.98
177	3ci	915.3	915.2	75.80	16.25	7.95	142	68	500	2.61
178	4	926.0	926.1	90.27	7.58	2.15	145	107	250	1.54
Well P4										
193	3a	913.0	913.0	36.53	35.36	28.11	15	11	500	3.66
194	3bii	913.9	914.0	66.61	17.79	15.60	176	48	500	3.62
195	3ci	916.4	916.4	67.84	15.38	16.79	139	46	1000	3.61
196	3ci	919.1	918.3	77.07	13.02	9.92	144	63	1000	2.76
197	3d	921.1	923.3	84.26	11.03	4.71	146	90	1000	2.10
198	4	927.9	928.7	90.16	6.99	2.85	151	113	500	1.74
Well I1										
200	3a	911.7	909.4	75.22	14.78	10.00	146	80	2000	3.29
201	3biii	912.7	910.4	82.15	7.49	10.36	143	72	1000	2.95
202	3d	917.8	915.5	91.31	7.65	1.04	144	115	500	1.22
203	4a	930.1	927.7	92.27	7.18	1.37	149	131	1000	1.11

[1] Sample numbers not listed are either shale samples, carbonate cemented, or repetitions of samples already analysed
[2] Depth - Log depths correspond to depths on geophysical well logs.

Table 3. Average Porosities[1]

Facies	Well 01	02	03	P1	P2	P3	P4	I1	Overall
3a	10	15	-	19	15	10	11	-	13
3bi	-	22	-	19	13	11	-	-	16
3bii	-	-	-	-	-	-	11	-	11
3biii	-	-	-	-	-	-	-	22	22
3ci	22	-	-	21	20	20	21	-	21
3cii	-	-	22	-	-	-	-	-	22
3d	25	25	26	27	25	27	25	26	26
4	26	27	29	28	27	27	29	27	27
5	25	25	29	-	-	-	-	-	26
6a	26	28	29	-	-	-	-	-	28
6b	23	22	27	-	-	-	-	-	24
6c	15	10	-	-	-	-	-	-	12

[1]Values from core analyses by Core Laboratories-Canada Ltd.

ripples (Plate 1–1), and small scour and fill structures (<3 cm diameter). Burrows and bioturbated zones are rare in subfacies 6b, and thin shale beds occur mainly in the lower portion. Bedding thickness is commonly greater than 20 centimetres. [4]. The SHOP project cores do not penetrate the base of the Glauconitic Sandstone but facies 6b is at least 6 to 9 metres thick.

Subfacies 6c is a a calcite–cemented siltstone or very fine grained sandstone. It is commonly laminated to lightly burrowed with some partially bioturbated, carbonaceous shale interbeds with syneresis cracks (Plate 1–2). This calcite–cemented zone may represent the lowermost Glauconitic Sandstone as suggested by well O2 or may be underlain by at least a meter of the noncarbonate–cemented subfacies 6b (well O1).

Subfacies 6a occurs in the upper portion of facies 6 and serves as a zone of transition from facies 6 to 5. This 2.5 to 3.2 metre thick zone is bioturbated, structureless, or indistinctly laminated (Plate 1–3). Grain size is slightly coarser than subfacies 6b but finer than facies 5.

Facies 5. Medium- to coarse-grained sandstone

Facies 5 is characterized by medium– to coarse–grained sandstone, interlaminated and interbedded with fine–grained sandstone. Coarser beds vary from <1 to 8 centimetres thick. The thicker beds commonly have scour bases and fine upwards (Plate 1–4). Low angle laminations (Plate 1–4) and flat beds are most common but rare steeper beds occur and the finer–grained portions of beds may be rippled. Grain size is bimodal and the coarser chert grains are relatively angular (Plate 3–1). Chert is the major grain component of the coarse sandstone in this facies (Table 1).

Facies 5 varies from 4.2 to 7.2 metres thick. Its base is marked by the presence of coarser–grained beds or laminations above the fine–grained sandstone of facies 6. [5] In one core (well O1) there is a 1 millimeter thick lamination of distinctly darker sandstone separating the underlying finer sandstone of facies 6 from the overlying coarser sandstone of facies 5. The transition from facies 5 to facies 4 is a poorly–defined

---

[4]The total thickness of beds cannot be determined because the core slabs are generally broken into pieces less than 20 cm long, and intervening portions removed for analyses.
[5]The actual contact between facies 6 and 5 was not seen in core. The core is broken into small pieces ranging from a few centimeters to ten's of centimetres long. Contacts commonly occur at the junction of two core pieces or within a piece which has been removed. Therefore, the contact may indeed be gradational and poorly defined, or it may be sharp and represented in a missing piece of core.

gradational contact; coarser interbeds gradually becoming less abundant upwards.

Facies 4. Laminated sandstone

Facies 4 consists of a relatively clean (1.4 – 3.7 % clay content), fine–grained sandstone, which characteristically has horizontal, planar laminations and low angle, cross–laminations (Plate 1–5 & 6). The sandstone is well sorted with concentrations of dark coloured chert grains defining the laminations rather than significant grain–size changes. No shale laminations or beds are present. Higher–angled laminations, bioturbated beds and disturbed laminations are minor in occurrence. Structureless beds, and beds showing cross–cutting relationships (Plate 1–5) are commonly 5 to 10 centimetres thick, whereas units with horizonatal, planar laminations are much thicker. Facies 4 is 14 metres to at least 20 metres in thickness. [6]

The oil/water interface in the wells from the SHOP project occurs within facies 4. In these wells, facies 4 represents the zone of highest and most continuous oil saturation.

Facies 3. Argillaceous sandstone

Facies 3 is represented by argillaceous, poorly–sorted, fine–grained sandstone with abundant bioturbated zones. Subfacies 3d, 3c, 3b, and 3a (ascending order) are arbitrary divisions representing a gradual increase in clay content and bioturbation. Subfacies 3a is the most argillaceous and occurs at the top of the Glauconitic Sandstone. Divisions of subfacies 3b (3bi, 3bii, and 3biii) represent variations from well to well within the same stratigraphic interval.

Subfacies 3d lies immediately above facies 4 with a poorly–defined, gradational contact. It is a 3 to 10 metre thick unit distinguished from facies 4 by the relative abundance of structureless and bioturbated zones, and clay–rich patches. This subfacies contains discontinuous zones which may be structureless, bioturbated, irregularly laminated, relatively high angle laminated, or brecciated (Plate 1–7). This high degree of variability characterizes subfacies 3d. In nonargillaceous zones, clay content can be as low as 1 percent (Table 2, well I1) and porosity as high as 37 percent. In the SHOP project cores, where facies 3 sits well above the oil/water interface, subfacies 3d has good oil–saturation in the cleaner zones. However, these zones have limited continuity. Clay–rich sandstone lenses, with no oil saturation, occur sporadically throughout

---

[6] Its maximum thickness is not known as several wells did not penetrate the entire facies.

subfacies 3d and limit its reservoir potential. Clay content varies from 1 to 6 percent in the samples analyzed from this subfacies. Angular, randomly oriented, breccia blocks (Plate 1-7) found in a 0.6 metre thick interval in well O2 are laminated. The matrix of the breccia is a slightly coarser clay-rich sandstone.

Subfacies 3c gradationally overlies subfacies 3d and represents the uppermost indication of bedding or lamination within the Glauconitic Sandstone (excluding facies 3biii). It differs from subfacies 3d in being more argillaceous (8-17% clay) and in lacking any regular bedding. The unit varies from 1.8 metres thick in well O1 to 5.2 metres thick in well P2, and is quite variable within a particular well. Zones of the sandstone may be bioturbated, structureless, or indistinctly bedded (Plate 2-1). Magnetite grains are concentrated along single, isolated laminations. In well O3 this zone has a green-grey colour and for this reason alone has been distinguished as facies 3cii in figure 5.

The sandstone at stratigraphic levels equivalent to subfacies 3c is commonly not significantly distinct from subfacies 3d and is therefore placed in subfacies 3d. In this case, subfacies 3b directly overlies 3d.

Subfacies 3b occurs as subfacies 3bi in most wells but as 3bii in well P4 and as 3biii in well I1. Subfacies 3bi is generally slightly more argillaceous then 3c, but its main distinguishing features are that it is structureless to bioturbated with no hint of laminations; clay streaks are common (Plate 2-2). Dark grey chert grains, slightly larger than the mean grain size, create a speckled appearance, distinctive in this subfacies because of its light grey rock colour. Subfacies 3bi varies in thickness from 0.8 to 2.1 metres but the lower contact with subfacies 3c or 3d is gradational and rather arbitrary.

Subfacies 3bii occurs in the same stratigraphic position as 3bi, but is distinctly different and present only in well P4. It is 2.2 metres thick and has a sharp base overlain by a structureless bed (3 cm thick) of fine-grained sandstone containing coarse-grained pyrite (Plate 2-3). The pyrite-rich sandstone grades upwards to a cross-laminated sandstone with bioturbated zones. A 0.3 metre thick breccia (Plate 2-3) is present at the top of the unit. The breccia appears as a disrupted zone with carbonaceous rootlets and irregularly-shaped or subrounded blocks. Breccia blocks are finer grained than the matrix.

Petrologically and texturally, subfacies 3bii is distinctive from the other facies. The thin section photograph on Plate 3-2 demonstrates the preferential horizontal fabric resulting from compaction flattening of soft rock fragments and the orientation of elongate chert grains. Feldspars (K-feldspar and plagioclase) are more abundant than in other facies. Also, illite content is 5 percent, an abnormally high percentage for a zone with such low porosity. Average porosity from core analyses is 11 percent, an average lower than other facies.

Facies 3biii also occurs in the same stratigraphic position as subfacies 3bi but is distinguished from both 3bi and 3bii by its low angle, planar laminations, defined by coarse sand sized magnetite grains (Plate 2-4). It is present only in well I1 and is 1.5 metres thick. The sandstone is light grey, fine grained, and clay-rich (10% clay), but porosity is relatively high (22%). The lower boundary of the unit is gradational and poorly defined. [7] The uppermost few centimetres of the unit are bioturbated and rooted, and there is a sharp, irregular contact with the overlying argillaceous sandstone of facies 3a.

Facies 3a is the most clay-rich sandstone facies and occurs at the top of the thick Glauconitic Sandstone in the SHOP project wells. It is typically a medium grey to light brown, very argillaceous, fine-grained sandstone with scattered coarser chert grains and carbonaceous rootlets (Plate 2-5). The sandstone is structureless to bioturbated. The high standard deviation of grain size (3.05-3.80, Table 2), indicates the very poor sorting. The contrast in the median grain size (fine-grained sand), and the mean grain size (silt-sized), (particularly in facies 3a of wells O2 and P3) also reflects this poor sorting. Facies 3a varies in thickness from 0.4 metres (well O3) to 1.3 metres (well P3). The transition from the underlying unit is gradational or an irregular sharp contact marked by a colour change.

Facies 2. Carbonaceous sandstone and shale

Facies 2 is a very carbonaceous unit at the top of the Glauconitic Sandstone. In some wells (P4 and O3), poor quality coal (Plate 2-6) is irregularly interbedded with carbonaceous shale (subfacies 2a). In other wells, this unit is represented by dark grey sandy shale (subfacies 2b, Plate 2-6) or dark grey argillaceous sandstone (subfacies 2c). Both these lithologies are very carbonaceous with abundant coal chips and are strongly

---

[7] Pieces of core demonstrating the contact of subfacies 3biii with subfacies 3d may be missing.

bioturbated. The transition from facies 3 to 2 is generally quite abrupt with an irregular boundary marked by a colour change from medium or light grey (facies 3), to dark grey (facies 2, Plate 2–6). Carbonaceous material in the underlying facies 3a is commonly most abundant near this boundary.

Facies 1. Very fine grained sandstone,siltstone, and shale

A maximum of 6 metres of rock above facies 2 is represented in the SHOP project cores and is described here as facies 1. Lowermost facies 1 overlies facies 2 gradationally and consists of structureless or laminated, medium grey shale with light grey silt interlaminations (Plate 2–7). Very small burrows and ripples (<1 mm) are present locally in the shale and carbonaceous chips are common. Silt interbeds and lenses gradually become more abundant upwards such that interbeds of shale and interlaminated silt and shale alternate on a one or two metre scale. Sedimentary structures (Plate 2–7) include ripples, planar laminations, burrow mottling to isolated burrows, contorted laminations, structureless beds, and rare rootlets. Pyrite is common as nodules averaging 1 centimetre in diameter and in pyrite–rich laminations. The uppermost metre of rock included in core (well P4) is a carbonate–cemented, very fine grained sandstone. Climbing ripples are outlined by carbonaceous debris. Microfaults and calcareous, bioturbated shale interbeds are also present. This sandstone lies with a sharp flat contact on the underlying thick (1.5 m) shale bed.

Regional Facies Descriptions

Although the facies descriptions in the preceding section are based entirely on core from the SHOP project wells, they can be adapted slightly to apply on a more regional scale. The characteristics of facies 6 on a regional scale are consistent with those described from the SHOP project cores. However, facies 5 varies considerably in grain size. Generally, it is a fine–grained sandstone interbedded with the coarsest–grained material in the well, which may consist of pebbles (well 12–32–20–8 W4) , coarse–grained sandstone or medium–grained sandstone. Structures are similar to those described from the SHOP project. Facies 4 may consist of medium– to coarse–grained sandstone (well 4–10–20–8 W4) rather than fine–grained sandstone, but is always low angle, planar laminated. In regional wells, facies 3 may be argillaceous, but a more general characteristic is the scarcity of sedimentary structures. It is commonly bioturbated or

structureless with only isolated laminated zones. A carbonaceous equivalent of facies 2 and a shale–siltstone sequence of facies 1 are represented in most wells.

B. Facies Interpretation

The criteria suggesting the deposition of the Glauconitic Sandstone (in the SHOP project area) in a prograding shoreline and nearshore environment are abundant: (1) Palynological analysis of shales from immediately below the Glauconitic Sandstone indicate restricted marine depositional conditions (See section on Palynological Results); (2) The contact of the Glauconitic Sandstone with the "ostracode zone" is gradational with the lower portion of the Glauconitic Sandstone coarsening upwards from silt or very fine grained sandstone; (3) The zones present on a modern day beach (shoreface, foreshore, backshore) are all represented in the Glauconitic Sandstone (Fig. 6); and (4) The uppermost part of the sandstone contains carbonaceous root markings and coal, and is overlain by low energy shales and siltstone of probable back–barrier origin.

Well–documented studies of modern barrier–island systems have resulted in a relatively good understanding of sedimentary structures and other features of sediments in beach environments. Several review papers (eg., Elliot, 1978; Reinson, 1980; and McCubbin, 1982) have both summarized the characteristics of barrier and strand–plain sandstone facies which have been recognized in modern environments, and described several ancient analogues. The most intensively studied modern barrier–island environments are the East Coast and Gulf Coast examples in the United States described in LeBlanc and Hodson, 1959; Shepard, 1960; Bernard, LeBlanc and Major, 1962; Hoyt and Weimer, 1963; and Kraft, 1971. Other well–known studies of modern shorelines include those by Hayes and Kana (1976) and Curray and Moore (1964). The following interpretation of each facies represented in the Glauconitic Sandstone is based on a comparison with facies from various barrier–island settings as described mainly in the review papers. A summary of the characteristics of each facies of the Glauconitic Sandstone, described in the previous section, is given in Table 4 and figure 6.

Facies 6

Facies 6 represents the lower to middle shoreface zone. The very fine grained sandstone and thin shale interbeds in the lower portion were deposited in the lower

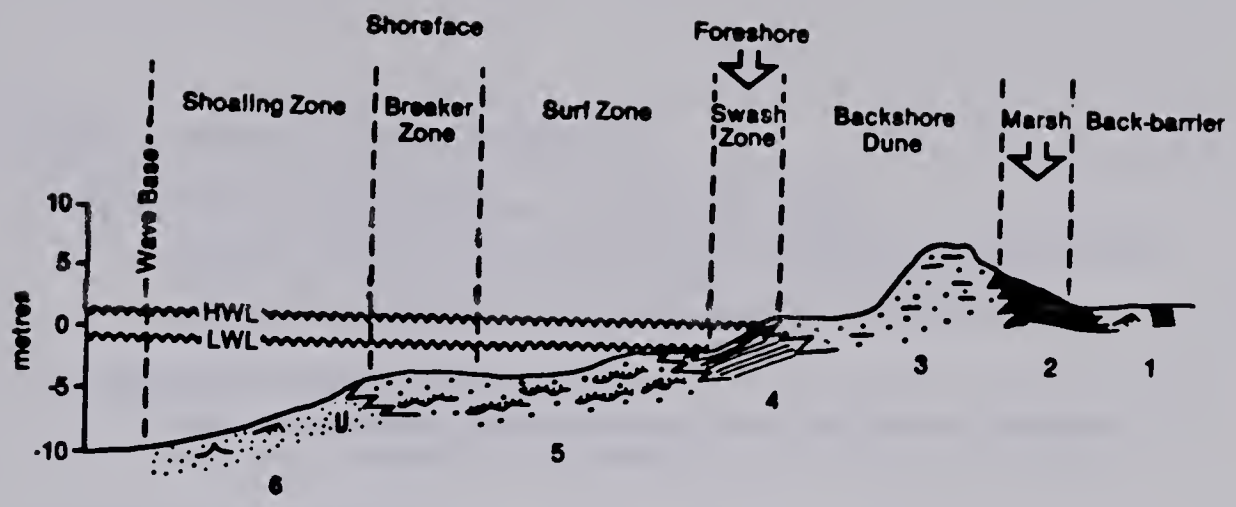

FIGURE 6a. Generalized profile of a barrier-beach environment showing the spatial relationships of the sedimentary facies and their positions on the shore. (Shore profile modified from Reinson, 1980)

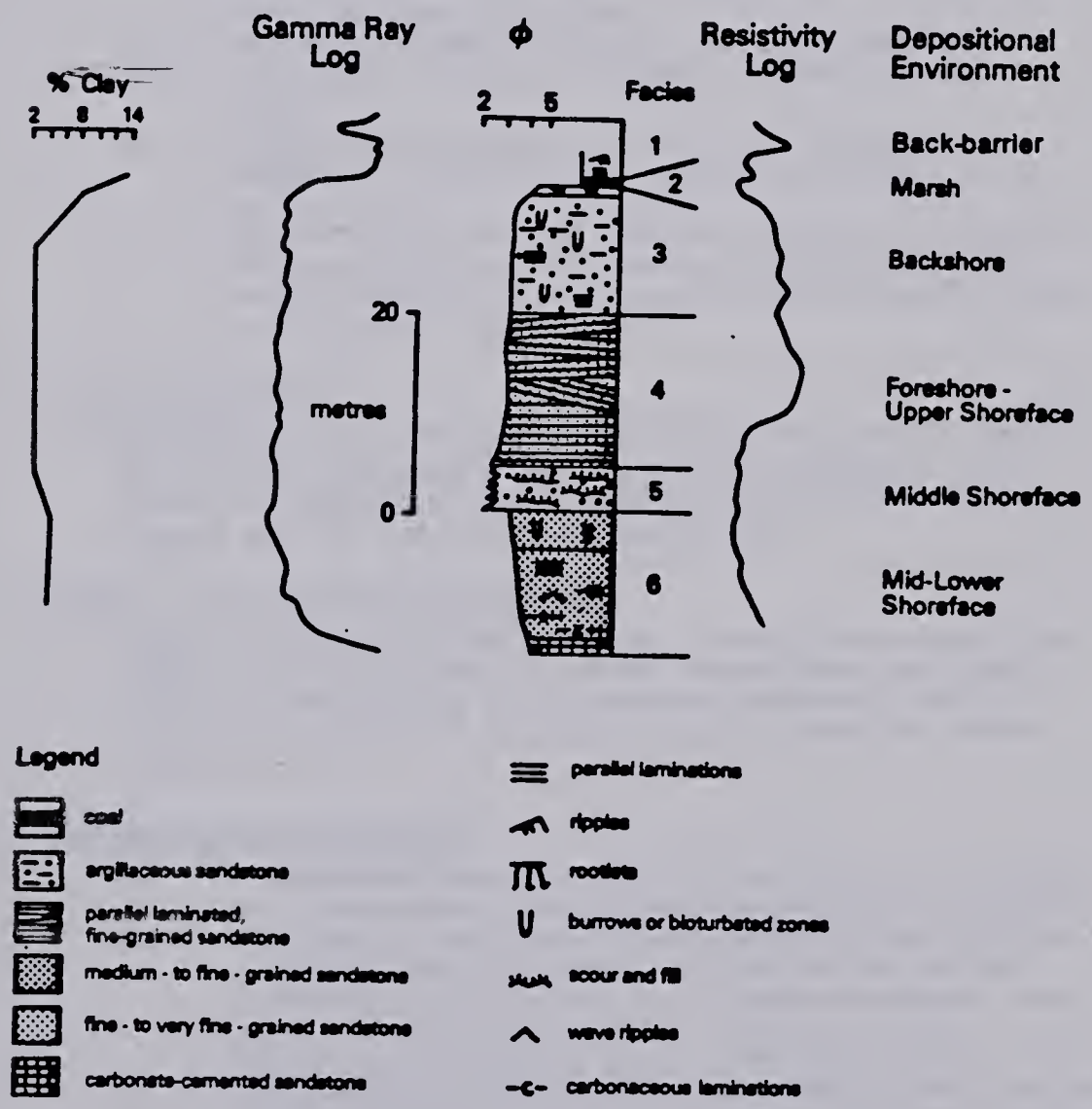

FIGURE 6b. Generalized litholog from SHOP project core showing the vertical sequence of facies, grain size, per cent clay, geophysical log shapes and the facies interpretations.

Table 4. Summary of Facies Descriptions

1. Very fine grained sandstone, siltstone and shale

   Interlaminated siltstone and shale interbedded with shale and sandstone; laminated, structureless, rippled or burrow mottled; contorted beds, burrows, pyrite, rare rootlets.

2. Carbonaceous sandstone and shale

   Coal, carbonaceous shaly-sandstone and sandy-shale; abundant coal chips; strongly bioturbated.

3. Argillaceous sandstone

   - 3a Very argillaceous sandstone; bioturbated, structureless, rooted; poorly sorted.
   - 3bi Argillaceous sandstone; structureless to bioturbated; clay streaks.
   - 3bii Green-grey sandstone; sharp base overlain by structureless sandstone with coarse-grained pyrite; grades up to cross-laminated sandstone with bioturbated zones, breccia at top; horizontal fabric in thin section; feldspar and illite abnormally abundant.
   - 3biii Low angle, planar-laminated, clay-rich sandstone; laminations defined by magnetite grains; rootlets at top.
   - 3c Argillaceous sandstone; indistinctly bedded, bioturbated or structureless; green-grey coloured in one well.
   - 3d Zones of clean and argillaceous sandstone; structureless, bioturbated, irregularly laminated, relatively high angle laminated, or brecciated; variable porosity, clay content and oil-saturation.

4. Laminated sandstone

   Relatively clean, fine-grained sandstone; well-sorted; horizontally planar-laminated to low angle cross-laminated; minor disturbed laminations, bioturbated or structureless beds; highest and most continuous oil saturations.

5. Medium- to coarse-grained sandstone

   Medium- to coarse-grained sandstone. interlaminated and interbedded with fine-grained sandstone; coarser beds have scour bases and fine upwards to fine-grained sandstone; chert is the major component of the coarse-grained sandstone; bimodal grain size.

6. Coarsening-upward sandstone

   - 6a Fine-grained sandstone slightly coarser than subfacies 6b; bioturbated, structureless or indistinctly laminated.
   - 6b Siltstone or very fine grained sandstone coarsening up to fine-grained sandstone; well-defined laminations, horizontal planar-laminations, cross-laminations, wave ripples, small scour and fill structures, rare burrows and bioturbated beds; carbonaceous debris in laminations and rare thin shale beds in lower portion.
   - 6c Carbonate-cemented, very fine grained sandstone and siltstone; laminated to lightly burrowed; carbonaceous shale interbed.

shoreface. In his review paper, Reinson (1980) described the lower shoreface as a relatively low energy transitional zone, where waves begin to affect the bottom, but where offshore shelf or basinal depositional processes also occur. The coarsening upwards to fine-grained sandstone represents the transition into the middle shoreface. The low angle cross-laminations, horizontal planar laminations, wave ripples (Plate 1-1) and scour and fill structures were produced by shoaling and breaking waves in this zone. The predominance of primary sedimentary structures, in the shoreface zone of the Glauconitic Sandstone, contrasts with the bioturbated shoreface zone described by Bernard et. al. (1962) for Galveston Island. The preservation of primary structures indicates a high wave energy setting where biogenic structures are not developed or have a low preservation potential (Elliot, 1978).

The calcite cement of subfacies 6c probably came into the lowermost portion of the Glauconitic Sandstone after pressure solution of the underlying calcareous "ostracode zone". The slightly coarser, generally structureless or bioturbated subfacies 6a (Plate 1-3) represents a part of the middle shoreface with a slightly higher energy and conditions more favourable for burrowing organisms.

Facies 5

The coarsest material available to a beach is commonly concentrated under the breaker zone of the middle shoreface (Harms et al., 1975). Facies 5 consists of the coarsest sandstone in the sequence from the pilot site and is sandwiched between coarsening-upward sandstone from the lower-middle shoreface and laminated sandstones of the foreshore zone. Therefore, the coarser sandstone of facies 5 probably was deposited in the breaker zone.

Pebble beds from some of the wells outside the pilot site (eg. 12-32-20-8 W4) have scour bases and fine upwards . These coarser beds suggest the interruption of normal shoreface deposition by pulses of storm-related sedimentation.

Facies 4

The horizontal, planar laminations and low angle cross-laminations in facies 4 (Plate 1-5 & 6) are typical of the upper shoreface to foreshore portion of a beach sequence (Reinson, 1980; Elliot, 1979; and McCubbin, 1982). These sedimentary structures, the good sorting, and the general lack of detrital clay indicate high energy

conditions of deposition such as occur in the wave zone. The swash-backwash mechanism is mainly responsible for the subhorizontal to low angle, planar laminations.

Facies 3

The depositional setting of facies 3 is the backshore zone of a beach. Subfacies 3d represents the transition from the foreshore to backshore zone. Periods of low energy conditions in local areas have allowed significant bioturbation. The laminated breccia blocks in well O2 (Plate 1-7) are probably collapsed portions of the banks of a small tidal creek. Upward increase in clay content from subfacies 3d to 3a signifies the gradual decrease in energy conditions along with an increase in bioturbation.

Carter (1978) describes a burrowed laminated sand facies above a laminated facies and below a peat facies. This facies, which is characterized by burrows, remnant stratification, and abundant heavy minerals, is probably very similar to facies 3 of the Glauconitic Sandstone. The burrowed laminated sand facies in the Cohansey Sand has a poorly-defined gradational contact with the laminated sand, an upward increase in burrowing and organic debris, and an upward decrease in heavy minerals and primary stratification. Similarily, in the Glauconitic Sandstone, the upward transition from subfacies 3d to 3a includes an upward increase in bioturbation and organic debris, and a decrease in primary stratification. Heavy minerals are present as laminations of magnetite but are relatively rare throughout the facies. Carter interpreted his burrowed facies as a backshore-lower eolian dune deposit. The remnant laminations indicate deposition on a horizontal to gently dipping plane surface. The upward increase in bioturbation and organic debris signify a slightly different, probably lower energy environment (Carter, 1978).

Subfacies 3bii may represent a small tidal creek cutting across the backshore zone. The mineralogical differences suggest a slight variation in sorting. The breccia at the top of the facies (Plate 2-3) represents blocks from the channel banks which collapsed into the channel.

The low angle, planar laminations of subfacies 3biii (Plate 2-4), in a stratigraphic position equivalent to backshore deposits, suggest a washover deposit. Washover deposits result when wind-generated storm surges overlap and cut through barriers creating lobate or sheet deposits of sand which extend into the lagoon (Reinson, 1980).

The deposits are generally thin, ranging from a few centimeters to two metres for each overwash event. Facies 3ciii is 1.5 metres thick, perhaps representing one washover event. The bioturbation and rootlets at the top suggest the development of vegetation on a sand flat.

Energy of the backshore environment fluctuates between low during calm periods and high during storms. Vegetated dunes occupy some of the area, whereas other areas are pools of shallow water. Facies 3 is variable with many discontinuous and irregularly-laminated, bioturbated, or clay-rich beds. This variability is due mainly to the irregularity of depositional energy within the backshore environment.

Facies 2

The carbonaceous material in facies 2 represents a marsh environment. The rootlets in facies 3a (Plate 2-5) indicate that the coal of facies 2 is *in situ* . The poor quality coal (Plate 2-6), containing much sand and clay material, indicates an unstable area of vegetation which collected wind-blown detritus and was periodicaliy flooded.

Facies 1

Facies 1 represents a back-barrier environment, including subaqueous lagoon and tidal-flat deposits. The shale immediately above facies 2 is structureless or laminated (Plate 2-7) and was probably deposited from suspension in a lagoon. Structures in the overlying interbeds of silt and shale (Plate 2-7) indicate some current activity and may represent a low energy, tidal flat. The carbonate-cemented, very fine grained sandstone may have been a washover deposit which formed a sand flat behind the barrier. The carbonate cement reflects diagenesis with some marine influence.

Summary

The Glauconitic Sandstone, represented in the SHOP project, was deposited as a prograding barrier island. Facies 6 through 1 represent the shoreface, foreshore, backshore and back-barrier environments. The major difference between the Glauconitic Sandstone and other ancient barrier-island sequences is the thickness. The Glauconitic Sandstone is 45 metres thick whereas typical models are only about ten to twelve metres thick (Galveston Island, Upper Tertiary Cohansey Sand, Gulf of Gaeta, Lower Cretaceous Muddy Sandstone; Elliot, 1979; Reinson, 1980; and McCubbin, 1982). A possible explanation for this abnormal thickness is discussed later.

III. PALYNOLOGY

Palynological results provide additional support for an environmental interpretation based on sedimentary structures and other rock properties. Shale and silty shale samples from below, above and within the Glauconitic Sandstone in regionally spaced wells, were examined for palymorphs and dinoflagellates. The distribution of samples within each well is indicated on two cross-sections in figure 7 and the geographic position of wells is shown in figure 8.

Samples containing dinoflagellates represent deposition in a marine environment (e.g., at the base or in the lower portion of the Glauconitic Sandstone in wells at 6-12-20-8 W4, 12-32-20-8 W4, and 2-8-19-8 W4; see Fig. 7). In these samples species diversity is extremely low; it is limited to one species (*Muderongia sp.*) in wells at 12-32-20-8 W4 and 2-8-19-8 W4, and 2 species (*Muderongia sp.* and *Ctenidodinium*) in the well at 6-12-20-8 W4. This low species diversity indicates that the lowermost Glauconitic Sandstone was deposited in a very restricted marine environment with low salinity (C.Singh, personal communication).

All other samples examined contain no dinoflagellates. Some have poorly preserved spores and pollen which include *Minerisporites, Erlansonisporites, Arcellites,* and megaspores, whereas others are completely barren. Samples above or within the upper portion of the Glauconitic Sandstone (uppermost samples in wells at 6-34-19-9 W4, 6-10-20-8 W4, 6-10-20-7 W4 and 11-17-21-9 W4) are in close proximity to coal beds, which suggests they are continental in origin. For other samples which lack dinoflagellates there is no conclusive evidence for a marine versus continental origin. However, since the lowermost samples in the wells at 6-34-19-9 W4 and 6-10-20-7 W4 are at stratigraphic positions similar to the marine specimens, these samples are probably also marine. Marine floras are often destroyed by wave energy along shorelines.

The conclusion from palynological data is that the Glauconitic Sandstone was deposited in a restricted, low salinity environment. Although some of the palynological data is inconclusive by itself, it does not contradict conclusions based on other evidence,

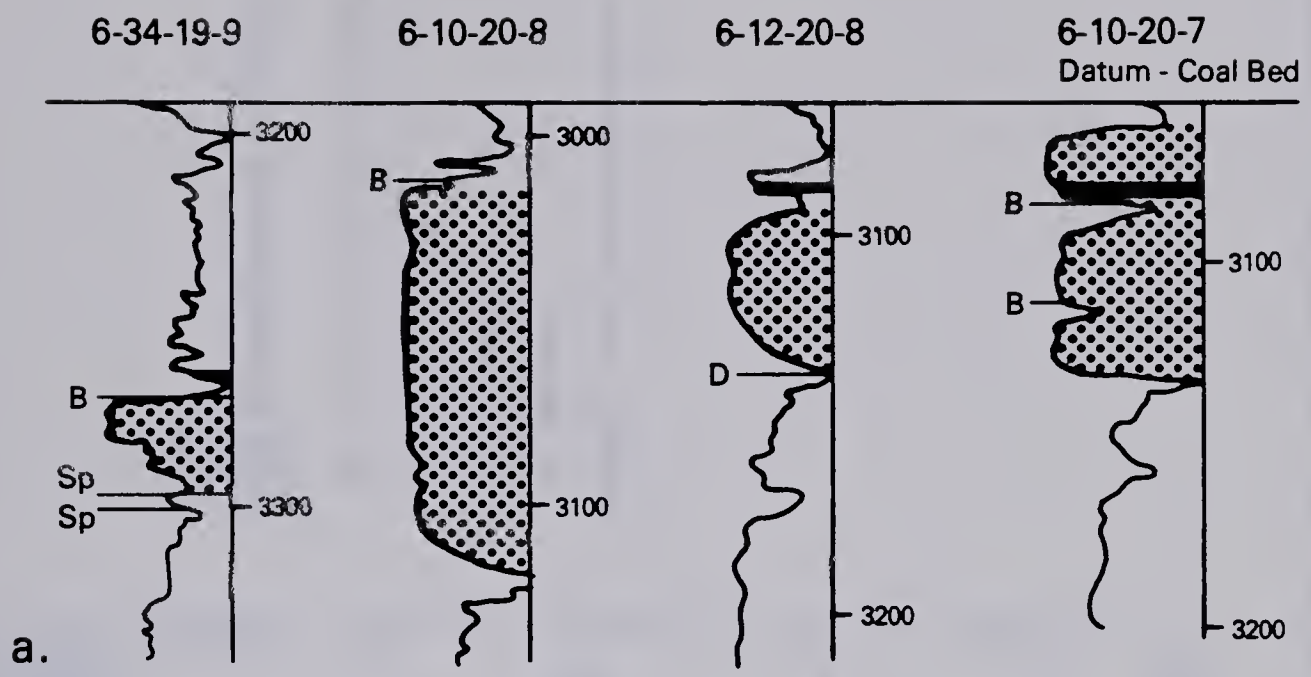

FIGURE 7. Gamma-ray log cross-sections showing the distribution of samples analyzed for palymorphs and dinoflagellates. The symbol indicating results of the palynological analyses is positioned at the depth in the well from which the sample was taken. Location of the wells is shown on figure 8.

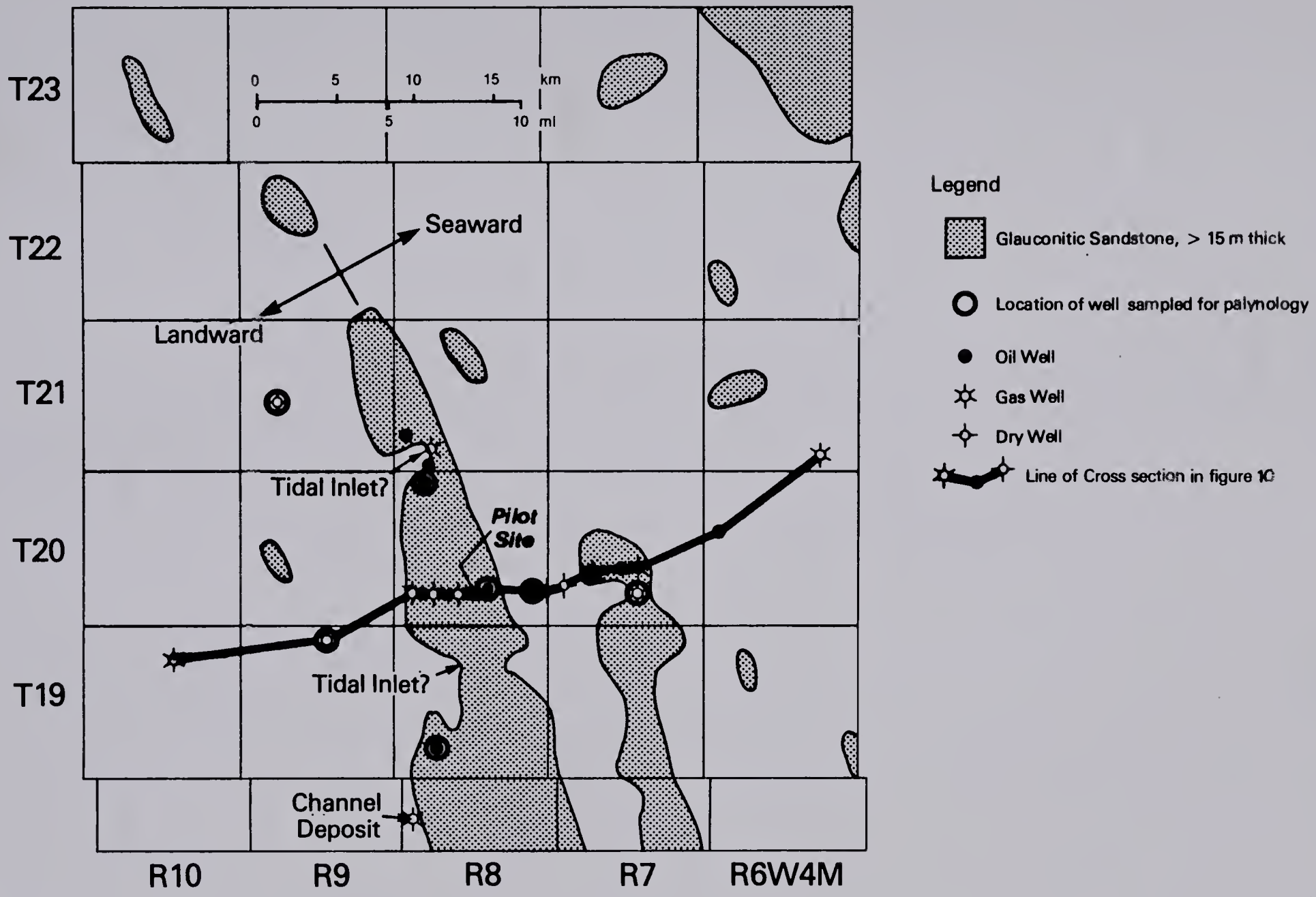

FIGURE 8. Map showing the 15 metre sandstone thickness contour for the Glauconitic Sandstone. The southeast to northwest trending broad arch defined by the sandstone represents an ancient shoreline position.

i.e., a prograding beach complex with restricted marine sediments at the base of the Glauconitic Sandstone to continental sediments at the top.

IV. REGIONAL DEPOSITIONAL SETTING

Map 1 (in pocket) is a computer-generated, sandstone thickness map for the Glauconitic Sandstone. Figure 8 is a simplified version of the same map showing the 15 metre sandstone thickness contour. A thick north-south trending sandstone is centred in Range 8, Township 20, and a thinner, less extensive trend is present to the east in Range 7. The linear geometry, combined with the sequence of facies represented by the sandstone (described in the previous section), suggests that the north-south trend represents the position of an ancient barrier-island complex. The focus of this study is on the more extensive western sandstone belt (Rge 8, Twp 20).

Palynological results, and the distribution of coals and sedimentary facies, provide evidence for western landward and eastern seaward directions. The shale at the top of the sandstone in well 6-34-19-9 W4 to the west of the sandstone belt is barren of palynological indicators but is overlain by a coal bed (Fig.7). The base of this sandstone also contains no marine indicators, although it has no *in situ* coal. The base of the Glauconitic Sandstone in well 6-12-20-8 W4 to the east of the thick Glauconitic Sandstone belt is marine (contains dinoflagellates, Fig.7). The marine shale in this well is at a stratigraphic position equivalent to the coal in the 6-34-19-9 W4 well. This suggests that continental conditions occurred to the west of the sandstone belt while marine conditions occurred to the east.

The distribution of facies provides additional support for a beach complex prograding seawards to the east. Figure 9 shows the distribution of facies within the sandstone on the western side of, within, and to the east of the sandstone belt. The Glauconitic Sandstone on the western side of the belt (represented by wells 2-8-19-8 W4 and 12-32-20-8 w4) is thinner than the sandstone in the central portion of the belt but all of facies 6 through 3 are represented. To the east of the sandstone belt, the 10 metre thick Glauconitic Sandstone consists mostly of facies 6 sandstone (at least all but the upper 2 metres, represented by a core from the 10-10-21-8 W4 well) and represents the shoreface portion of the beach to the west.

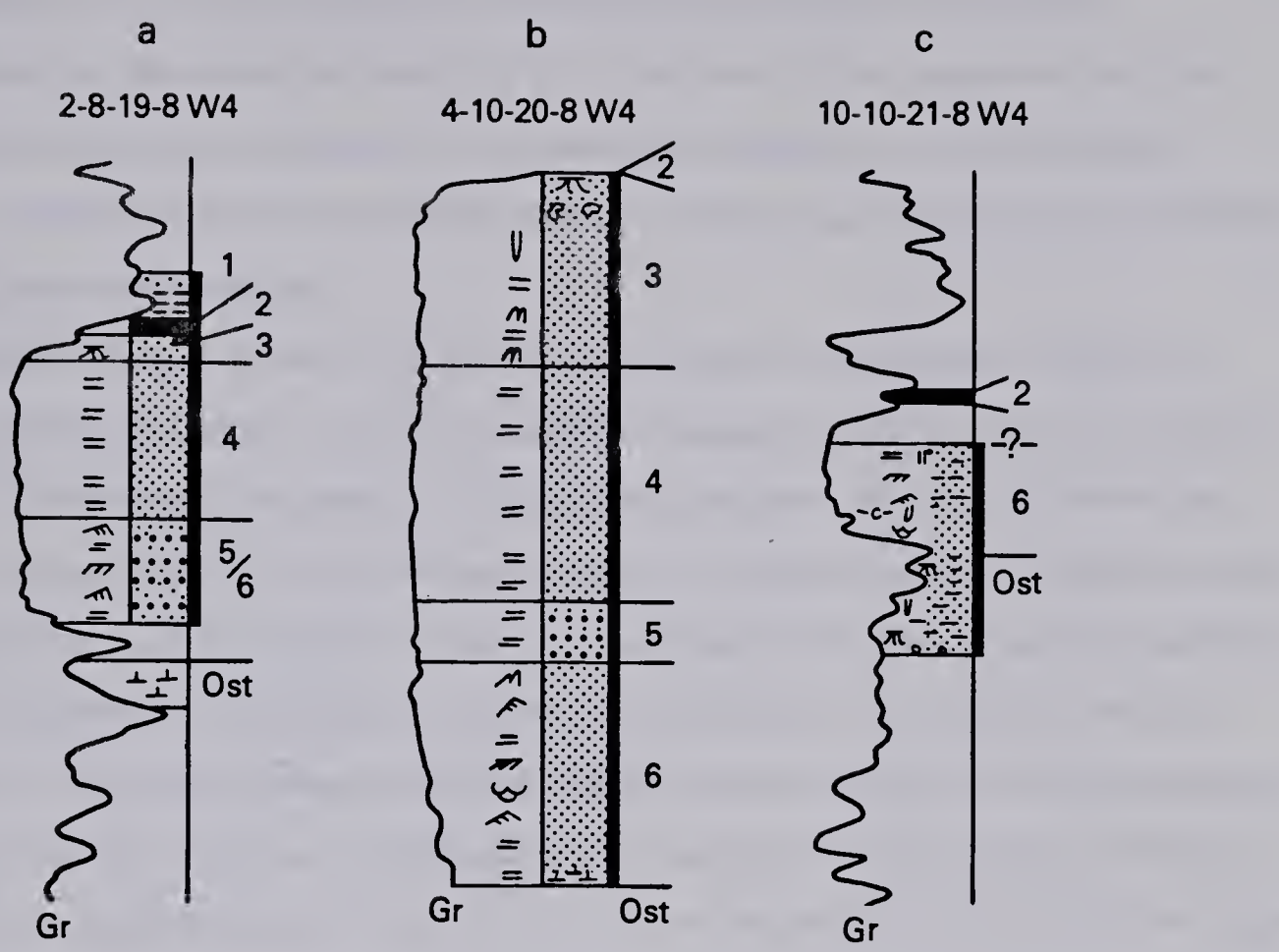

FIGURE 9. Sequence of sedimentary facies within regionally spaced wells from (a) the western side of; (b) within; and (c) the eastern side of the thick sandstone belt.

Figure 10 is a cross-section of the Glauconitic Sandstone extending perpendicular to the sandstone belts (Fig. 8). To the west of the sandstone belt, the Glauconitic Sandstone is replaced by an interbedded sequence of thin sandstones, siltstones, shales and coal of continental origin. To the far east the Glauconitic Sandstone loses its distinctive character.

Comparison of facies in the thinner sandstones, on the western side of the sandstone belt, with facies in the thick sandstone sequences, shows that no one facies has been preferentially thickened at the expense of another. The thickest sandstones represent areas where the shoreline was stable with a balance between sediment imput and subsidence such that vertical buildup of facies dominated rather than progradation. A possible mechanism controlling the subsidence is discussed in the section 'Tectonic Setting'. The fluctuating energy conditions in the backshore zone, and the accumulation of washover deposits, produce a considerable local variation in the thickness of facies 3 sandstone (compare the well at 2-8-19-8 W4 with the well at 12-32-20-8 W4, Fig.9).

Storm and washover processes played a significant role in the deposition of the Glauconitic Sandstone. The interbedding of coarse-grained sandstone and pebbles with fine-grained sandstone (facies 5) is a result of storm activities in the shoreface zone. The shape of the major sandstone belt (Fig.8) suggests the presence of washover lobes on the landward (western) side of the belt (Fig.8). The eastern side of the belt is relatively straight, whereas the western side is more irregular. The variety in the thickness of facies 3 sandstone (<1-12 m thick) and the scattered, remnant, low angle, planar laminations suggest that much of facies 3 was deposited as a series of washover lobes which formed washover terraces on the landward side of the beach complex. Burrowing organisms, wind processes, and small tidal creeks destroyed much of the original sedimentary structure during quiet times between storms.

Although abundant washover features indicate a microtidal environment where tidal inlets are infrequent (Hayes and Kana, 1977), tidal inlets and channels are present in the Glauconitic Sandstone. Two possible positions of tidal inlets based on the shape of the sandstone belt are shown in figure 8. At 14-5-21-8 W4, geophysical logs (no core available) for the Glauconitic Sandstone interval indicate a sequence of interbedded silty sandstone and shale (Fig. 11) that is dissimilar to any of the facies described. This well is

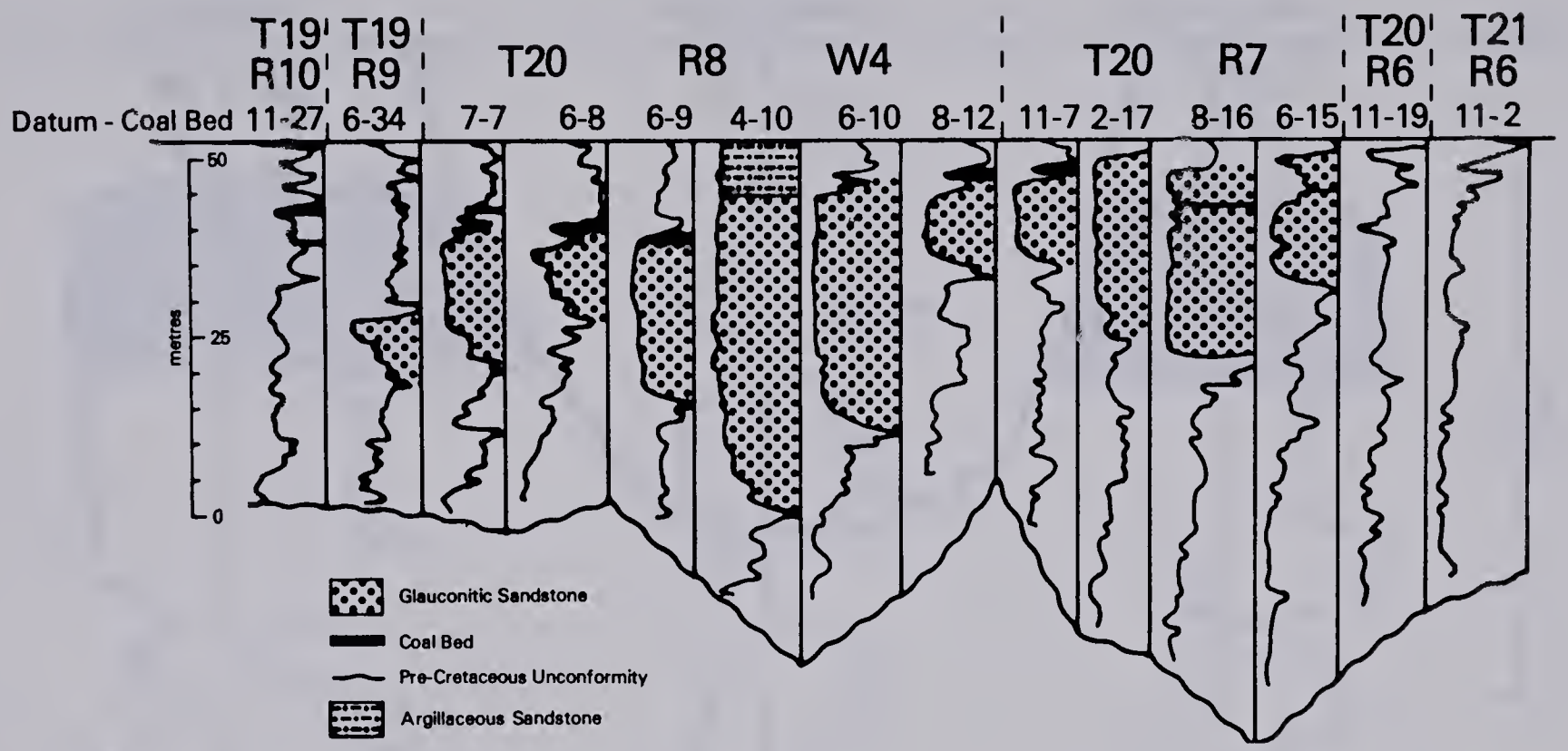

FIGURE 10. Gamma-ray log, stratigraphic cross-section illustrating the relative vertical position of sandstone bodies when the datum coal bed was deposited. The cross-section location is shown on Figure 8. As the datum coal bed is not detectable in wells at 8-16-20-7W4 and 11-19-20-6W4, positioning relative to adjacent wells is based on correlations of geophysical log shapes. The argillaceous sandstone zone in the 4-10-20-8W4 well is equivalent to the backshore zone (facies 3) in the SHOP project wells.

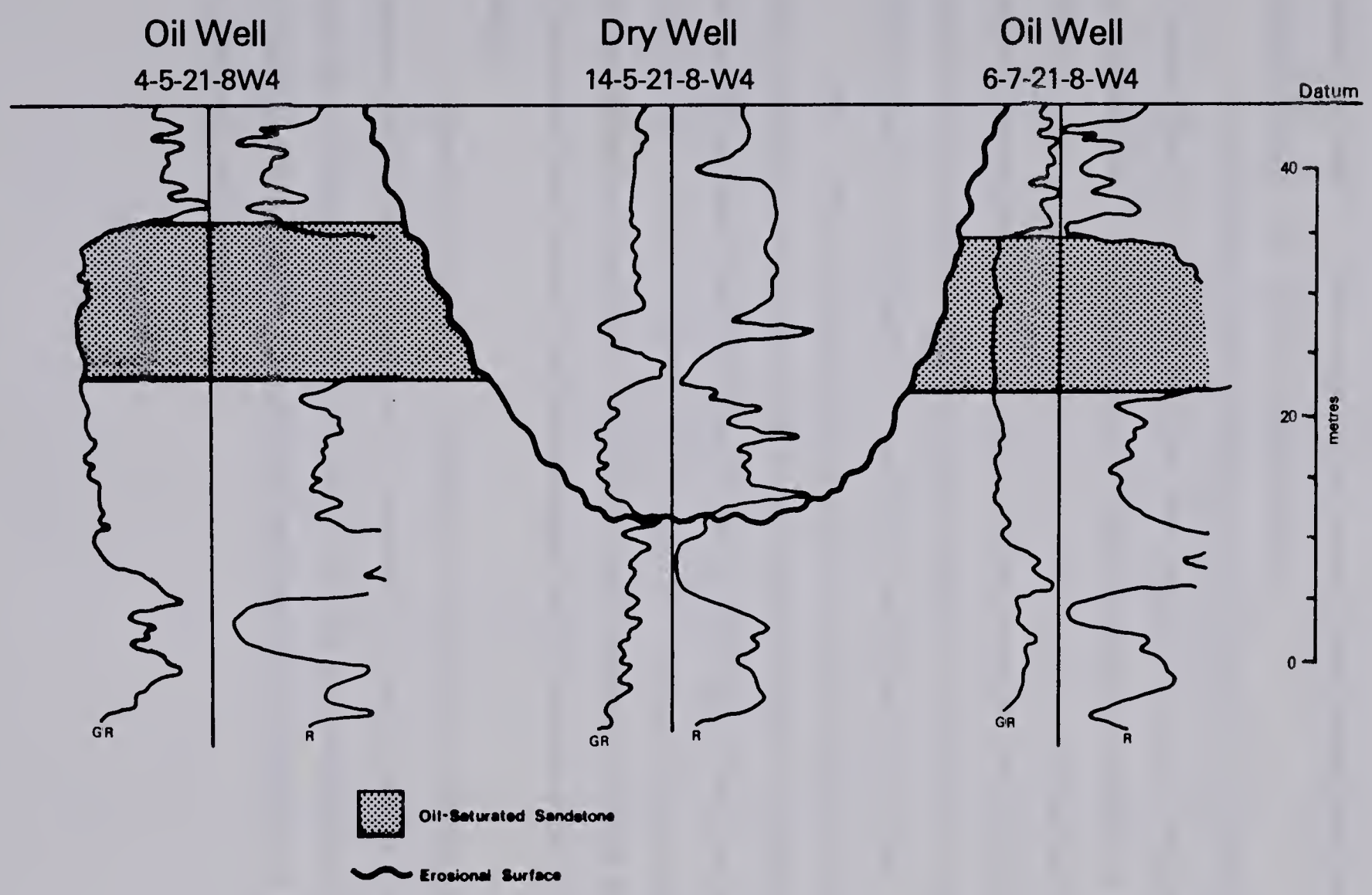

FIGURE 11. Geophysical log, stratigraphic cross-section showing an interruption in the continuity of the sandstone reservoir by a facies change. The fine-grained sediments in the dry well represent the abandonment of either a tidal inlet which cut across the beach trend, or a later stage fluvial channel.

dry, whereas wells immediately to the north and south (4-5-21-8 W4 and 6-7-21-8 W4, Fig.11) have the typical Glauconitic Sandstone beach facies and are oil producers. The silty sandstone of the dry well represents a facies change from the beach facies in the surrounding wells and probably is the fill of an abandoned portion of a tidal inlet or the abandonment of a later stage fluvial channel. Similar abandoned portions of tidal inlets are described by Tye (1978) in South Carolina.

A 10 metre thick channel sandstone occurs at 6-30-18-8 W4 (Fig.12). The base of the sandstone is erosional into the underlying calcareous silt, shale and sand of the "ostracode zone". The lower portion of the sandstone unit consists of a series of fining-upward cycles with erosional bases, from cobbles and pebble conglomerates to coarse-grained sandstone. In the upper portion of the unit, the sandstone has fined upwards to fine-grained sandstone and is topped by a rooted coal. Cross-laminations dipping at about 15 degrees are the dominant sedimentary structures.

Other wells probably penetrate tidal inlet or channel deposits. Unfortunately, cores rarely include the base of the Glauconitic Sandstone. The difficulty in identifying channel versus beach deposits based on geophysical log character alone is demonstrated by the 6-30-18-8 W4 well (Fig.12). The gamma-ray log indicates a good coarsening-upward sequence (suggesting a beach deposit), whereas the SP-log indicates a convincing fining-upward sequence (suggesting a channel deposit) for the same depth interval.

In summary, the depositional setting is a north-south trending barrier-island complex with the seaward direction to the east. The thick sandstone trend can be expected to extend to the south into the undrilled area. Interruptions in the continuity of the reservoir on a regional scale can be expected due to dissection of the sandstone belt by tidal inlets and channels.

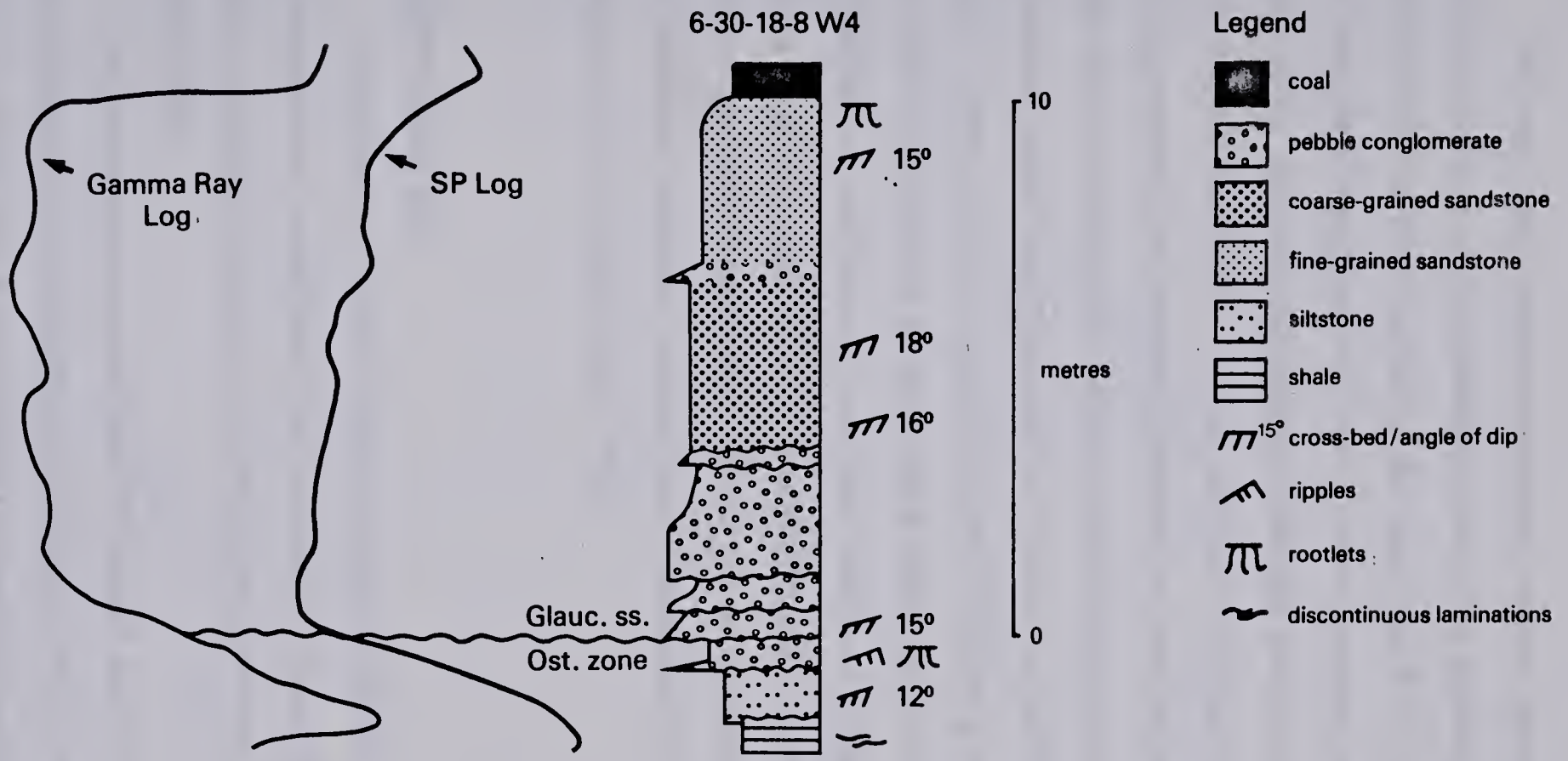

FIGURE 12. Litholog of a channel deposit within the Glauconitic Sandstone interval.

V. TECTONIC SETTING

The study area is located immediately west of the North Battleford Arch, a northward extension of the Sweetgrass Arch. The westernmost ridge-line from the arch extends into the northern portion of the study area (Fig. 13). Evidence for periods of uplift along the Sweetgrass Arch from Late Precambrian time to the Tertiary is given by Herbaly (1974). By close examination of the rock units he noted that there were several cycles of uplift and erosion and long periods of nondeposition. The Sweetgrass Arch dipped southward from the North Battleford Arch during the Pennsylvanian, Permian, and Triassic time, as evidenced by subcrop patterns and thinning isopachs across the axes of the positive trends. Major reactivation of the arch occurred during the late Cretaceous and Early Tertiary Laramide Orogeny (Tovell, 1958) and a northward plunge of axis of the arch resulted. To the north of the Suffield Saddle (Fig. 13) formed during this orogeny, the North Battleford Arch retained its original southward plunge. Hayes (1982) summarized evidence cited by various authors for uplift along the Sweetgrass Arch before and during the Early Cretaceous. The present well control shows that extensive faulting of various types displaces Cretaceous, Jurassic and Mississippian strata in the vicinity of the Sweetgrass Arch complex (Hayes, 1982).

A. SHOP Project Site

The dense core control within the SHOP project site offers a unique opportunity for correlation on a small scale. Such correlation shows that basement faults, probably related to movement associated with the North Battleford Arch, were active during late Mannville time.

Two very closely spaced wells (70 metres apart) show considerable structural relief on the top of the foreshore zone (facies 4) and on the top of the Glauconitic Sandstone unit. Figure 14 shows these two wells, P2 and O2, in a series of relative vertical positions. The horizontal to subhorizontal lines between the two wells join correlative beds and represent surfaces which were near horizontal during deposition of

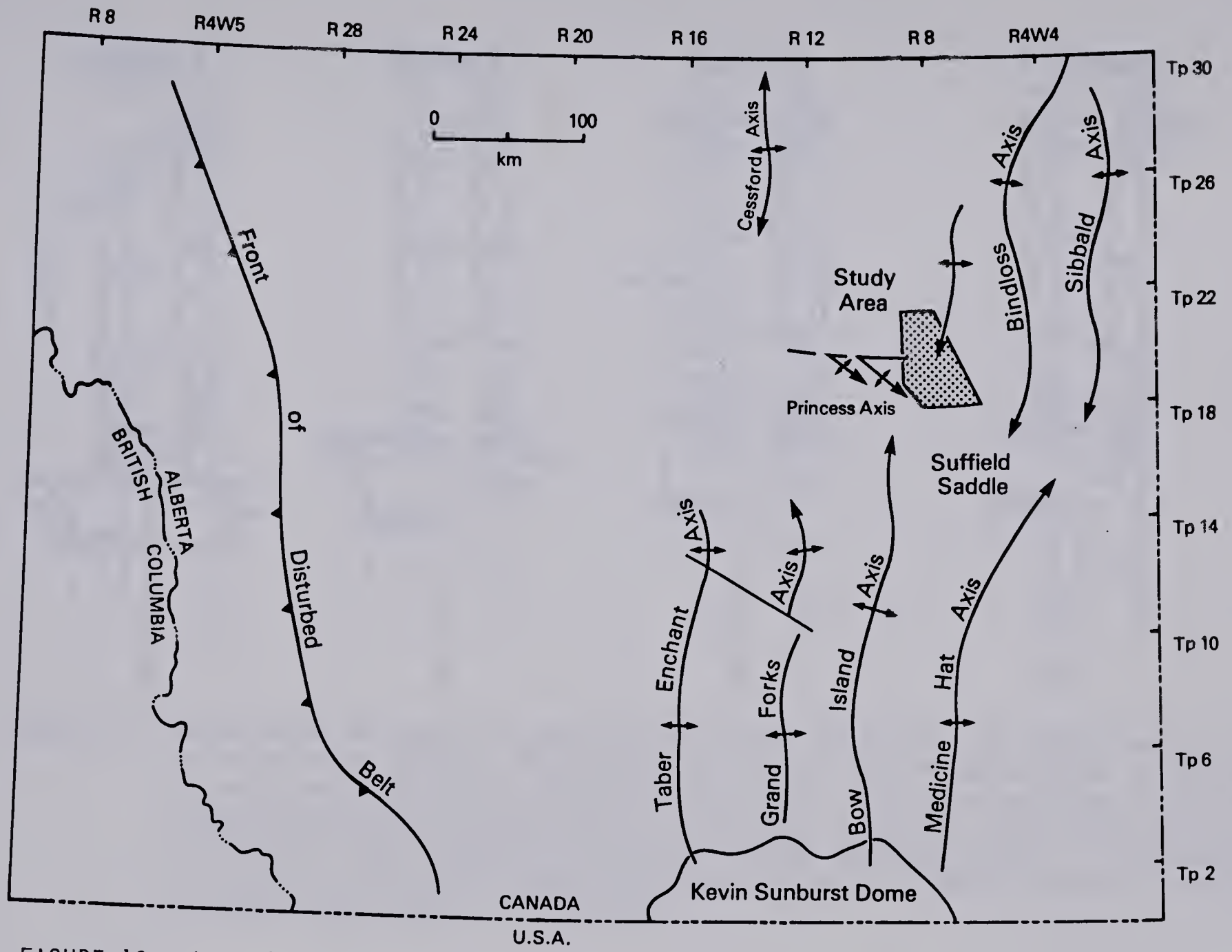

FIGURE 13. Location of the study area relative to various components of the North Battleford Arch, a northern extension of the Sweetgrass Arch. From Herbaly (1974): contours on top Devonian System.

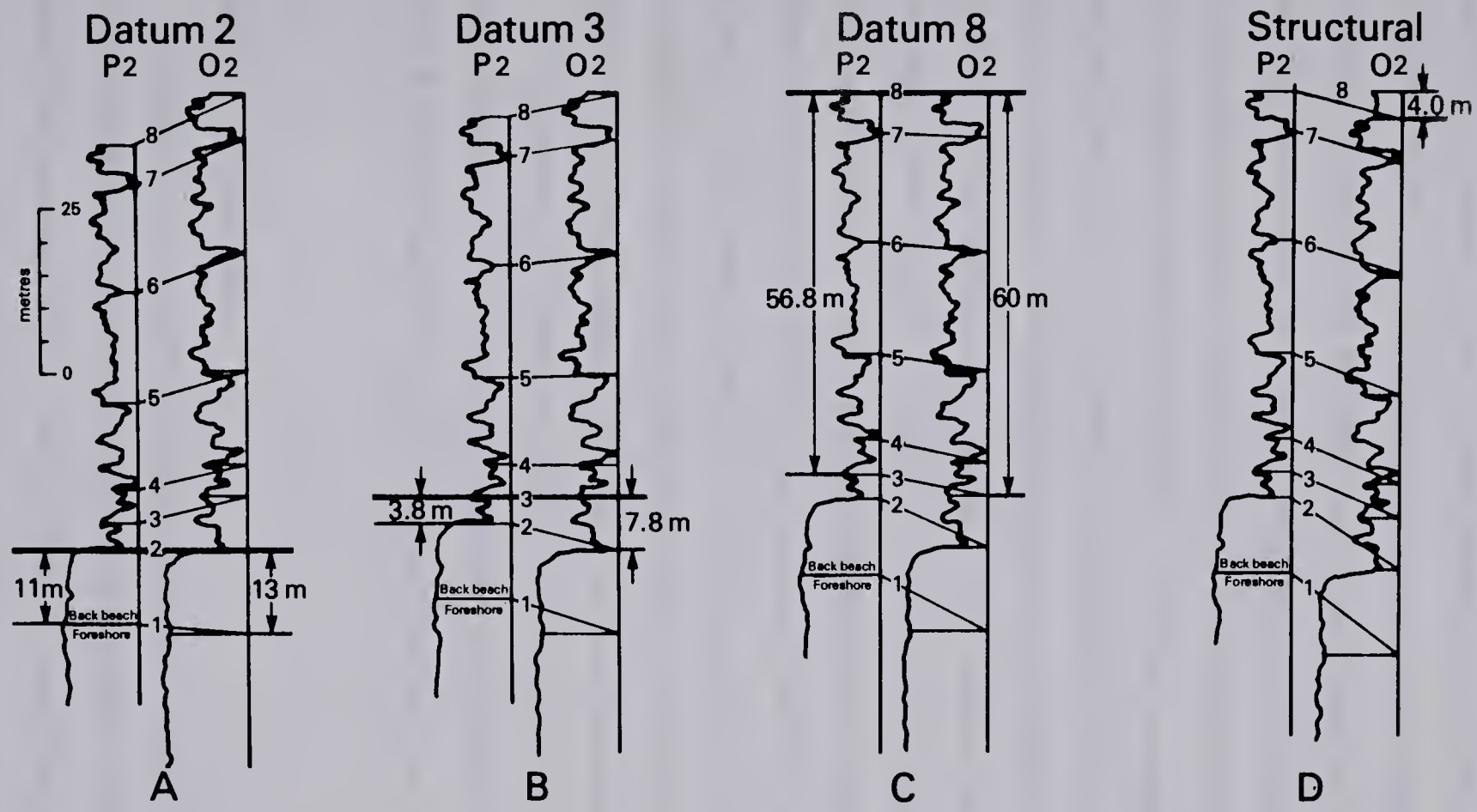

FIGURE 14. Correlation of gamma-ray logs for two wells (P2 and 02, 70 metres apart), hung on a series of datums. The heavier horizontal line between wells is the datum in each case. Thickness of sediment in each well between each datum is given and demonstrates the main intervals of thickening. A total cumulative thickening of 9.2 metres within Mannville deposition (below correlation 8) is illustrated in A, B and C. Figure 14D shows additional relief of 4 metres caused by structural movement after Mannville deposition.

that particular datum. Figure 14A shows the position of the two wells with the carbonaceous bed on the top of the sandstone as the datum (#2). Note that the interval from the top of the foreshore zone, facies 4, to the carbonaceous bed at the top of the sand, is thicker in well O2 by 2 metres. Figure 14B, where the datum is #3, shows a thickening of 4 metres in well O2 from datum #2 to #3. This is the interval of most significant thickening within Upper Mannville deposition. Figure 14C shows the top of the Mannville as the datum (#8). Between datum lines #3 and #8, an additional 3.2 metres of thickening has occurred. Thus, within deposition of the Mannville itself a total thickening of at least 9.2 metres has occurred. Figure 14D shows the present structural position of the two wells. Since Mannville deposition, structural movement of 4.0 metres has occurred. Thus a total of 13.2 metres vertical adjustment from the present structural positions, is needed to reconstruct the top of the foreshore zone. An elevation difference of 13.2 metres over a distance of 70 metres requires an 11 degree beach slope. Such a steep slope is unrealistic for fine-grained sandstone beaches which typically have slopes of only 3 degrees (Shepard, 1973). Figures 4 and 5 support the argument that the beach had a very low slope by illustrating that the top of the sandstone in all SHOP project wells, except P2, is approximately at the same structural level. Well P2 is structurally higher than all the other wells by a significant amount. A fault between wells P2 and O2 is the simplest explanation for such an elevation difference.

A basement fault between wells P2 and O2 was probably active during the latter stage of deposition of the Glauconitic Sandstone. This fault caused gradual subsidence of wells to the east of well P2 and a consequent thickening of sediment in those wells.

B. Regional Suffield Area

Comparison of the structural cross-section in figure 15 with the stratigraphic cross-section (Fig. 10) demonstrates the vertical shifting of wells in the regional setting necessary for sedimentological interpretation. Although the present relief on the approximate horizon correlated in figure 15 appears excessive, when one considers that there is a structural relief of 13.2 metres over a distance of only 70 metres (between wells P2 and O2 in the SHOP project; see Fig. 14), the relief shown in figure 15 stretched

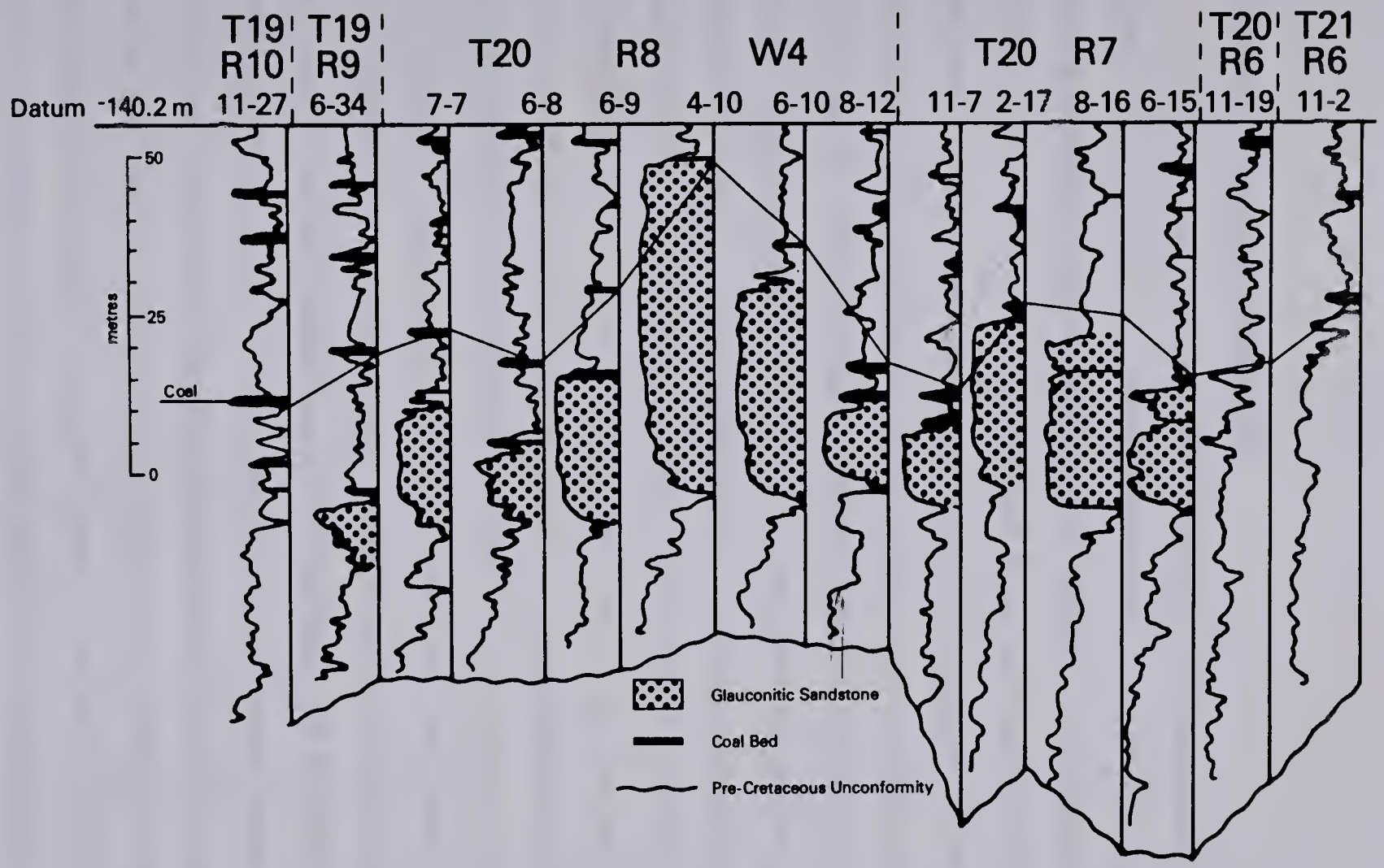

FIGURE 15. Gamma-ray log, structural cross-section with a correlation line joining approximate correlative horizons. Correlation of these particular coal beds is based on the vertical, sequential arrangement of sands, shales and coals throughout the Mannville interval as indicated by geophysical log characteristics and core where available.

over a much larger distance (40 km) is not so dramatic. In fact, if wells are not adjusted so that the correlated coal horizon is horizontal, the sedimentological picture becomes very complex; for example, coals would occur on both sides of the thick beach sandstone sequence in the 4-10-20-8 W4 well.

C. Petroleum Trapping Mechanism

Trapping of petroleum in the Suffield area is stratigraphically controlled. Oil is trapped by facies changes, from the clean sandstone of the beach sequence (facies 4) to the more argillaceous sandstones (facies 3), siltstones, and shales (facies 1) of the backshore zone, or to tidal inlet or channel deposits. However, faults have also played a significant role in producing traps by vertically shifting blocks from their original depositional positions, where no facies changes occurred within the depth interval of oil impregnation, to relative positions such that facies changes do occur at this same structural level. Figure 16 shows two cross-sections demonstrating the effect of structural movements on the relative position of the oil/water interface in an oil well and a nearby potential oil well. Figure 16A shows the present structural position of the oil/water interface in each of the two wells, 14-27-19-8 W4 and 6-34-19-8 W4. The 14-27-19-8 W4 well is a potential oil well with a possible pay zone only 9 metres in thickness, whereas the 6-34-19-8 W4 well is an oil well with a pay zone 21 metres thick. The level of the oil/water interface is within the clean sandstone interval of the 6-34-19-8 W4 well, but is relatively higher in the 14-27-19-8 W4 well, where it is very close to the more argillaceous sandstone facies. The continuity in the upper portion of the petroleum reservoir is interrupted by a facies change. However, if these two wells are adjusted to reflect their relative vertical positions at time of sedimentation (Fig. 16B), it can be seen that the depth of the oil/water interface, shown by the 6-34-19-8 W4 well, is deep within the clean sandstone facies in the 14-27-19-8 W4 well. If no structural movement had occurred after deposition of the sandstone, the 14-27-19-8 W4 well would have been an oil producer with a pay zone more than twice its present thickness. Thus, although the overall trapping mechanism is stratigraphic, there are local structural complications as a result of basement faulting.

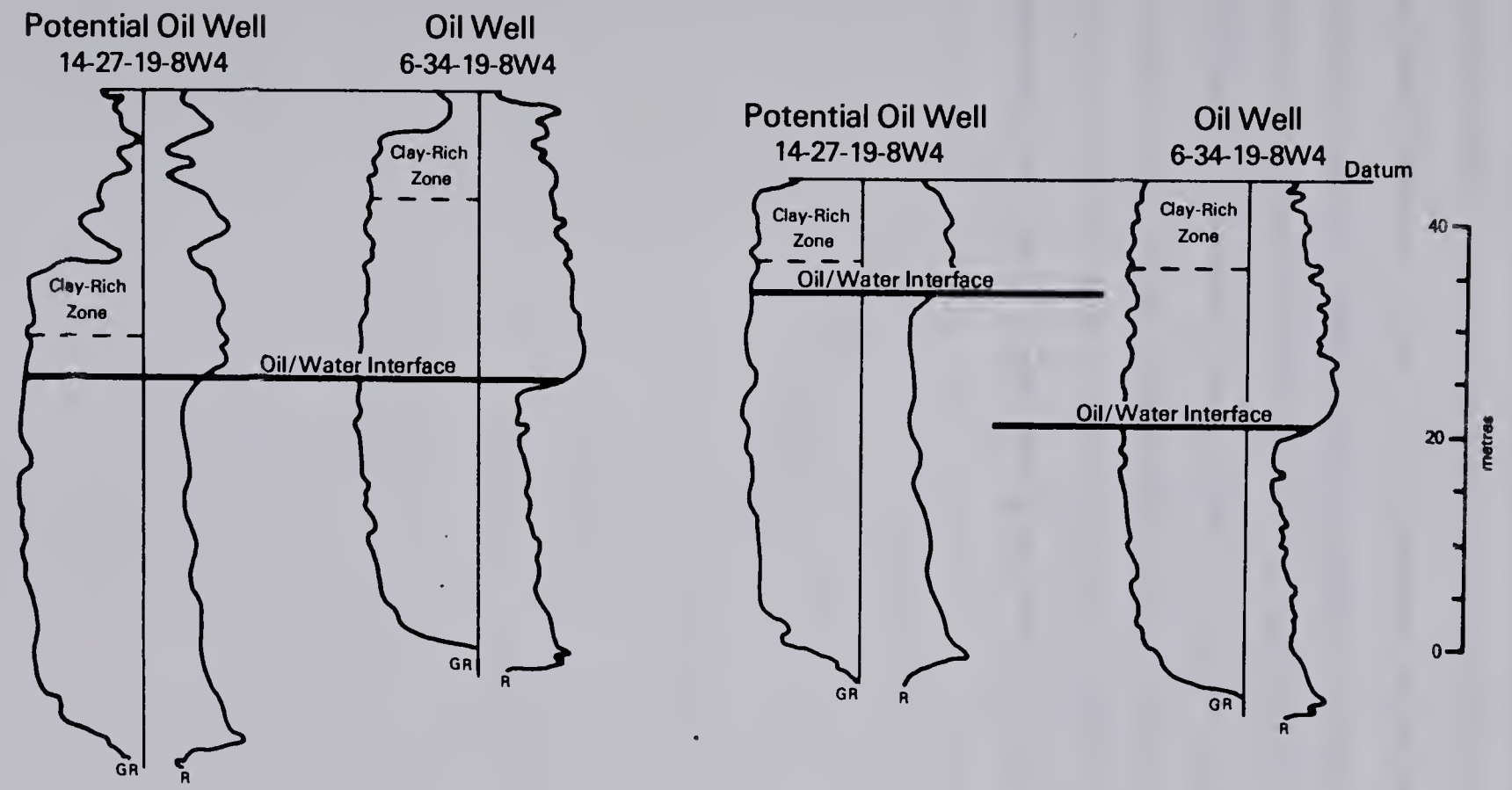

A. Structural Cross Section

B. Stratigraphic Cross Section

FIGURE 16. Two cross-sections demonstrating the effect of structural movements on the relative positions of the oil/water interface. If no structural movements had occurred after deposition of the sandstone, the 14-27-19-8W4 well would have been an oil producer with a pay zone more than twice its present thickness.

D. Tectonic Control on the Glauconitic Sandstone Thickness

As mentioned previously, parts of the Glauconitic Sandstone are unusually thick for a beach sequence. In light of the evidence for tectonic activity immediately after deposition of the sandstone, it seems probable that movement on basement faults was also responsible for controlling the rate of subsidence during deposition of the Glauconitic Sandstone. Figure 17 is a schematic cross-section showing the thickening of sediment in a zone of relatively rapid subsidence. Wells A, B, and C represent wells to the west of; within; and to the east of the thick sandstone belt, respectively. The thicknesses of the facies, representing the shoreface, foreshore and backshore zones, are shown as they occur in each of the representative cores. The greater sediment accumulation in well B was the result of relatively rapid subsidence, probably caused by the downfaulting of basement blocks below well B, during deposition of the sandstone.

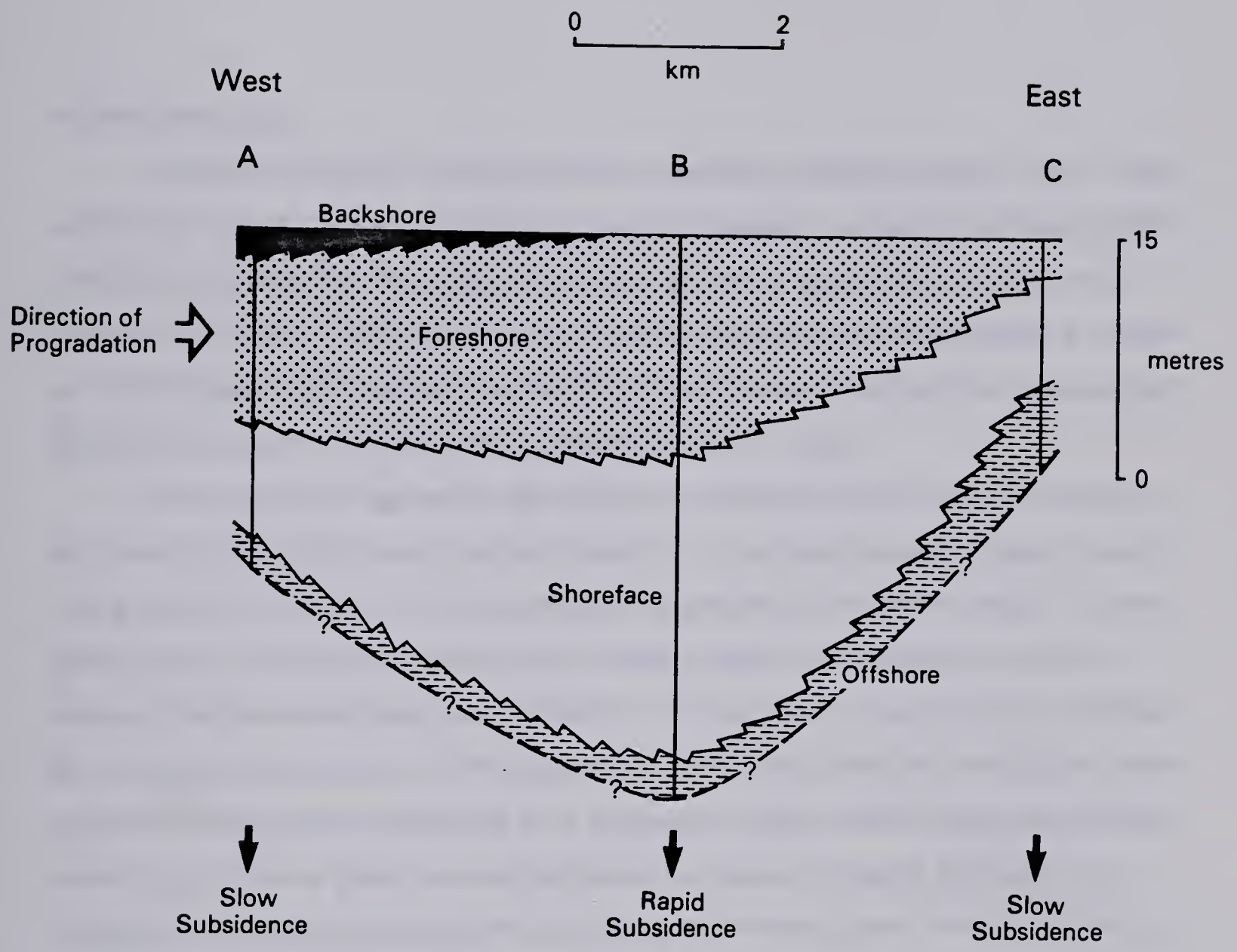

FIGURE 17. Schematic cross-section showing the thickening of sediment over a zone of relatively rapid subsidence. Wells A, B and C represent wells to the west of, within, and to the east of, the thick sandstone belt, respectively. The thickness of the facies, representing the shoreface, foreshore and backshore zones, are shown as they occur in each of the representative cores. The relatively rapid subsidence in well B was probably caused by downfaulting basement blocks.

VI. MINERALOGY

A. Bulk Mineralogy

The grain mineralogy of the Glauconitic Sandstone consists of quartz, chert, other sedimentary rock fragments, and minor amounts of feldspar . According to Folk's (1968) sandstone classification, the rock is a litharenite, and more specifically a chert arenite with 60–70% quartz, 10–50% chert, 5–20% other sedimentary rock fragments and trace to <10% feldspar. Grain percentages based on point counts of thin sections representing each facies present in well O1 (SHOP project) are given in Table 1.

Quartz grains are generally subrounded to rounded and vary in size from coarse silt–sized in lowermost facies 6 to fine–grained in all overlying facies. Authigenic quartz overgrowths are common in the less argillaceous sandstone. The detrital shape of some quartz grains is defined by a thin line of abundant inclusions trapped at the boundary between detrital and authigenic quartz (Plate 4–1). Other quartz overgrowths are defined by the euhedral terminations of the overgrowth, or the interlocking of overgrowths from adjacent grains (Scholle, 1979) (Plate 4–1), making the original detrital shape less obvious. Interlocking of quartz grains can also be caused by pressure solution. The open pore structure of these sandstones and the abundance of euhedral quartz terminations favour the overgrowth origin. In the most argillaceous sandstones of facies 3, quartz overgrowths are rare and may have rounded or broken terminations. These overgrowths are probably inherited from a previous depositional cycle (Scholle, 1979).

Chert grains are commonly coarser grained and more angular than quartz grains. Facies 5, the coarsest sandstone, is composed of approximately 50 per cent chert and only 30 per cent quartz. The chert grains are larger than quartz, although less durable, simply because they started out much larger in the original sedimentary source as chert nodules: the chert is more angular because it tends to chip and split rather than round with abrasion (Folk, 1968). Chert grains are microcrystalline or macrocrystalline (Plate 4–2), and commonly have opaque inclusions or alteration products.

Other sedimentary rock fragments consist of siltstone, shale and silty shale. Grains within siltstone fragments are dominantly quartz with some chert. Some siltstone fragments have been so deformed that they are almost indistinguishable from the matrix (Plate 4-3). Rock fragments with a significant clay content tend to be deformed as a result of compaction (Plate 4-4). Rock fragments are most abundant (20%) in facies 4 and subfacies 3bii; their compaction is a significant cause of porosity reduction.

Feldspar grains are present in minor amounts in most samples. The distribution of feldspar is largely related to grain size. Feldspar cleaves relatively easily and breaks into smaller grains. It most commonly occurs as silt grains within rock fragments or as grains in the very fine grained sandstone of facies 6. Facies 2bii is exceptional in its relatively high abundance of feldspar (Plate 3-2), including plagioclase and K-feldspar. Many feldspars are corroded and only their skeletal framework remains (Plate 5-1), thus producing a minor amount of secondary porosity.

Carbonate grains (dolomite or siderite) and carbonate cement are present in the less argillaceous sandstones. Some of the carbonate is approximately median grain size (fine-grained) and has interlocking contacts with adjacent detrital grains (Plate 5-2). The interlocking contacts may result from remobilization of a carbonate grain or be due to a combination of both quartz and carbonate overgrowths. Other carbonate zones are larger than median grain size and also have interlocking contacts with detrital grains (Plate 5-2). This carbonate probably represents a very local, early diagenetic cement. Authigenic calcite prisms also occur.

Pyrite occurs as isolated cubes associated with clay on the pore walls (Plate 5-3), and in spherical clusters. It also replaces what looks like an organic structure (Plate 5-4). Pyrite generally shows no signs of abrasion, and is probably authigenic.

Although the unit is called the "Glauconitic Sandstone", glauconite is very rare. It occurs in thin section as a round, silt-sized, pleochroic, green mineral with medium birefringence.

B. Clay Mineralogy

Descriptive Clay Mineralogy

Kaolinite

Kaolinite is the dominant clay mineral in all samples. Its proportion in the <2 micrometre fraction varies from 100 per cent in the most argillaceous sandstones at the top of the Glauconitic Sandstone (Tables 5 and 6) to only 45 per cent in a shale interbed at the base of the Glauconitic Sandstone (sample 34-165, Table 6). The cleanest sandstones contain 80 to 90 per cent kaolinite in the clay fraction. X-ray powder camera analysis of a sample in which a 7A phase is the only clay mineral present, confirms that the polytype is kaolinite (Table 7). In X-ray diffractograms (Figs. 18-24), kaolinite is represented by a sharp, intense 7A peak and well-defined, lower-order basal reflections; some nonbasal reflections are also present on most diffractograms.

Kaolinite in the most argillaceous sandstones occurs as masses of very fine clays whose crystal structure can only be distinguished under high magnification (Plate 5-5). These masses of kaolinite coating grains and filling pores consist of very fine platelets with ragged edges . The clay is dispersed with silt-sized quartz as matrix surrounding fine- to medium-sized sand grains (Plate 5-6), and is detrital in origin (Wilson and Pittman, 1977).

In the slightly less argillaceous sandstones, ridges or sheets of very fine clay are commonly attached to grains and extend into the pore space (Plate 6-1) or form bridges between grains. These ridges or sheets are present in argillaceous sandstones of facies 3, in which the clay composition is almost 100 per cent kaolinite. The kaolinite is probably detrital in origin and may represent an infiltration clay which moved into the interstices of sand by downward or lateral migration of water (Wilson and Pittman, 1977).

Very fine detrital clay may fill the majority of pore space in the less argillaceous sandstones, but authigenic kaolinite and quartz overgrowths fill the remaining pore space (Plate 6-2). Kaolinite is one of the most abundant authigenic phases and is present in all the sandstones which had sufficient primary pore space to allow its growth (especially facies 4, 5, and 6). Authigenic kaolinite abundance is inversely proportional to the amount

Table 5. Relative Percentages of Clay Minerals in SHOP Project Samples, <2μm Size-Fraction

Well No.	Sample	Log Depth	Facies	Clay Minerals[1] (relative %) Kaol	Ill	Sm	Chl	ML	Total Clay (Wt %)	
01	147	911.3	3ai	100	tr	-	-	tr	9.74	
	148	912.3	3ci	100	tr	-	-	tr	9.61	
	149	915.3	3d	100	tr	-	-	tr	5.94	
	151	929.0	4	90	10	tr	-	tr	2.12	oil-saturated
	152	940.5	5	90	10	tr	tr	-	3.55	water-saturated
	153	944.2	6a	95	5	tr	tr	tr	4.35	
	155	953.4	6b	95	5	-	tr	tr	2.60	
02	157	910.1	3ai	100	-	-	-	-	13.69	
	158	911.6	3bi	100	tr	-	-	tr	8.04	
	159	918.1	3d	95	5	tr	-	tr	2.72	
	160	929.9	4	90	10	tr	-	tr	2.79	oil-saturated
	161	940.2	5	90	10	tr	-	tr	3.12	water-saturated
	162	944.6	6a	95	5	tr	-	tr	4.61	
	164	952.8	6b	90	10	tr	-	tr	4.42	
	165	954.6	6c	90	10	-	-	tr	no data	
03	167	914.7	3bi	100	tr	*	*	*	19.54	
	168	916.8	3cii	100	*	*	*	*	14.47	
	169	922.0	3d	100	tr	-	-	-	5.42	
	170	932.9	4b	90	10	-	-	*	3.07	oil-saturated
	171	941.7	5	80	15	5	-	*	3.36	water-saturated
	172	950.7	6a	95	5	tr	-	tr	6.07	
	173	956.6	6b	90	10	-	tr	tr	5.50	
P1[2]	186	910.4	3ai	100	-	-	-	tr	19.50	
	187	915.0	3ci	100	tr	-	-	tr	11.42	
	188	926.3	4b	90	10	-	-	tr	3.09	
P2[2]	189	901.6	3bi	100	tr	-	-	tr	15.89	
	190	904.6	3ci	100	-	-	-	tr	8.46	
	191	907.7	3d	100	tr	-	-	tr	3.26	
	192	919.6	4a	100	tr	-	-	tr	3.76	
P3[2]	176	911.5	3ai	100	-	-	-	tr	21.80	
	204	912.7	3bi	100	tr	-	-	tr	9.59	
	177	915.3	3ci	100	tr	-	-	tr	7.95	
	178	926.0	4	95	5	-	-	tr	2.15	
P4[2]	193	915.9	3ai	100	tr	-	-	tr	28.11	
	194	916.8	3bii	95	5	-	tr	tr	15.60	
	195	919.3	3ci	100	-	-	-	tr	16.79	
	196	922.0	3ci	100	-	-	tr	tr	9.92	
	197	924.0	3d	100	tr	-	-	tr	4.71	
	198	930.8	4	90	20	-	-	tr	2.85	
I1[2]	200	911.7	3ai	100	tr	-	-	tr	10.00	
	201	912.7	3biii	100	tr	-	-	tr	10.36	
	202	917.8	3d	95	5	-	tr	tr	1.04	
	203	930.1	4a	95	5	-	-	tr	1.37	
Shale Samples										
01	146	910.3	1	60	40	-	-	tr		
02	156	909.1	1	80	20	-	-	tr		
	163	948.1	6b	90	10	tr	tr	-		
	166	955.5	6c	45	55	tr	-	tr		
P3	175	910.4	1	65	35	-	-	tr		

[1] Kaol, kaolinite; Ill, illite; Sm, smectite; Chl, chlorite; ML, mixed-layer clays

[2] All samples were taken above the oil/water contact

* May be present in trace amounts, not detectable due to the sensitivity at which the XRD patterns were obtained for these particular samples

Table 6. Percentages of Clay Minerals in the <2μm Size-fraction From Detailed XRD Analyses*

Sample #	Well Location	Log Depth(m)	Sample Description	Relative Percent Clay Minerals Kaol.	Ill.	Sm.	Chl.
10-56	10-33-19-7 W4	945.8	fine ss., above heavier oil-sat. zone	75	20	5	-
10-59	10-33-19-7 W4	958.0	coarser ss. interbed. oil-sat.	82	20	trace	trace
10-62	10-33-19-7 W4	961.9	coarse ss., below O/W interface	90	10	<5	trace
16-86	8-3-20-7 W4	962.5	fine ss., below O/W interface	70	20	10	trace
30-132	6-15-20-7 W4	957.7	light grey shale with rootlets	<5	-	>95	-
14-82	2-8-19-8 W4	961.6	shale above coal overlying Glauc. ss	55	45	-	-
8-39	6-27-19-8 W4	959.2	coarser ss., no oil-sat.	90	10	<5	trace
8-42	6-27-19-8 W4	968.3	fine ss., oil-sat.	95	5	-	-
2-4	16-9-20-8 W4	905.0	calcite-cemented fine ss.	95	5	-	-
7-34	4-10-20-8 W4	900.1	coarser ss. at top of Glauc. ss.	80	15	5	trace
7-23	4-10-20-8 W4	902.0	fine ss., oil-sat.	95	5	<5	trace
7-24	4-10-20-8 W4	907.1	fine ss., less oil-sat. than above & below	95	5	-	-
7-35	4-10-20-8 W4	910.4	coarse & fine interbedded ss., oil-sat.	90	10	trace	-
7-28	4-10-20-8 W4	922.3	fine ss., oil-sat.	70	25	<5	trace
7-30	4-10-20-8 W4	928.7	coarse ss., below O/W contact	65	25	10	trace
7-32	4-10-20-8 W4	933.0	fine ss., below O/W contact	80	10	5	trace
9-47	12-28-20-8 W4	949.8	fine ss., light oil-stain, dry well	70	20	10	trace
5-179	12-32-20-8 W4	920.8	fine ss., light oil-stained	95	5	-	-
5-180	12-32-20-8 W4	923.8	fine ss., oil-sat.	90	10	trace	-
5-181	12-32-20-8 W4	925.7	bioturbated fine ss., oil-stained	95	5	-	-
5-182	12-32-20-8 W4	929.9	fine ss., oil-sat.	90	10	trace	trace
5-183	12-32-20-8 W4	936.0	fine-medium ss., below O/W contact	85	10	<5	trace
5-184	12-32-20-8 W4	938.5	congl. with sand matrix	80	20	<5	trace
5-185	12-32-20-8 W4	948.4	siltst. to very fine ss.	90	10	trace	-
6-18	14-7-21-8 W4	949.1	argillaceous fine ss.	100	-	-	-
6-19	14-7-21-8 W4	956.5	medium ss., light oil-stain	95	5	-	-
6-20	14-7-21-8 W4	959.5	medium ss., oil-sat.	90	5	<5	trace
6-21	14-7-21-8 W4	961.3	medium ss., below O/W contact	90	10	<5	trace
19-100	10-10-21-8 W4	975.1	fine ss.	100	trace	-	-
19-101	10-10-21-8 W4	981.9	dark grey shale below Glauc. ss.	60	40	-	-
11-49	6-34-19-9 W4	999.1	fine ss., oil-sat.	90	10	trace	trace
12-78	11-17-21-9 W4	931.3	medium ss. above Glauc. ss.	90	10	-	-
12-75	11-17-21-9 W4	952.5	interlam. siltst. & very fine ss.	80	20	-	-
			Samples From SHOP Project Wells Located at 4-10-20-8 W4				
34-156	02	909.1	medium grey shale above Glauc. ss.	80	20	-	-
34-157	02	910.1	rooted, argillaceous ss.	100	trace	-	-
34-158	02	911.6	ss., less argillaceous than sample 157	100	<5	-	-
34-159	02	918.1	fine ss., discontinuous oil-sat.	90	10	trace	-
34-160	02	929.9	fine ss., oil-sat.	80	20	trace	-
34-161	02	940.2	interlam. coarse & fine ss.	90	10	trace	-
34-162	02	944.6	bioturbated fine ss. below O/W contact	95	5	trace	-
34-163	02	948.1	sandy-shale lamination	90	10	trace	-
34-164	02	952.8	very fine ss.	90	10	trace	-
34-165	02	954.6	calcite-cemented very fine ss.	90	10	-	-
34-166	02	955.5	shale lamination within calcite-cemented ss.	45	55	trace	-
33-146	01	910.3	shale above Glauc. ss.	60	40	-	-
36-175	P3	910.4	shale above Glauc. ss.	65	35	-	-

Abbreviations: Kaol, kaolinite; Ill, illite; Sm, smectite; Chl, chlorite; Glauc. ss., Glauconitic sandstone; interlam., interlaminated; O/W contact, oil/water contact; oil-sat., oil-saturated

* For analytical methods see Appendix B

Table 7. X-ray Powder Camera Results for Sample 6-18

Line No.	d-spacing	$I_{est.}$	hkl
1	7.167	9B	K(001)
2	4.479	5	K(020)
3	4.370	7	K(1$\bar{1}$0)
4	4.271	6	Q(100)
5	4.168	6B	K(11$\bar{1}$)
6	3.842	5	*K(02$\bar{1}$)
7	3.735	3	K(021)
8	3.583	8	K(002)
9	3.345	10	Q(101),K(111)
10	3.116	1B	*K(11$\bar{2}$, 1$\bar{1}\bar{2}$)
11	2.750	1	*K(022)
12	2.567	5	K(1$\bar{3}$0, 20$\bar{1}$)
13	2.532	1	K(13$\bar{1}$)
14	2.498	5	K(1$\bar{3}\bar{1}$, 200+)
15	2.458	3	Q(110)
16	2.386	1	K(003)
17	2.341	7B	*K(20$\bar{2}$, 1$\bar{3}$1)
18	2.290	6	*K(131)Q(102)
19	2.242	1	K(13$\bar{2}$)Q(111)
20	2.186	1	*K(201)
21	2.129	3	K(02$\bar{3}$)Q(200)
22	1.988	5B	*K(20$\bar{3}$, 1$\bar{3}$2)
23	1.942	.5	K(132)
24	1.902	.5	K(13$\bar{3}$)
25	1.839	.5	*K(1$\bar{3}\bar{3}$, 202)
26	1.819	5	Q(112)
27	1.792	.5	K(11$\bar{4}$, 2$\bar{2}\bar{3}$)
28	1.787	5B	K(004)
29	1.622	2	K(133, 1$\bar{5}$1)
30	1.590	1	K(13$\bar{4}$)
31	1.544	5	*K(2$\bar{2}\bar{4}$, 1$\bar{3}\bar{4}$)Q(211)
32	1.534	6	*K(203, 31$\bar{3}$)
33	1.454	2B	Q(113)
34	1.382	1	Q(212)
35	1.375	5	Q(203, 301)
36	1.342	1	*K(13$\bar{5}$)
37	1.308	1	*K(1$\bar{3}\bar{5}$)
38	1.287	2B	Q(104)
39	1.260	1B	Q(302)
40	1.238	1B	Q(220)
41	1.200	3	Q(213)
42	1.828	3	Q(114, 310)
43	1.153	.5	Q(311)

* diagnostic d-spacings for kaolinite (Brindley, 1980)

K - kaolinite; Q - quartz

of detrital clay present. Authigenic kaolinite is distinguished by its crystalline habit, the delicate aggregrate morphology which precludes extended transport, and/or because it covers earlier diagenetic phases (Wilson and Pittman, 1977). Large, authigenic, vermicular kaolinite extends across pores to act as bridges (Plate 6-3), and together with quartz overgrowths totally blocks some pores (Plate 6-4). Smaller vermicular and booklet forms of kaolinite commonly sit on larger vermicular forms (Plate 6-3). Masses of small, authigenic kaolinite booklets (Plate 6-5) and silt-sized clusters of authigenic quartz and kaolinite (Plate 6-6) rim, bridge, or fill pores.

Illite

The second most abundant clay mineral is an illitic phase. The proportion of illitic clay minerals in the <2 micrometre size fraction varies from trace amounts in argillaceous sandstone (facies 3), to 10-20 per cent in cleaner sandstones (facies 4, 5 and 6), and 20-55 per cent in shales (Tables 5 and 6).

The behaviour of the 10A reflection, I(001), on XRD patterns, particularly in shale samples, suggests the presence of discrete illite which is partially depotassified and chloritized. Figure 20 shows the XRD patterns for a shale sample containing about 30 per cent illite, and is representative of most shale samples analyzed. The 10A reflection is sharp (Ca-disc, 54% humidity) but is asymmetrical towards its low angle side (Fig. 20A). The asymmetry extends from 10A to 15-16A. Upon saturation with ethylene glycol, the apex of the 10A reflection remains sharp and unmoved but the asymmetrical portion expands towards higher d-spacings and a broad reflection occurs at about 13-14A. The asymmetry and swelling properties may result from edge weathering of illite (Fanning and Keramedas, 1977). Edge weathering produces a 10A peak (unaltered core) and a series of less intense irregular spacings at higher d-spacings. The process of edge weathering involves the simultaneous opening of many clay interlayers along edges and fractures of the mica particle. Potassium is released from these sites and replaced by hydrated, exchangeable cations. Depotassified illite has a larger layer thickness at the opened edges than in the unaltered core (Fanning and Keramedas, 1977)

The presence of chloritic material within the illitic phase is indicated by the low angle asymmetry which remains on the 10A peak after K-saturation (Fig. 20). Upon

heating to 550°C, the reflection at 5–10 degrees two theta, caused by uncollapsed layers, is enhanced. Grim and Johns (1954) described interlayer, chloritic material as 'islands' of brucite occurring with sufficient frequency to keep the layers apart on heating, but too few in number to prevent expansion with glycol.

Sandstone samples contain significantly less illite than the shale samples, and variations in the character of the 10A reflection upon the different treatments are less pronounced (Fig. 19). Some expansion occurs upon glycolation, asymmetry develops on the low angle side of the 10A peak following K–saturation (0% humidity), and a very broad peak in the 13–14A range develops upon heating to 550°C. These characteristics suggest that the illite in the sandstones is depotassified and chloritized.

The morphology of most illite in the Glauconitic Sandstone is not that of typical authigenic illite (i.e., short or long lath–like projections; Wilson and Pittman, 1977). Rather, illite most commonly appears as ridges on detrital grains (Plate 7–1). The internal structure of these ridges is too fine to be resolved even under highest magnification with our SEM. Only because potassium is detected by the energy dispersive unit (EDA) attached to the SEM are these ridges presumed to contain illite. The ridges may be composed of: (1) very fine detrital kaolinite and illite; (2) illite or mixed layer illite–smectite; or (3) an illite–Fe–chlorite intergrade. EDA detects Fe as well as K in some sheet–like clusters or ridges of fine clay. Iron may occur as $Fe(OH)_3$ in positively charged hydroxy–Al interlayers (Barnhisel, 1977). Thus its presence in these sheets is compatible with the an illite–Fe–chlorite intergrade.

Rarely, very fine clay forms delicate coatings on kaolinite booklets or bridges between larger clays (Plate 7–2) in argillaceous sandstones of facies 3. As no smectite is present in these samples, it is likely that this clay coating is illite or a mixed–layer clay. The clay is probably diagenetic and formed after the kaolinite booklets.

No conclusive evidence exists for a detrital versus authigenic origin for the majority of the illite but a detrital origin is favoured for several reasons: (1) The depotassified, chloritized nature of the illite suggests that it was formed under the following conditions: moderately active weathering to furnish Al ions; moderately acid pH; low organic matter; and frequent wetting and drying of the material (Rich, 1968). (2) The detrital illite in the shale samples is similar to the illite from the sandstones and (3) Illite

generally does not have a distinct authigenic morphology.

Interstratified Clay Minerals

Some clay samples have a XRD reflection which forms a broad peak at about 12A (Ca–disc, 54% humidity) (Figs. 21 & 22) in addition to the asymmetrical 10A reflection described earlier. Upon glycolation the broad 12A reflection loses intensity and shifts to about 14A. Much material does not collapse completely to 10A when K–saturated (0% humidity). This behaviour results in a 10A peak which has a greater intensity but is still broadly asymmetrical on the low angle side. The behaviour of the XRD reflections after the other treatments is similar to that of the chloritized hydrous illites. These clays may be randomly interstratified illite–smectite. They also are more chloritized than the illites previously described.

Interstratified clay minerals are present in shales and silty shales within the lowermost Glauconitic Sandstone (facies 6) and fine–grained, bioturbated, and/or carbonate–cemented sandstones (facies 3 and 6). It seems unlikely that the mixed–layer clay formed diagenetically for two reasons: (1) Interstratified clay minerals are present in both shale and bioturbated sandstone; and (2) The distribution of sandstones containing interstratified clay minerals is no different from those with only kaolinite and illite. More probably, the interstratified clay minerals are detrital and represent advanced weathering in the source area.

The " illites " and interlayered clays described above have characteristics of phases which have been called " glauconites " in the literature. Brindley (1980) describes glauconite as a mineral with Fe^{3+}–rich, mica–like, non–expanding layers, with fewer than normal interlayer K^{+} ions, interstratified with varying proportions of expanding montmorillonite–like layers. Thompson and Hower (1975) state that the " the occurrence of interlayer hydroxy–metal complexes seems to be far less common in aluminous illite–smectite then in glauconite " and describe glauconite as an iron–rich illite–smectite. However, the AIPEA nomenclature committee (1980) definition of glauconite indicates that glauconite is a single phase, ideally non–interstratified mineral. As the clays from the Glauconitic Sandstone have only been studied by XRD, SEM and EDA , it can be suggested that they are interlayered illite–smectites which contain iron, but nothing is

known about the abundance of potassium, or the position or abundance of the iron. Thus it would be incorrect to call these clays glauconite. Moreover, the popular useage of the term glauconite is for a small greenish pellet. Such pellets are rarely found in the Glauconitic Sandstone within the study area.

Smectite

Some samples contain up to about 10 per cent smectite in the <2 micrometre size fraction (Table 6). The smectite is usually represented on XRD charts by a broad 15A reflection which expands to 17A upon saturation with ethylene glycol (Fig. 24). For a few samples these peaks are relatively sharp (Fig. 23); for most specimens they occur as rounded, asymmetrical humps. The smectite may be partially chloritized in a manner similar to that described for illite.

Very rarely, smectite occurs in a honeycomb-like growth habit in the Glauconitic Sandstone (Plate 7-3). This is one of the few occurrences of the typical morphology for authigenic smectite (Wilson and Pittman, 1977). More normally, in samples which contain more than trace amounts of smectite according to XRD analyses, there is a distinctive abundance of clay ridges on grains (Plate 7-4), but no honeycomb-like or crenulated clay structures.

Several factors suggest that smectite is mainly a late diagenetic phase even though its morphology is seldom typical of authigenic clays: (1) Smectite is absent in associated shales; (2) In most cases, smectite is present only in the most porous sandstones; and (3) Smectite is most abundant below the oil/water interface where nondescript clay coatings occur on large vermicular kaolinite. The absence of smectite in associated shales and its presence only in the nonargillaceous porous sandstones suggest that it is not generally a detrital component (Shelton, 1964). The greater abundance of smectite below the oil/water interface suggests that smectite is a late diagenetic phase which continued to form in the water zone after petroleum emplacement.

Chlorite

Discrete chlorite occurs in trace amounts, most commonly in samples that also contain smectite (Figs. 23–24). For these samples, the chlorite (001) basal reflection is generally masked by the reflections of other phases after all treatments except upon heating to 550°C. After heating, the chlorite (001) peak is enhanced and shows as a low intensity broad peak at 13 or 14A (Figs. 23B & 24B).

Chlorite occurs in insufficient amounts to determine its morphology. No morphologies typical of authigenic chlorite (i.e. Wilson & Pittman, 1977) are present in detectable amounts in thin section or under the SEM. The association of chlorite with smectite suggests that chlorite is authigenic.

Other Clay-size Minerals

All samples contain quartz in the <2 micrometre size fraction. Clay–size feldspar occurs in trace amounts (Figs.18–24). Calcite is detected in the clay–size fraction of sandstone samples which are carbonate–cemented.

Assemblages of Clay Minerals

The analyzed sandstone and shale samples from both the regional setting and well O2 in the SHOP project can be classified into four types according to their clay mineral assemblages.

1. Type I: 100% kaolinite
2. Type II: Almost 100% kaolinite; trace illite [8]
3. Type III: Kaolinite, illite [8] ± randomly interstratified illite–smectite
4. Type IV: Kaolinite, illite[8], discrete smectite, usually discrete chlorite

. Examples of XRD patterns for each type are given in figures 18 to 24.

---

[8]All illites are depotassified and chloritized

Distribution of Clay Mineral Assemblages

Type 1 samples (Fig. 18) are from the argillaceous, rooted sandstone (subfacies 3a) at the top of the Glauconitic Sandstone immediately below a coal or very carbonaceous horizon. The detrital clay within the sandstone was probably leached shortly after deposition, resulting in the degradation of illite to kaolinite. Conditions for degradation of illlite to kaolinite are; pH of 4–5, reduced K, Mg, and Fe concentration, fluctuating wet and dry conditions, and the presence of organic substances provided by plants (Dixon, 1977). These conditions probably occurred in subfacies 3a sandstones as a result of the progradation of marsh deposits (facies 2).

Type II samples (Fig. 19) represent sandstones of facies 3, located stratigraphically below those of type I. The appearance of illite may be the result of less effective leaching than in type I, or a variation in the composition of the detrital clay at time of deposition. The total clay content is significantly lower than in type I samples.

Type III samples (Figs. 20, 21 & 22) include shales with 20–45% illite (Fig. 20), shales with 55% illite (Fig. 22), and sandstone with <10% illite (Fig. 21). The shales occur immediately above and below the Glauconitic Sandstone. Sandstones in this group include a very fine grained sandstone of facies 6, and a bioturbated sandstone (9% total clay) of facies 3. Both these sandstones probably have a significant detrital clay component.

The type IV group of samples (Figs. 23 & 24) encompasses the clean oil–saturated and water–saturated sandstones of facies 4, 5 and 6 which have only 1 to 2 per cent total clay. Any samples with more than a few percent clay content do not contain smectite. This implies that the origin of clay in the cleanest sandstones is different from that in the more argillaceous sandstones. Either the detrital source varies or clays in the cleanest sandstones are largely authigenic in origin. Based on the well–crystallized morphologies of kaolinite, the latter seems most probable.

In contrast to samples from the main western sandstone belt described above, smectite in samples from the eastern sandstone belt (Twp. 19–20, Rge. 7), occurs both in shales and argillaceous sandstones (Table 6). A bentonitic shale immediately above the sandstone (at 6–15–20–7 W4) consists of >95 per cent smectite and <5 per cent kaolinite. In a well at 10–33–19–7 W4, a clay–rich sample in facies 3 contains 5 per cent smectite, whereas a cleaner, oil–saturated sandstone from facies 4 contains only

trace amounts of smectite. Therefore, smectite in samples from this eastern sandstone belt is probably detrital in origin. The bentonitic shale probably represents deposition of a volcanic ash. Its deposition may have occurred sometime after that of the shales within, and immediately above, the Glauconitic Sandstone of the western belt.

Figure 18 A and B.
Typical X-ray diffractograms of the <2 micrometre fraction for type 1 samples. Type 1 samples represent the most argillaceous sandstone at the top of the Glauconitic Sandstone (uppermost facies 3). This sample contains almost 100 per cent kaolinite (K), a minor amount of quartz (Q), and trace amounts of feldspar (F). Basal reflections for the clay minerals are indicated in brackets after the symbol for the clay. The 7A, K(001), peak of kaolinite is sharp and intense. The clay symbols with no adjacent bracket indicate nonbasal reflections.

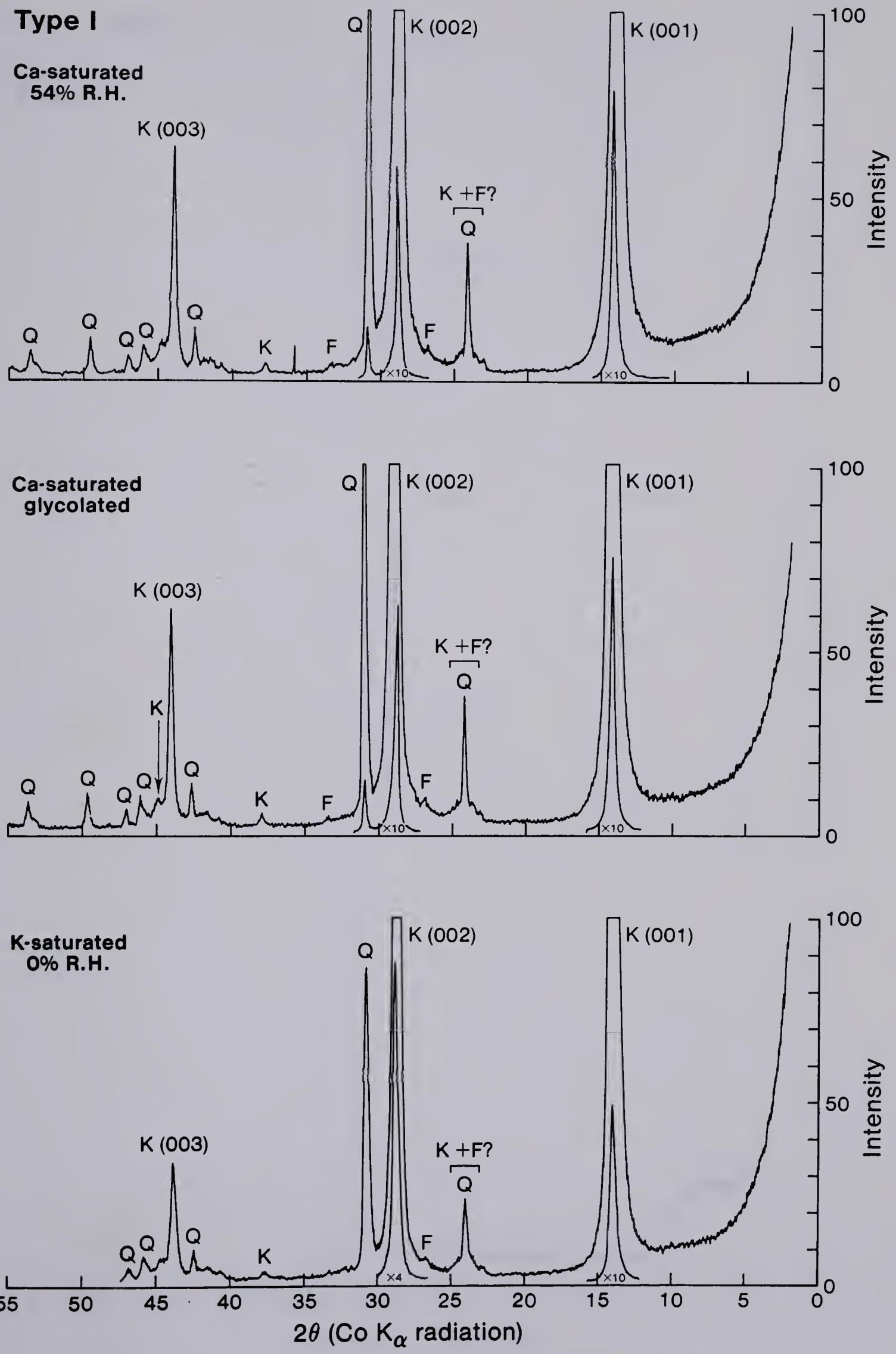
Type I
Ca-saturated
54% R.H.
K (003)
Q
K (002)
K (001)
K +F?
Q
Q
Q
Q
Q
Q
K
F
F
×10
×10
100
50
0
Intensity
Ca-saturated
glycolated
K (003)
Q
K (002)
K (001)
K +F?
Q
K
Q
Q
Q
Q
Q
K
F
F
×10
×10
100
50
0
Intensity
K-saturated
0% R.H.
K (003)
Q
K (002)
K (001)
K +F?
Q
Q
Q
Q
Q
K
F
×4
×10
100
50
0
Intensity
55
50
45
40
35
30
25
20
15
10
5
0
2θ (Co Kα radiation)

Type I cont.

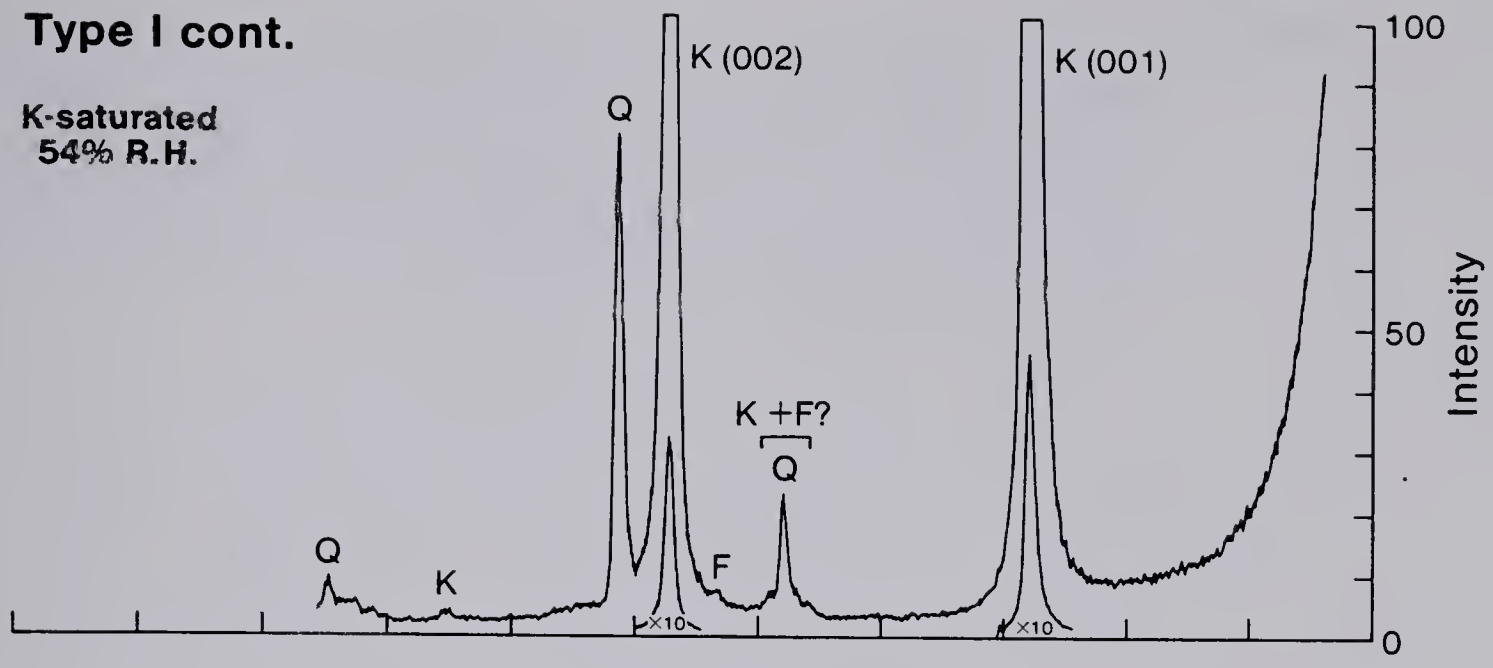
K-saturated
54% R.H.
Q
K (002)
K (001)
K
F
K +F?
Q
×10
×10
100
50
0
Intensity

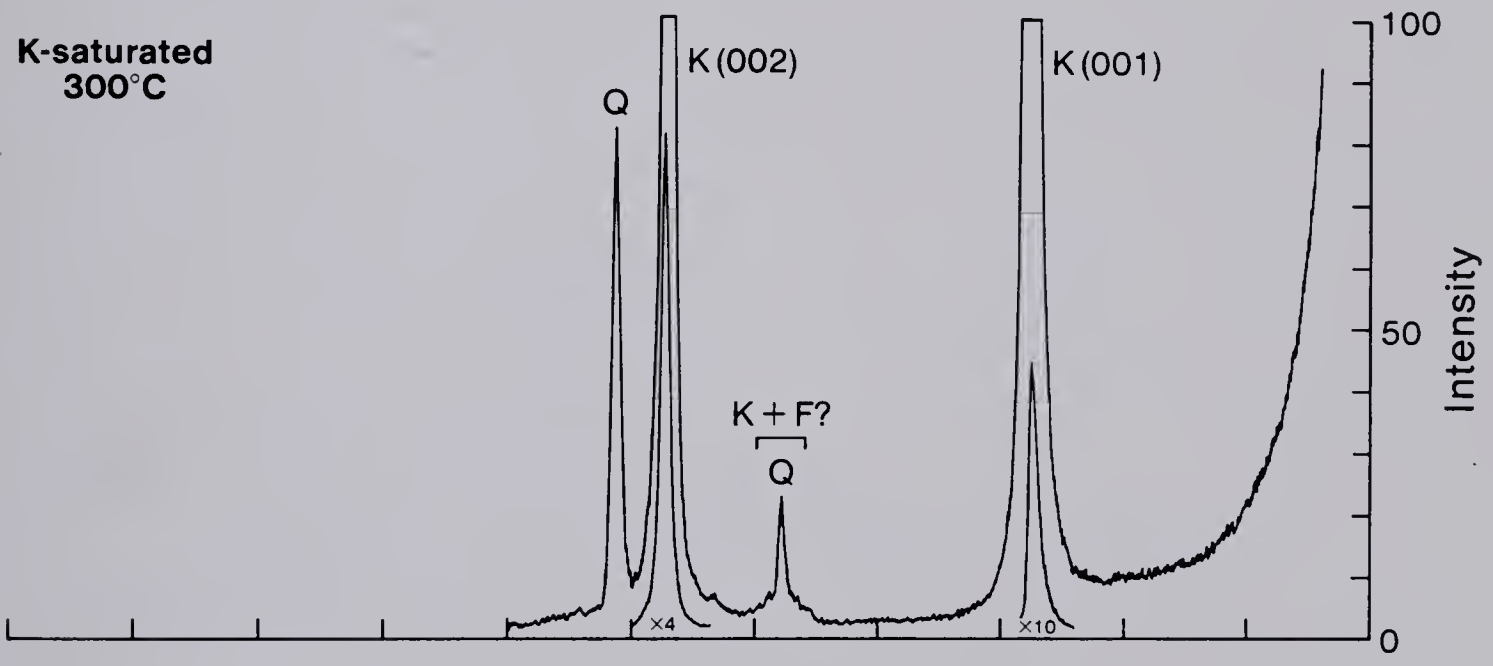
K-saturated
300°C
Q
K (002)
K (001)
K + F?
Q
×4
×10
100
50
0
Intensity

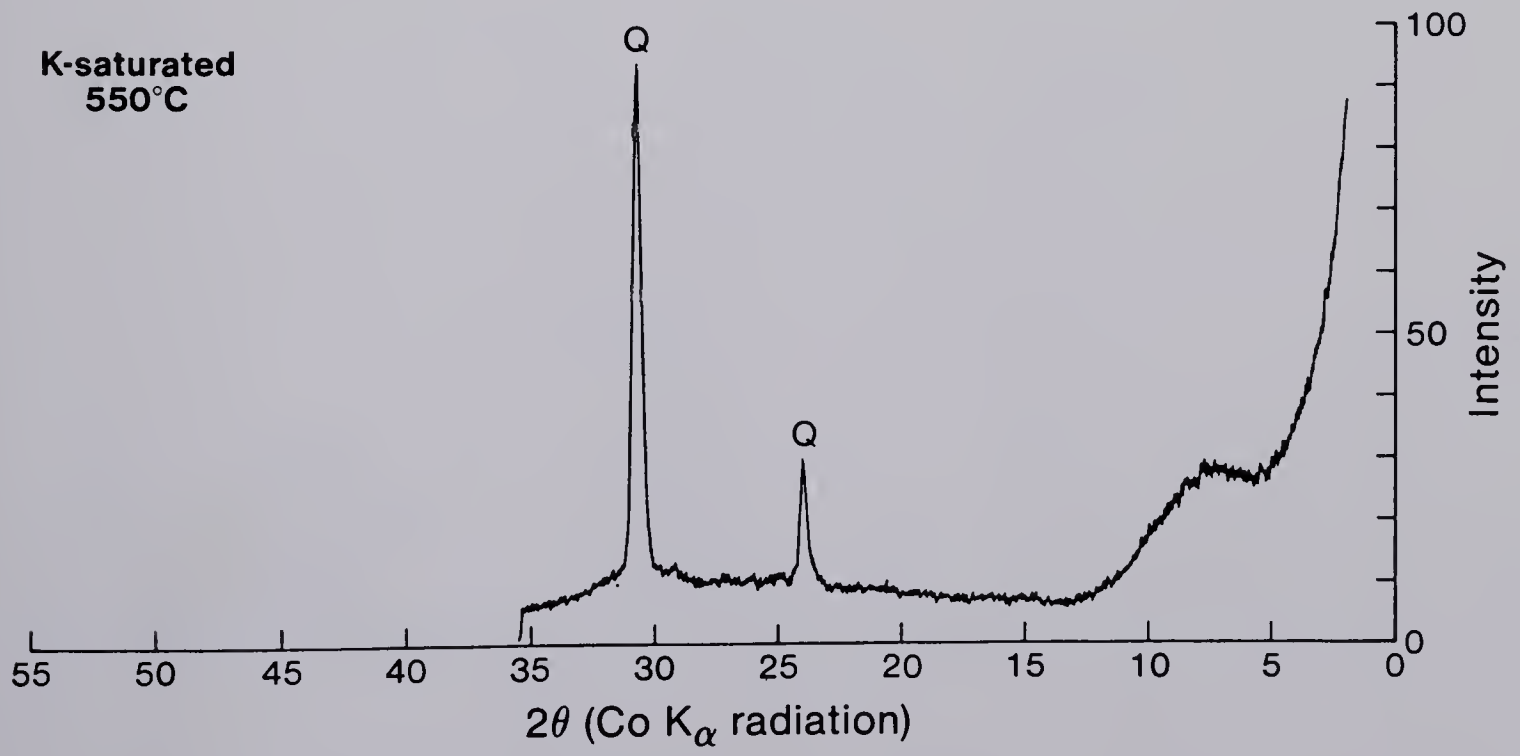
K-saturated
550°C
Q
Q
100
50
0
Intensity
55
50
45
40
35
30
25
20
15
10
5
0
2θ (Co Kα radiation)

Figure 19 A and B.
Typical X-ray diffractograms of the <2 micrometre fraction for type II samples. Type II samples represent sandstones of facies 3, located stratigraphically below those of type 1. The total clay content in the sandstone is significantly lower than in type 1 samples. Illitic clay minerals (I) are present in trace amounts. The low angle asymmetry which remains on the 10A peak, I(001), after K-saturation (Fig. 19A) indicates the presence of chloritic material within the illitic phase.

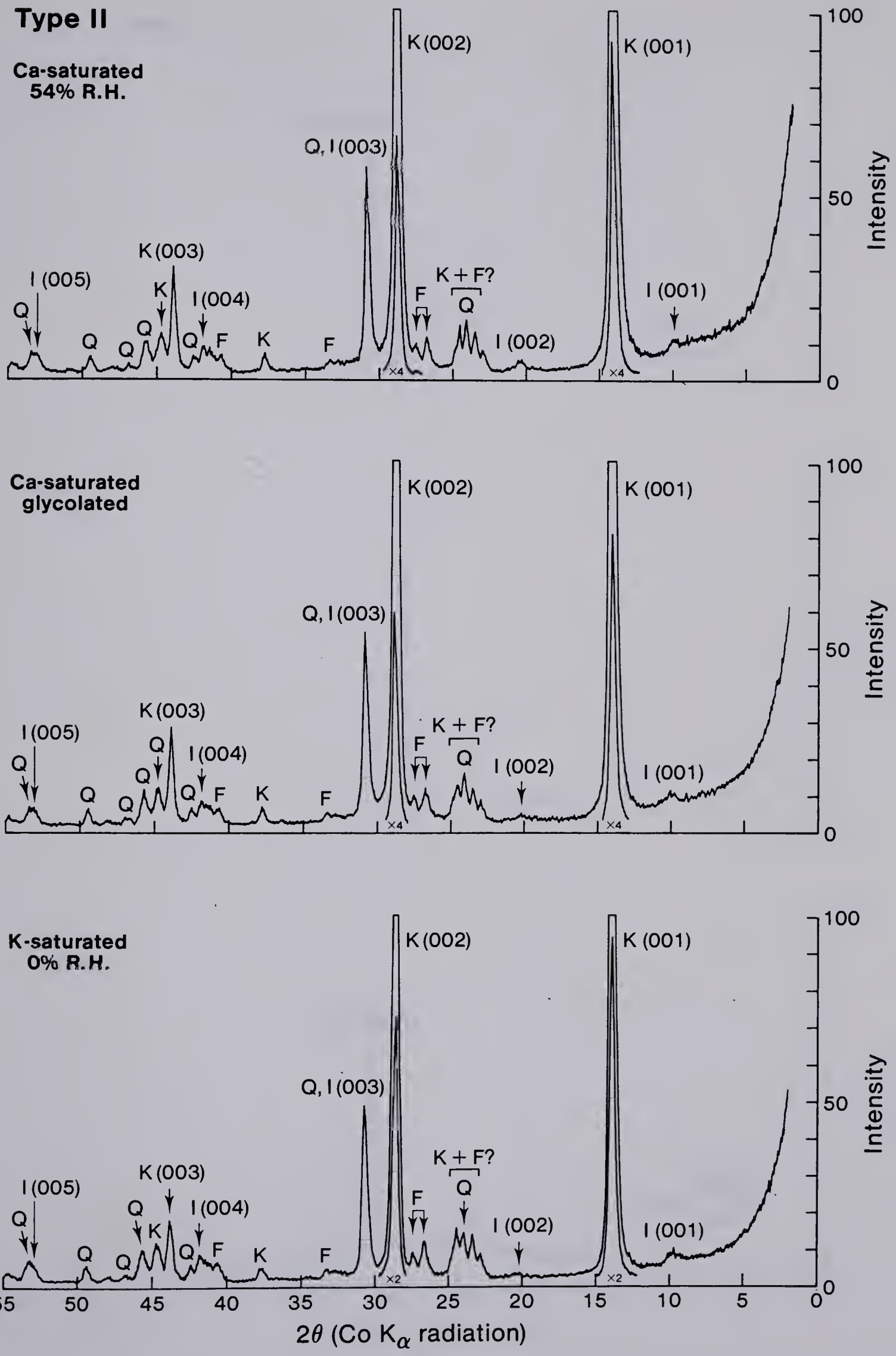
Type II
Ca-saturated
54% R.H.
K(002)
K (001)
Q, I (003)
K(003)
I (005)
K
I (004)
K + F?
F
Q
I (001)
Q
Q
Q
Q
F
K
F
I (002)
×4
×4
100
50
0
Intensity
Ca-saturated
glycolated
K(002)
K (001)
Q, I (003)
K(003)
I (005)
Q
I (004)
K + F?
F
Q
I (002)
I (001)
Q
Q
Q
Q
F
K
F
×4
×4
100
50
0
Intensity
K-saturated
0% R.H.
K(002)
K (001)
Q, I (003)
K(003)
I (005)
Q
K
I (004)
K + F?
F
Q
I (002)
I (001)
Q
Q
Q
F
K
F
×2
×2
100
50
0
Intensity
55
50
45
40
35
30
25
20
15
10
5
0
2θ (Co Kα radiation)

Type II cont.

K-saturated
54% R.H.

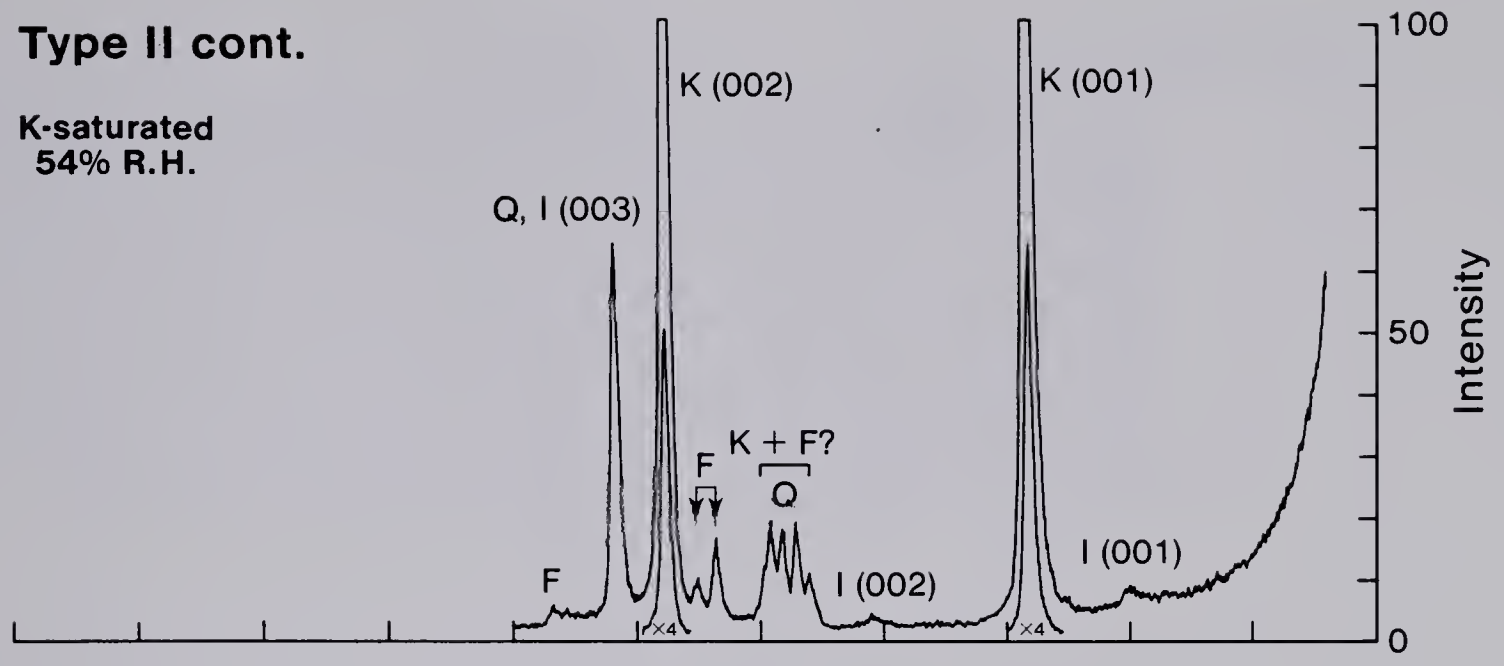

K-saturated
300°C

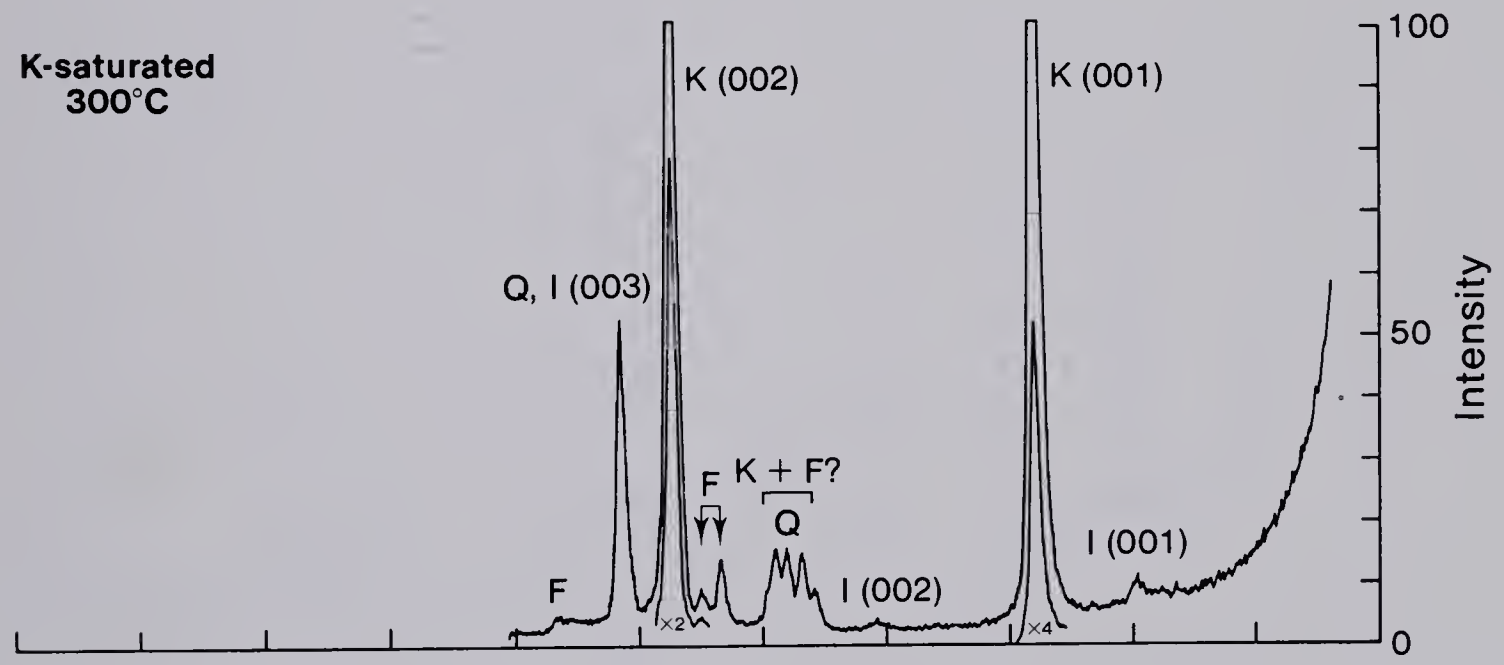

K-saturated
550°C

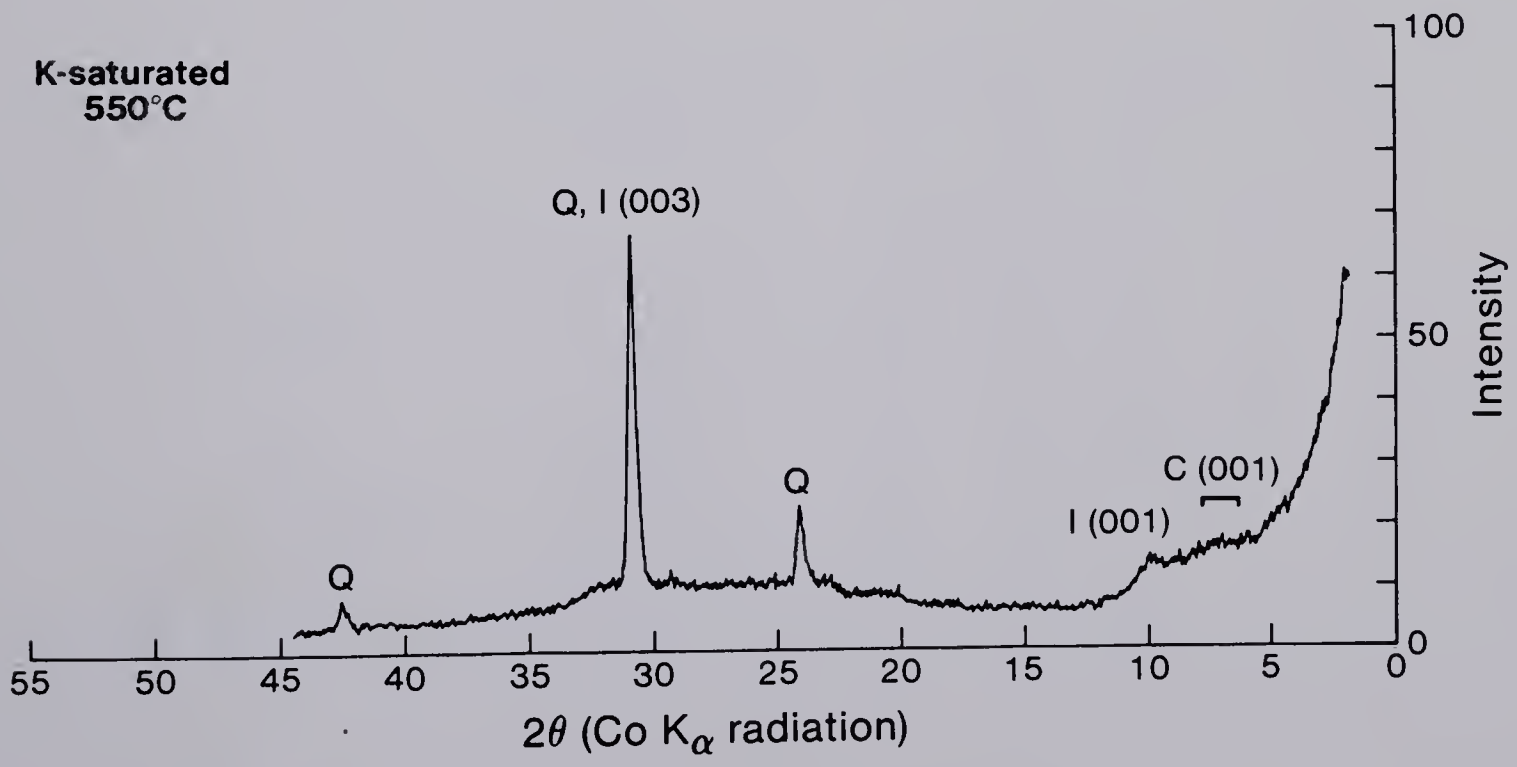

Figure 20 A and B.

X-ray diffractograms representative of shale samples from immediately above and below the Glauconitic Sandstone, type III clay assemblage. This sample contains about 30% illite (I). The 10A (I(001)) reflection is sharp (Ca-disc, 54% humidity) but is asymmetrical toward its low angle side. The asymmetry extends from 10A to 15-16A. Upon saturation with ethylene glycol, the 10A reflection remains sharp but the asymmetrical portion expands towards higher d-spacings and a broad peak is produced at 13-14A. The asymmetry and swelling properties may result from edge weathering of illite. The presence of chloritic material within the illitic phase is indicated by the low angle asymmetry which remains on the 10A peak after K-saturation (Fig. 20A, lower portion). Upon heating to 550°C, (Fig. 20B, lower pattern) the reflection (5-10° 2θ) caused by uncollapsed layers is enhanced.

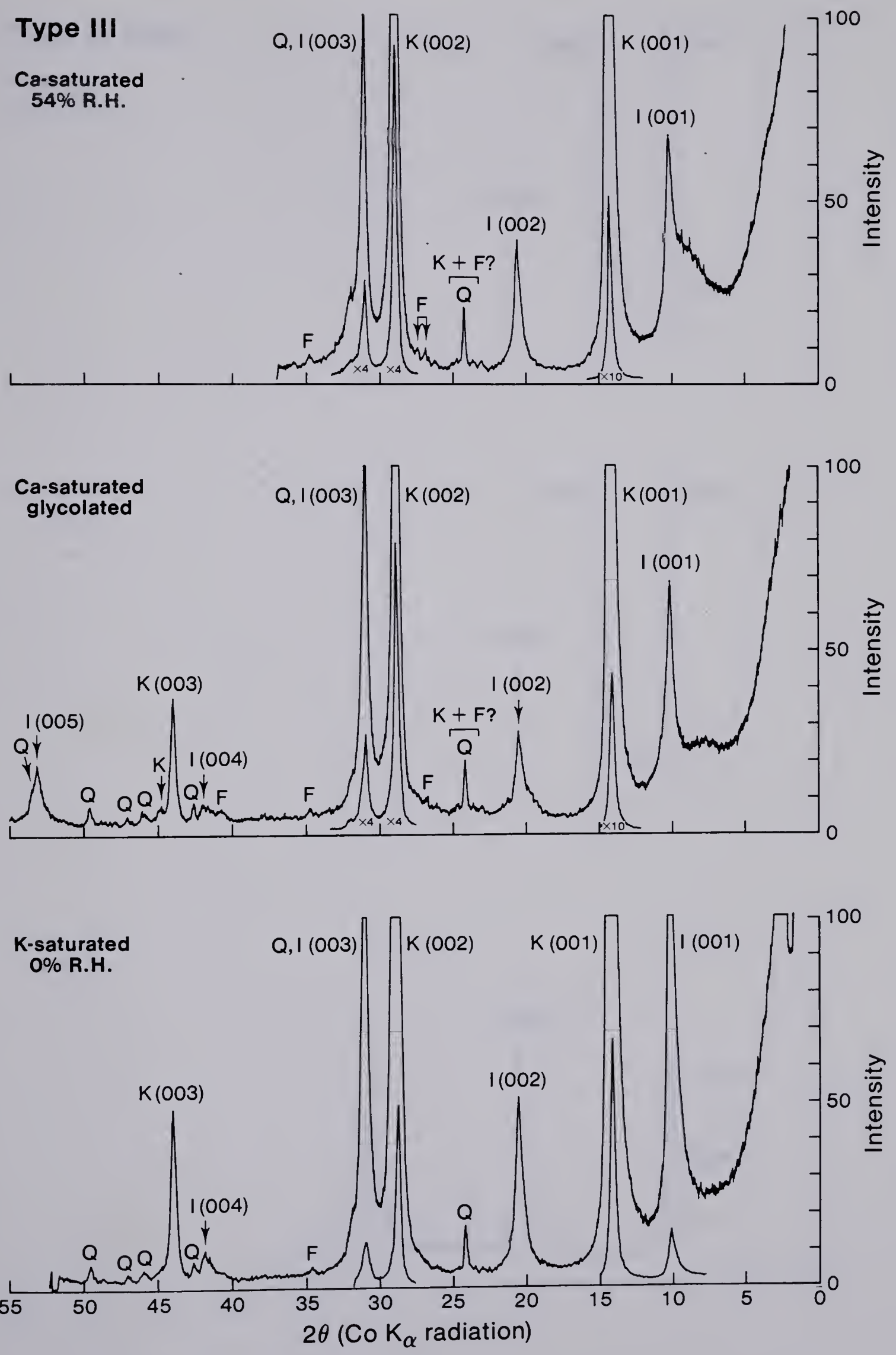
Type III
Ca-saturated
54% R.H.
Q, I (003)
K (002)
K (001)
I (001)
I (002)
K + F?
Q
F
F
×4
×4
×10
100
50
0
Intensity
Ca-saturated
glycolated
Q, I (003)
K (002)
K (001)
I (001)
K (003)
I (005)
Q
K
I (004)
Q
F
F
I (002)
K + F?
Q
F
×4
×4
×10
100
50
0
Intensity
K-saturated
0% R.H.
Q, I (003)
K (002)
K (001)
I (001)
K (003)
I (004)
Q
F
I (002)
Q
100
50
0
Intensity
55
50
45
40
35
30
25
20
15
10
5
0
2θ (Co Kα radiation)

Type III cont.

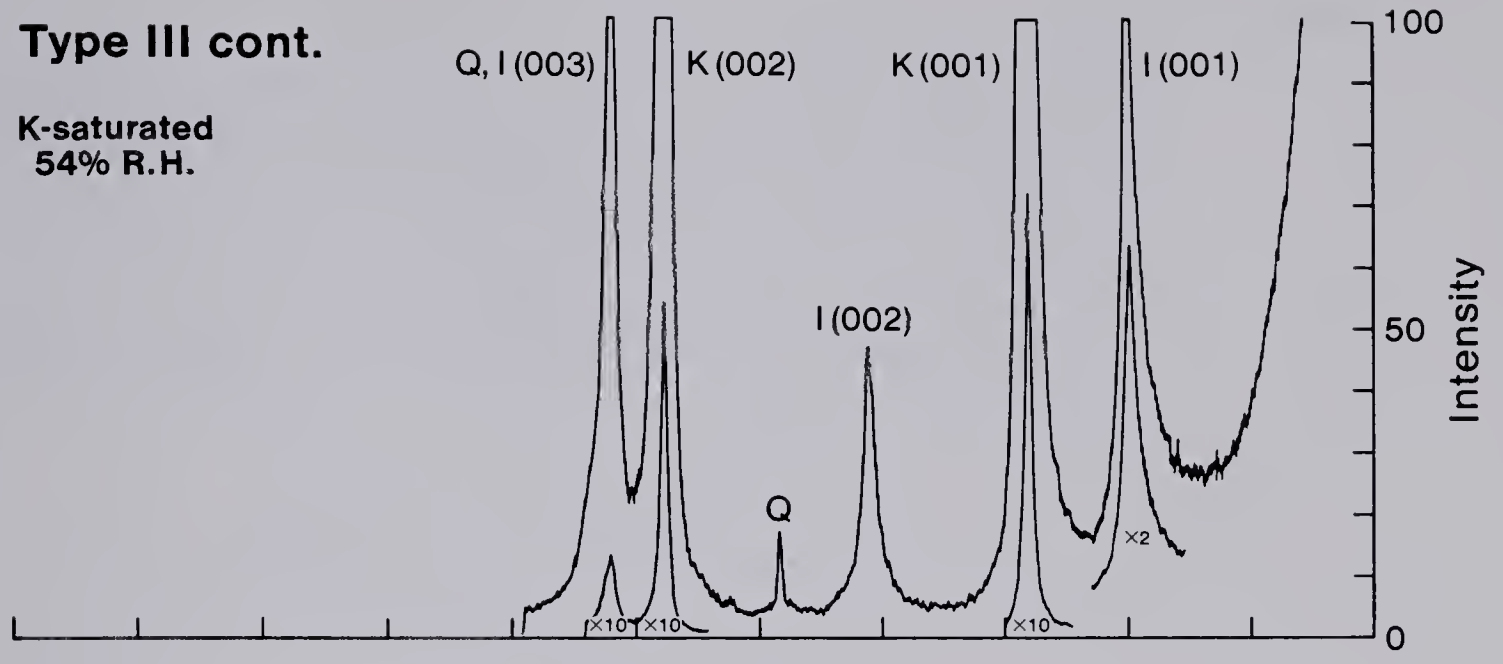

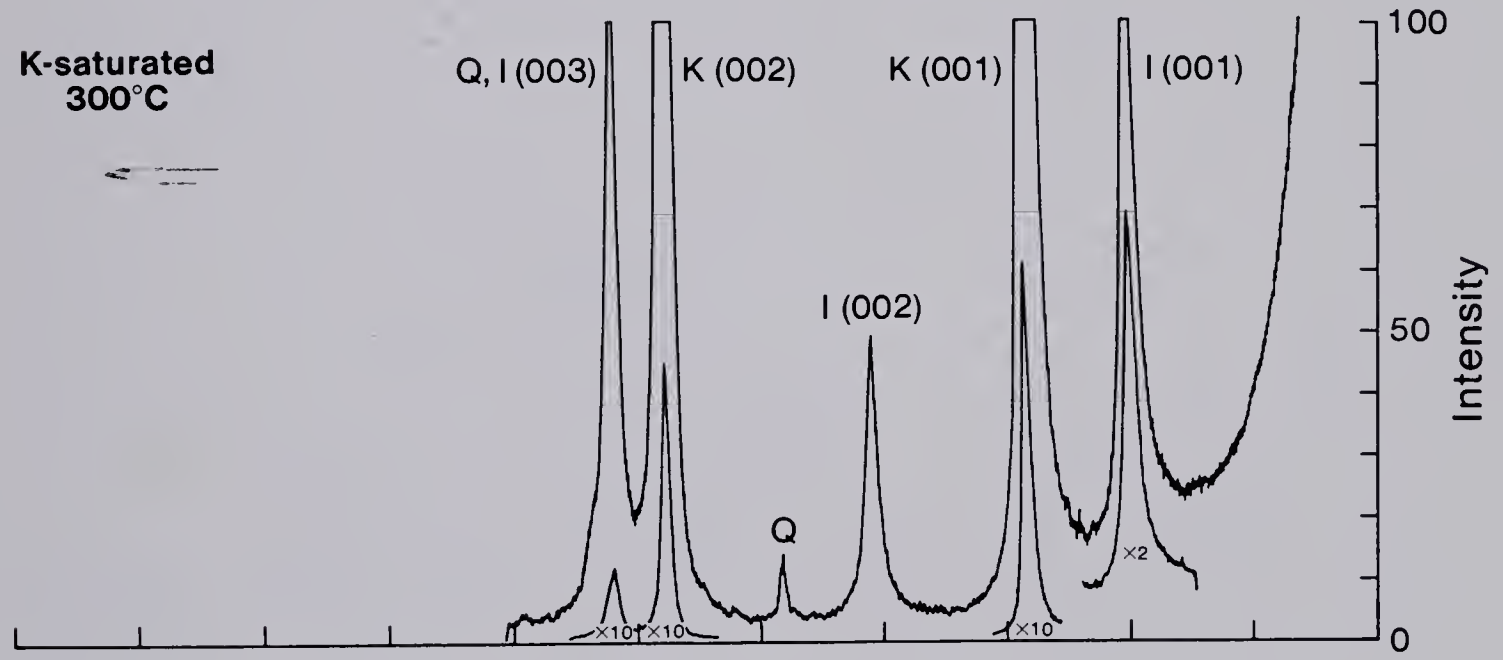

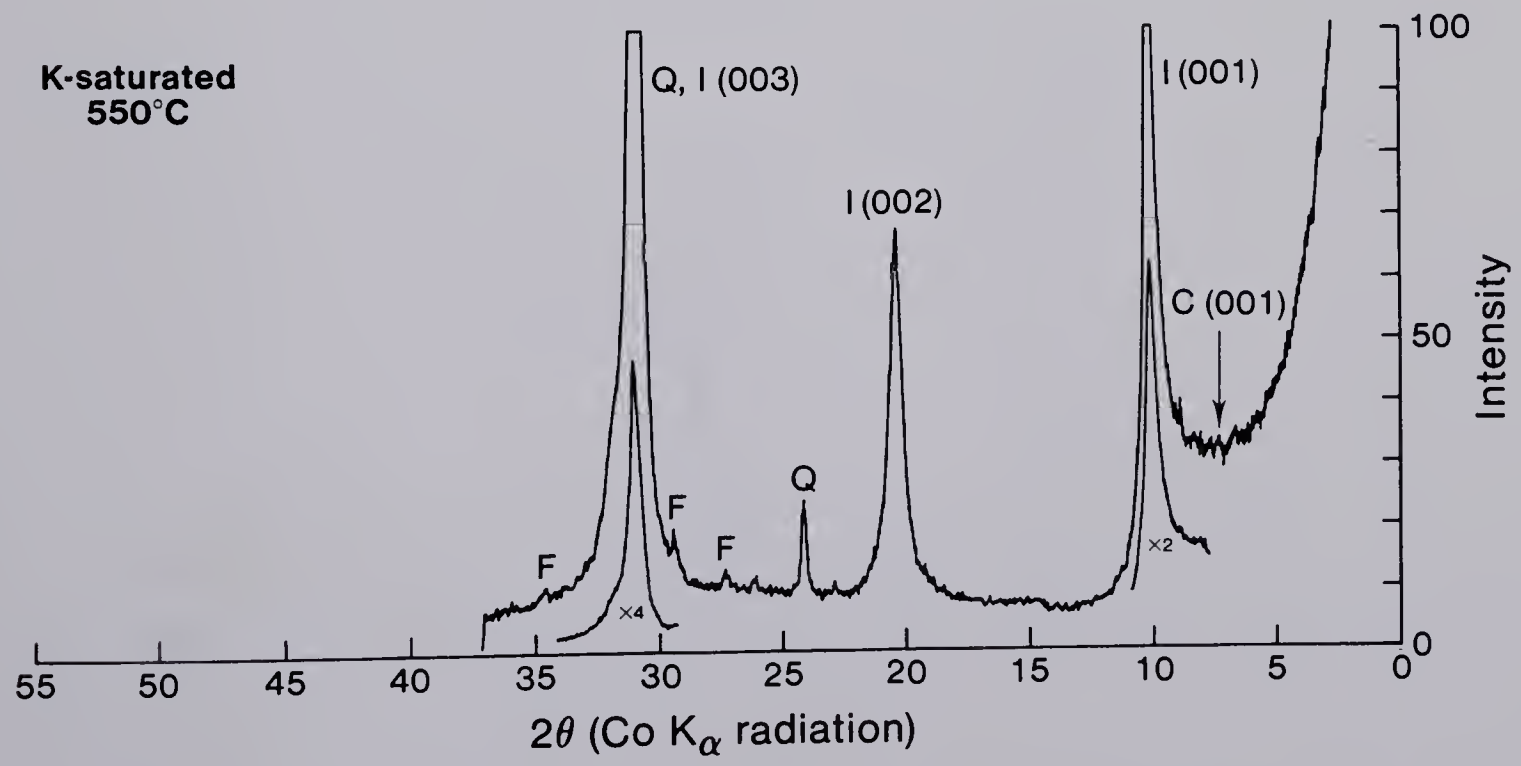

Figure 21 A and B.
X-ray diffractograms representative of a very fine grained sandstone in facies 6, and a bioturbated sandstone of facies 3, type III clay assemblage. Both these sandstones probably have a significant detrital clay component. Note the broad peak at about 12A (labelled I-S) on the Ca-saturated 54% R.H. pattern (Fig. 21A). Upon glycolation, the broad 12A reflection loses intensity and shifts to about 14A. Much material does not collapse completely to 10A when K-saturated (0% humidity). This behaviour results in a 10A peak which has greater intensity but is still broadly asymmetrical on the low angle side. This clay is probably a randomly interstratified illite-smectite. The behaviour of the low angle reflections upon heating (Fig. 21B) suggests that the clay is also chloritized.

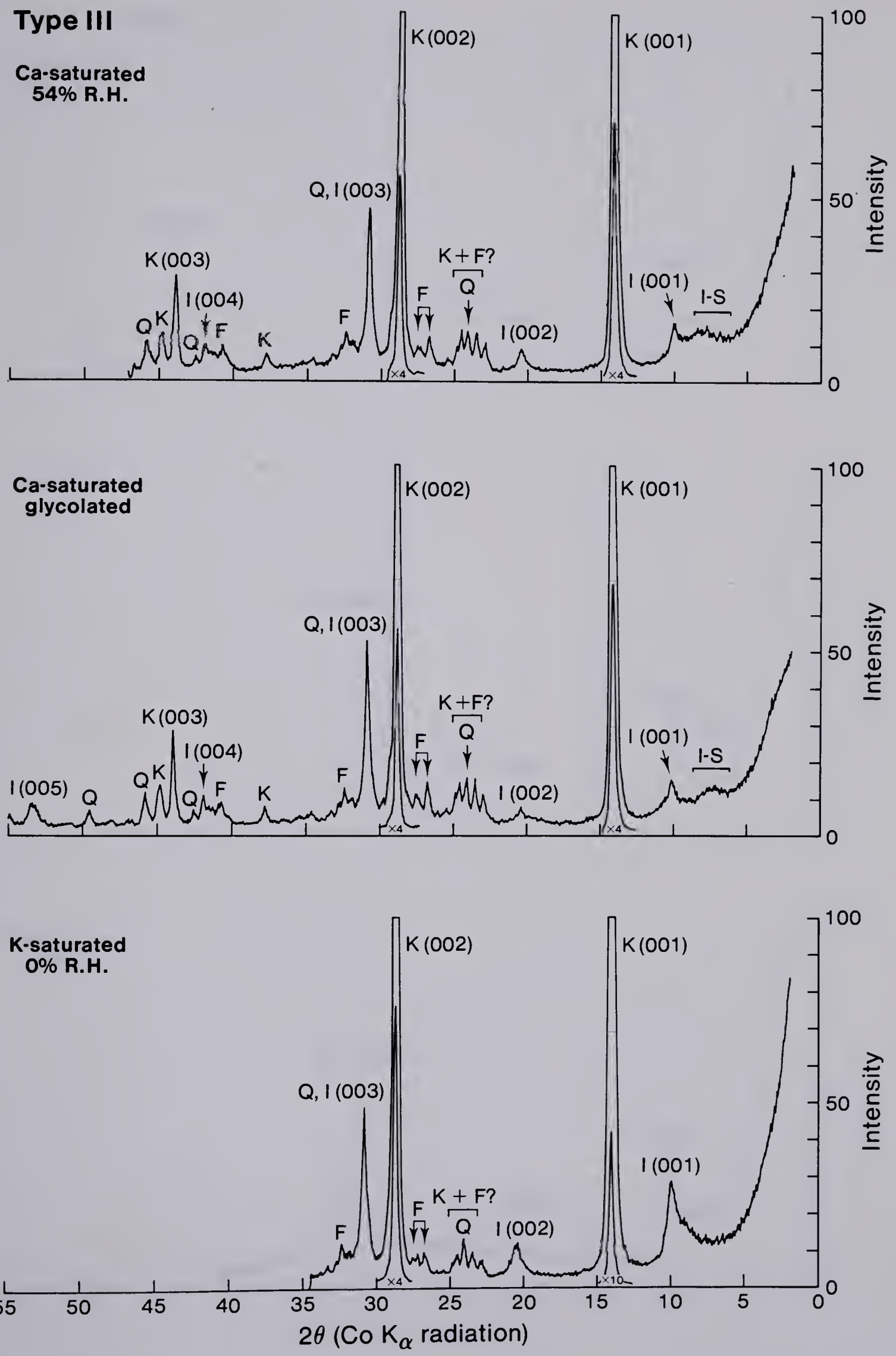
Type III
Ca-saturated
54% R.H.
K(002)
K (001)
Q, I (003)
K(003)
K + F?
I (001)
I-S
I(004)
I (002)
Q
K
F
×4
100
50
0
Intensity
Ca-saturated
glycolated
I(005)
K-saturated
0% R.H.
55
50
45
40
35
30
25
20
15
10
5
0
2θ (Co Kα radiation)

Type III cont.

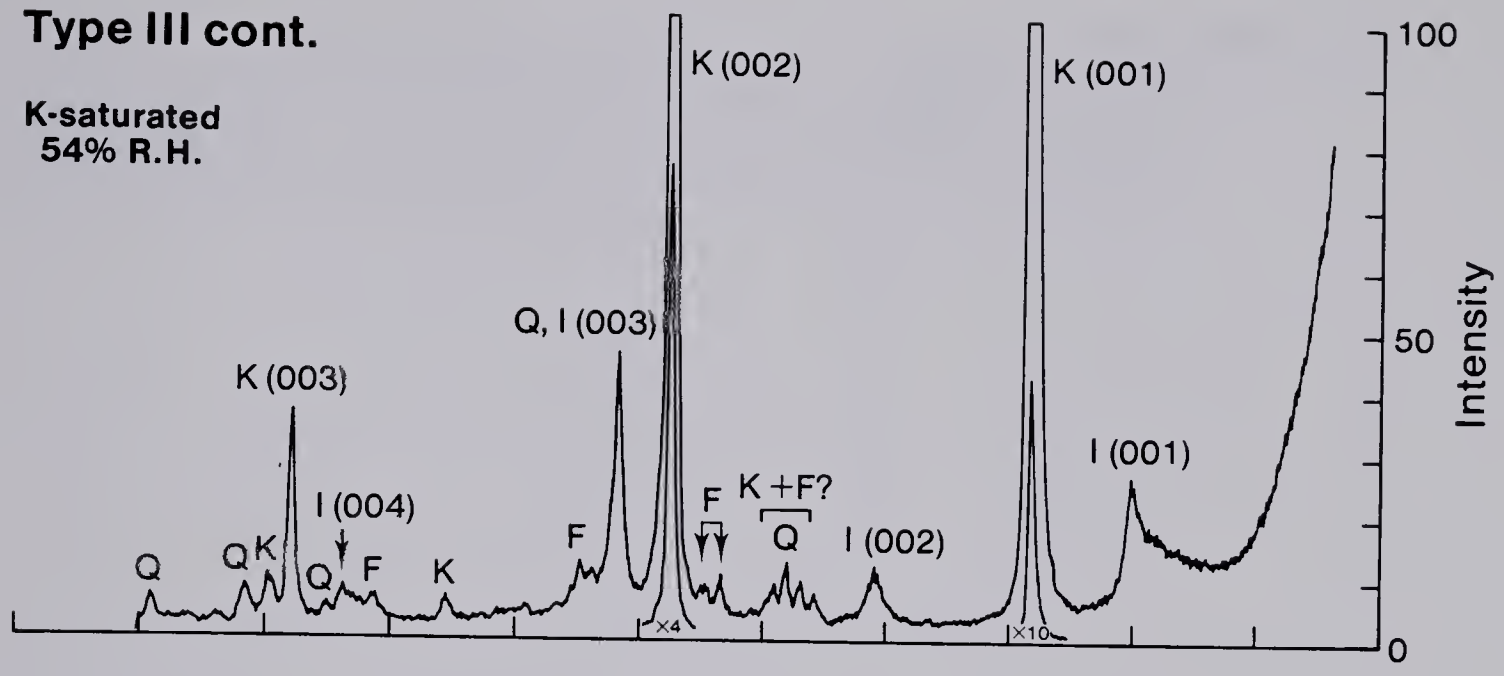

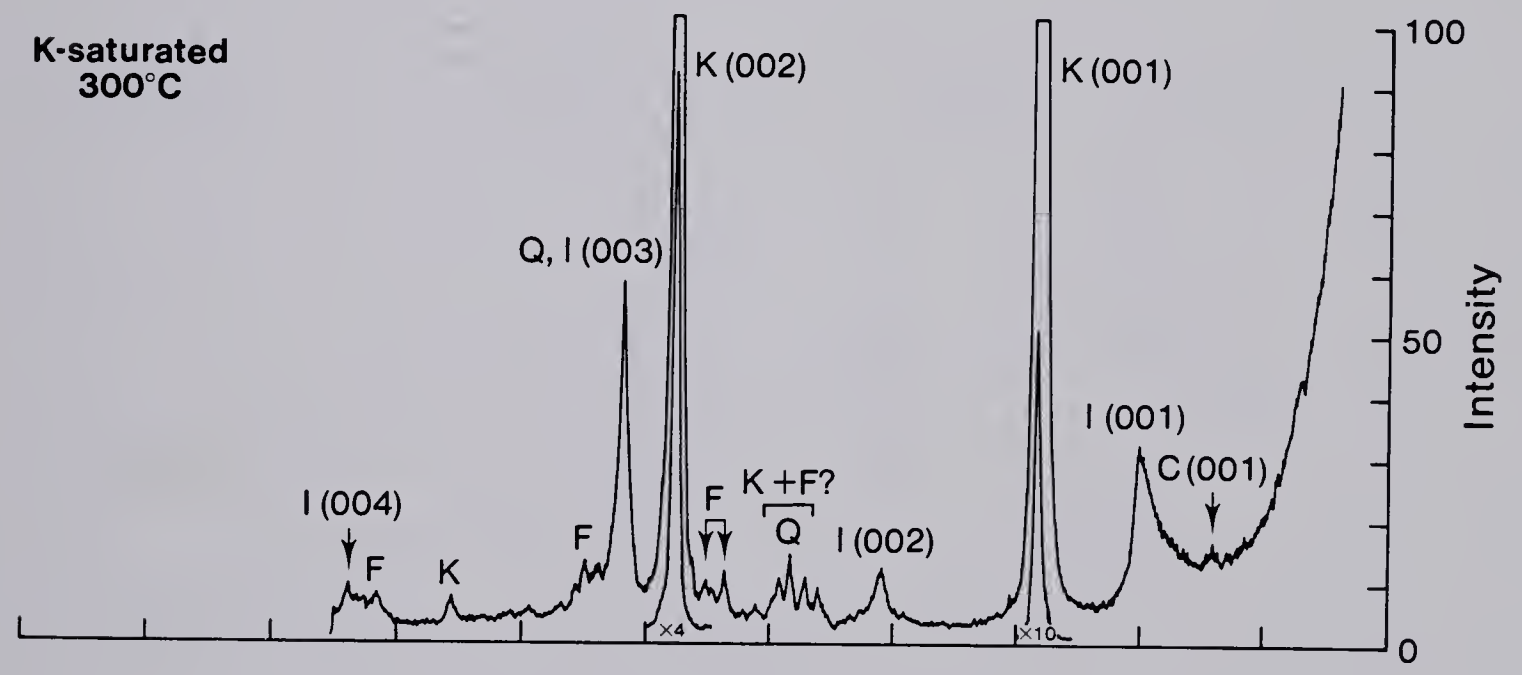

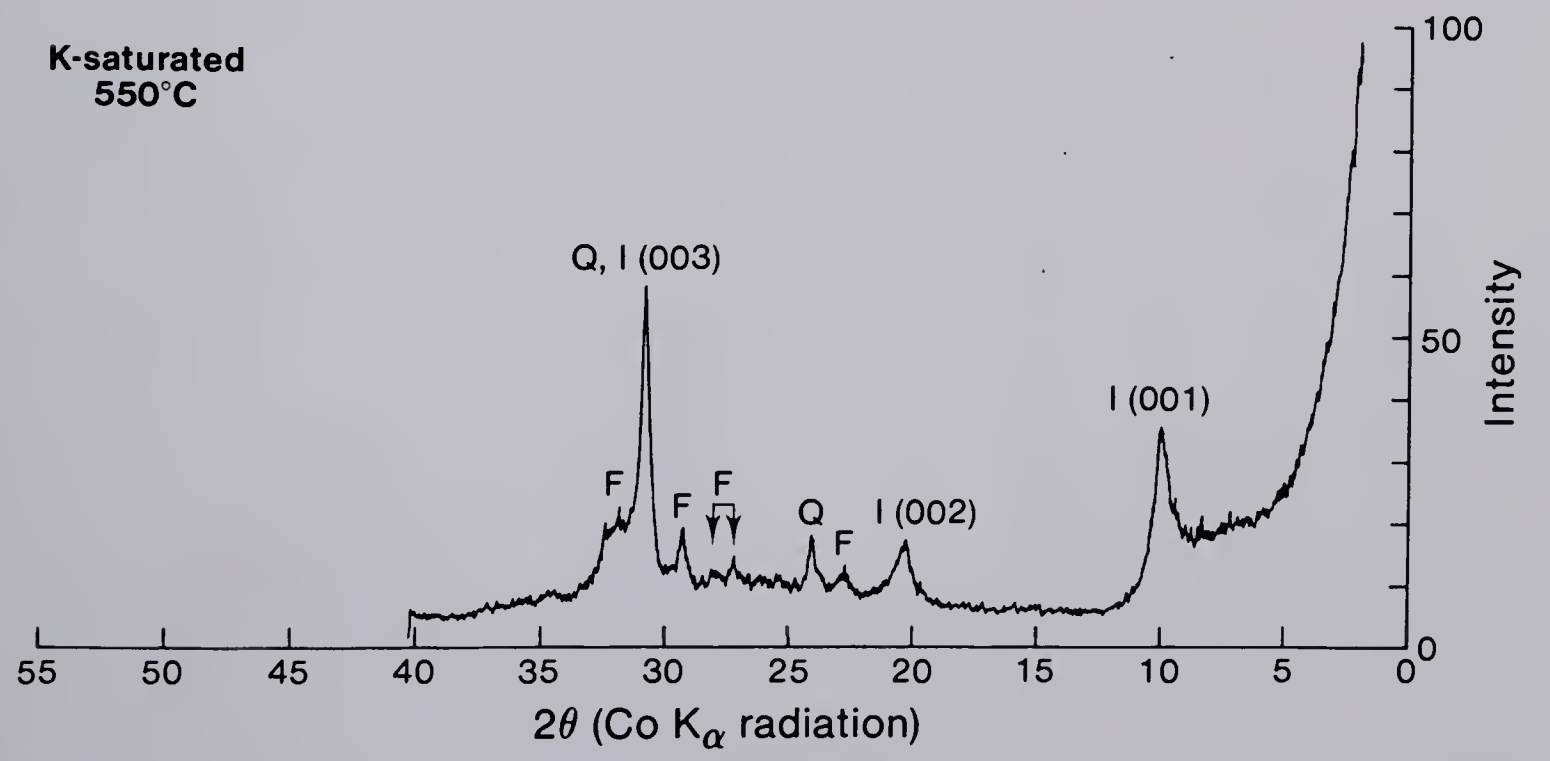

Figure 22A and B.
X-ray diffractograms representing a shale interbed in the carbonate-cemented sandstone of facies 6, type III clay assemblage. This sample contains 55 per cent illite. Note the peak at 12A (labelled I-S). Upon glycolation, the 12A reflection loses intensity and shifts to about 14A. This reflection probably represents a randomly interstratified illite-smectite.

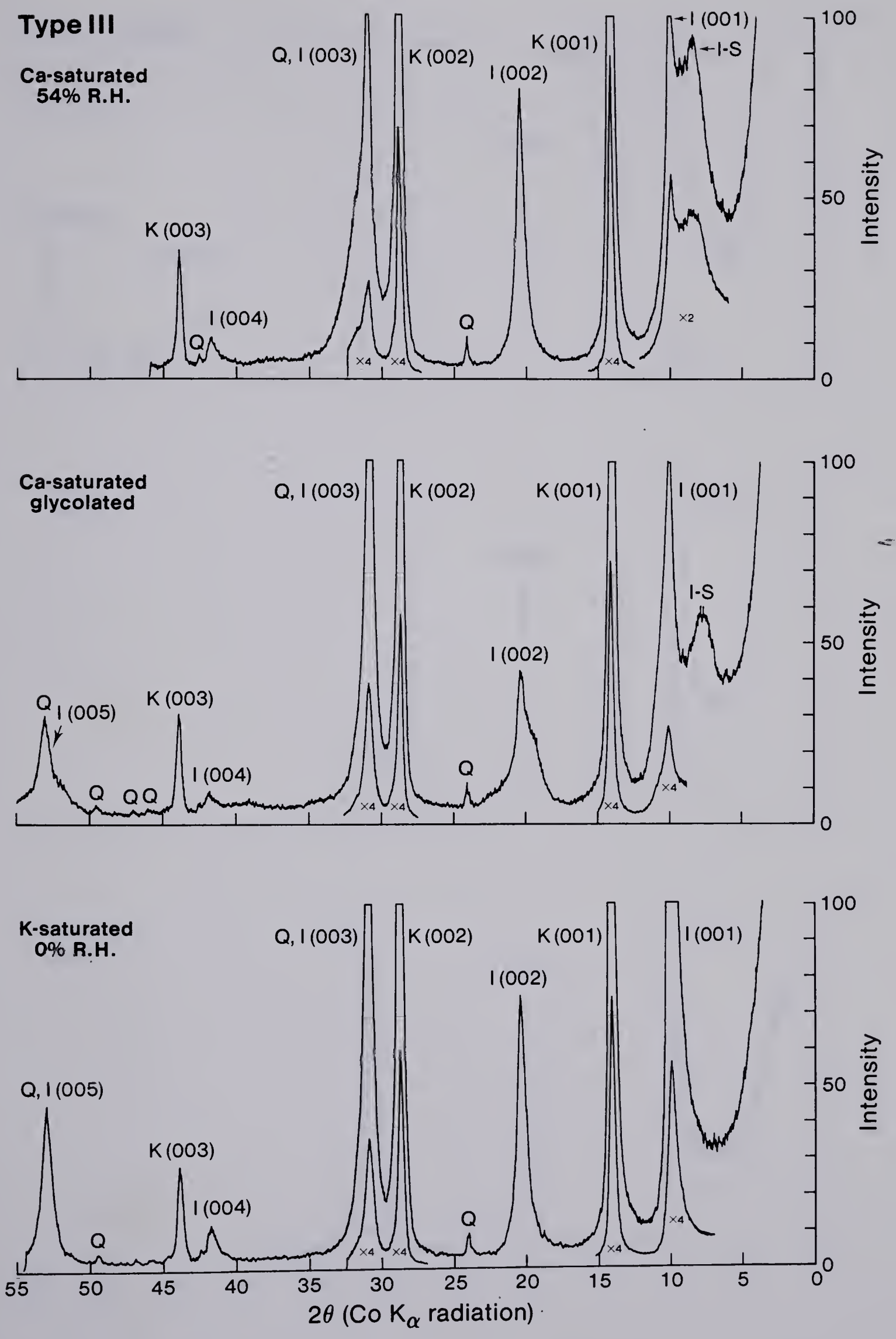
Type III
Ca-saturated
54% R.H.
Q, I (003)
K (002)
I (002)
K (001)
I (001)
I-S
K (003)
I (004)
Q
×4
×2
100
50
0
Intensity
Ca-saturated
glycolated
Q, I (005)
K (003)
I (004)
Q
I (002)
K (001)
I (001)
I-S
K-saturated
0% R.H.
55
50
45
40
35
30
25
20
15
10
5
0
2θ (Co Kα radiation)

Type III cont.

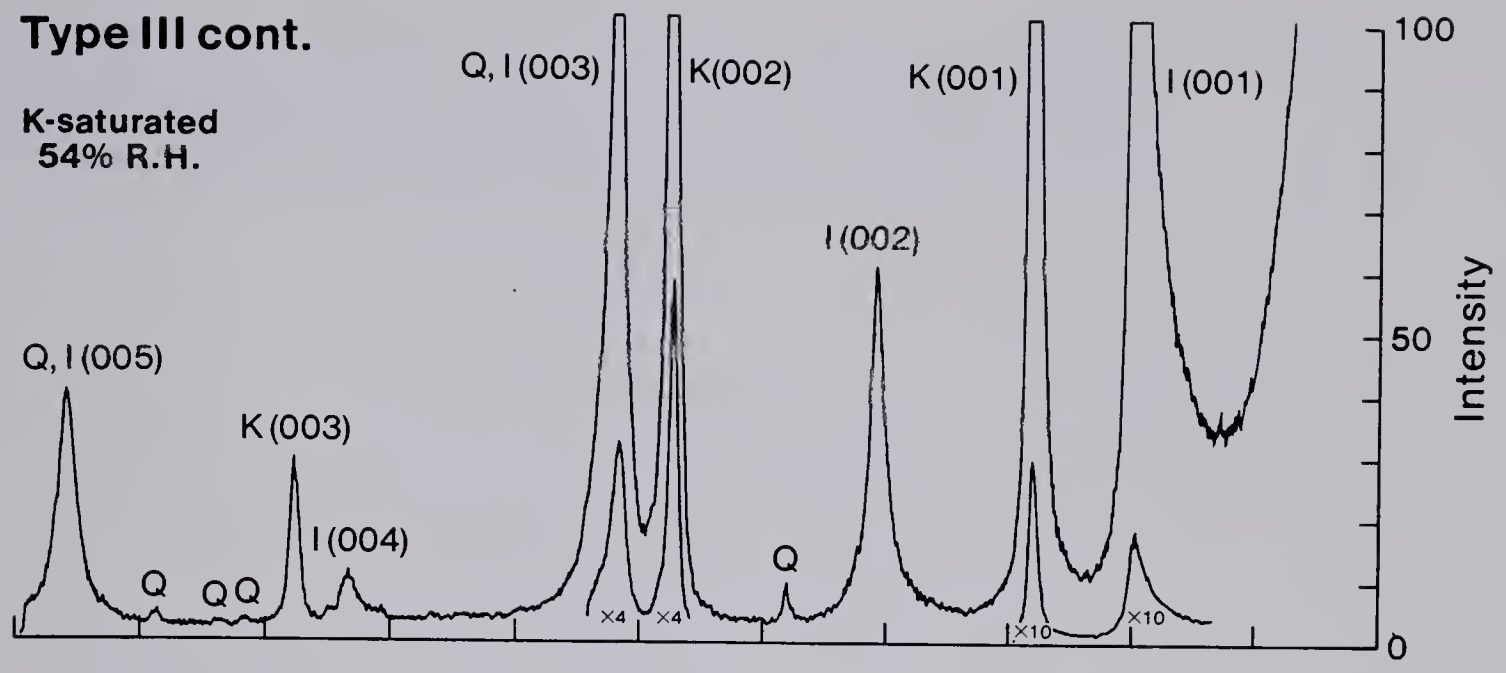

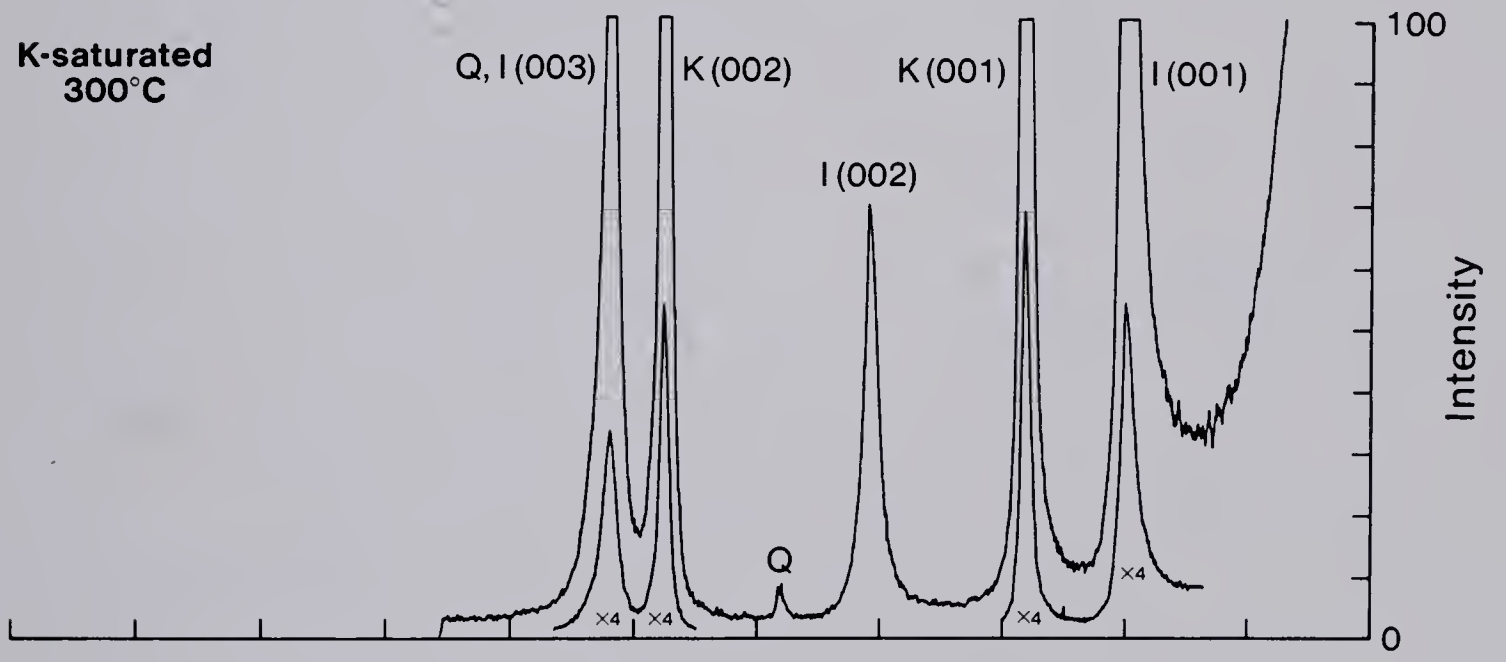

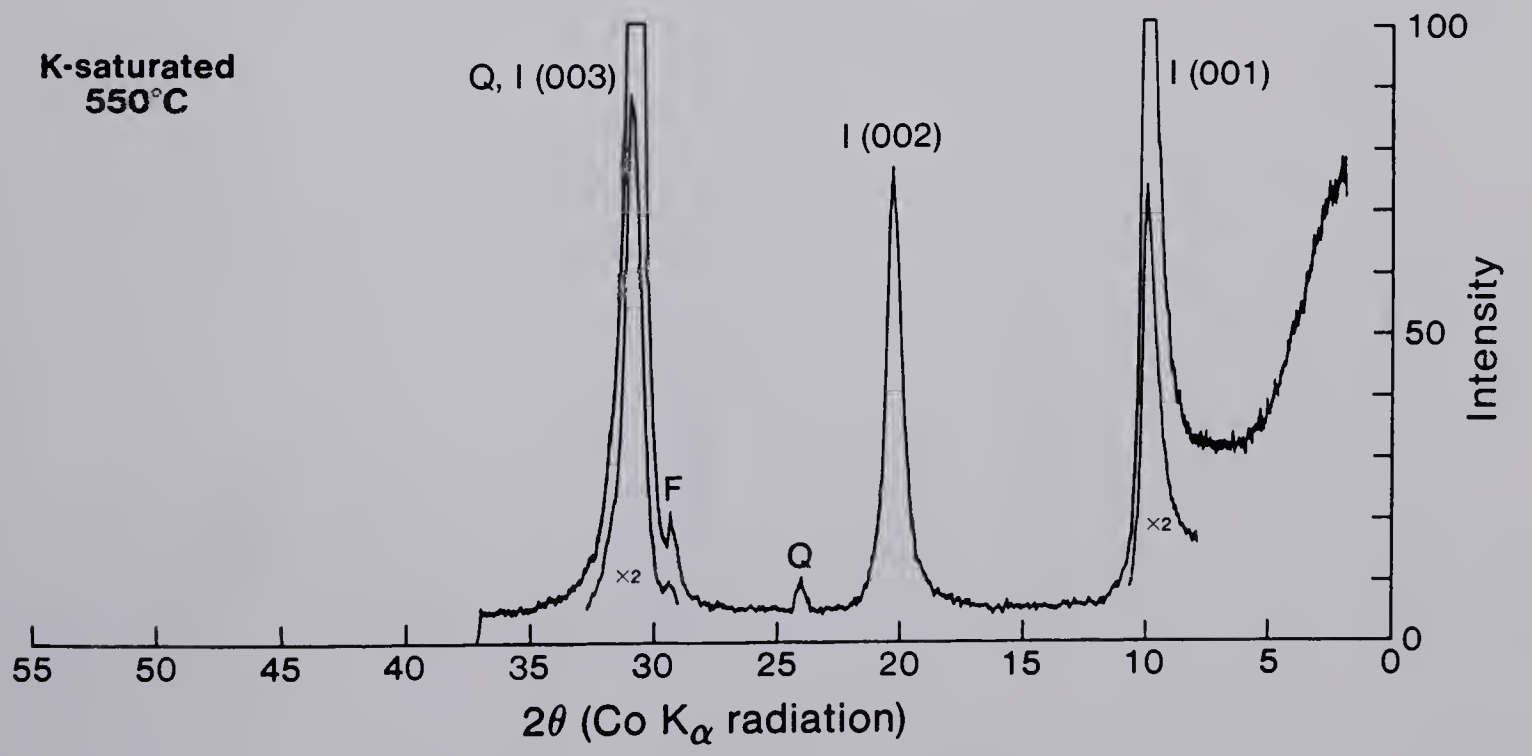

Figure 23 A and B.
X-ray diffractograms representing the <2 micrometre fraction of an oil-saturated sandstone of facies 4, type IV clay assemblage. Smectite (S) content is less than 5 per cent. The smectite (001) peak is relatively sharp (Ca-saturated patterns). Discrete chlorite (C) occurs in trace amounts.

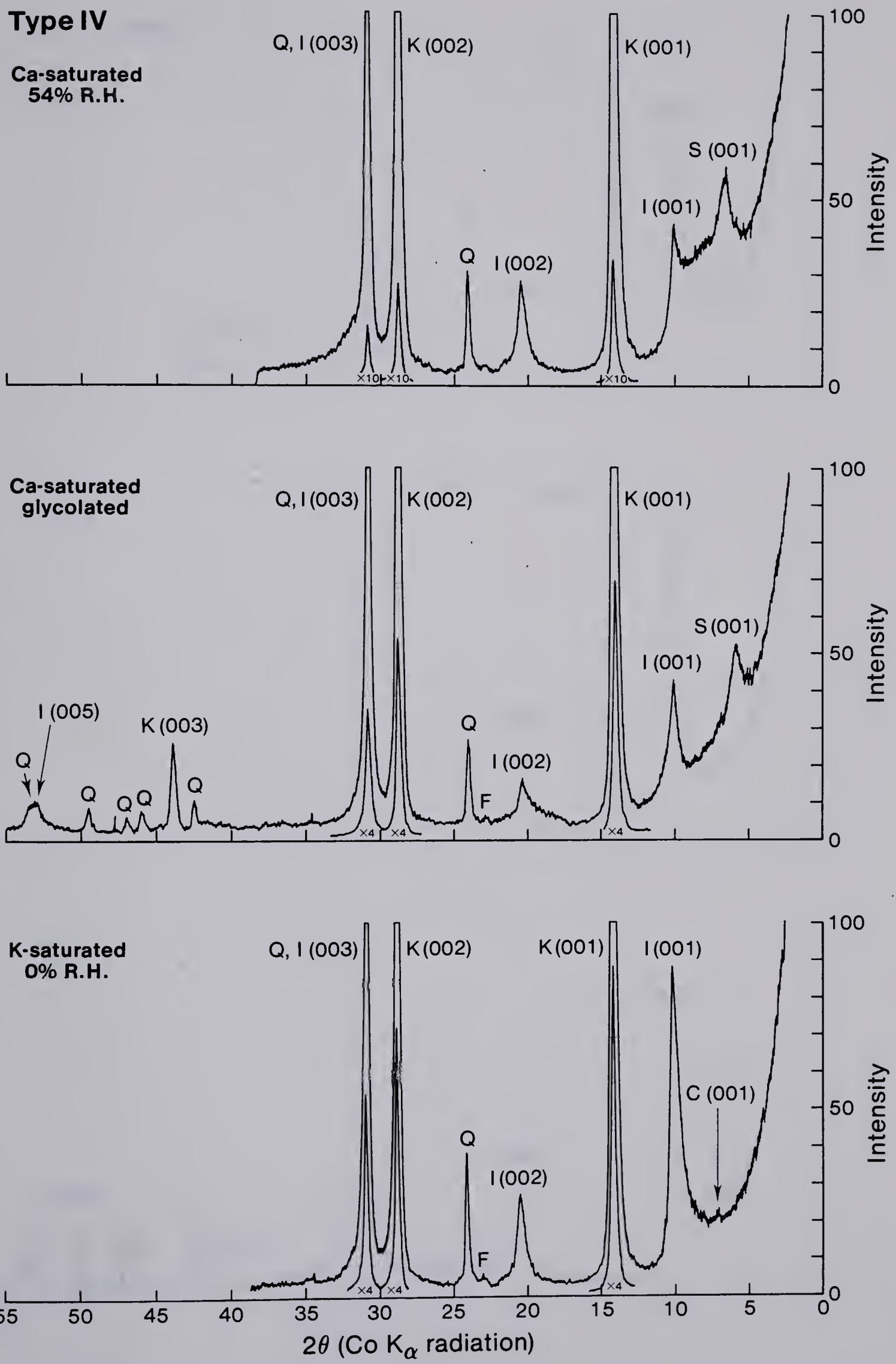
Type IV
Ca-saturated
54% R.H.
Q, I (003)
K (002)
K (001)
S (001)
I (001)
Q
I (002)
×10
×10
×10
100
50
0
Intensity
Ca-saturated
glycolated
Q, I (003)
K (002)
K (001)
S (001)
I (001)
I (005)
K (003)
Q
Q
Q
Q
Q
Q
I (002)
F
×4
×4
×4
100
50
0
Intensity
K-saturated
0% R.H.
Q, I (003)
K (002)
K (001)
I (001)
C (001)
Q
I (002)
F
×4
×4
×4
100
50
0
Intensity
55
50
45
40
35
30
25
20
15
10
5
0
2θ (Co Kα radiation)

Type IV cont.

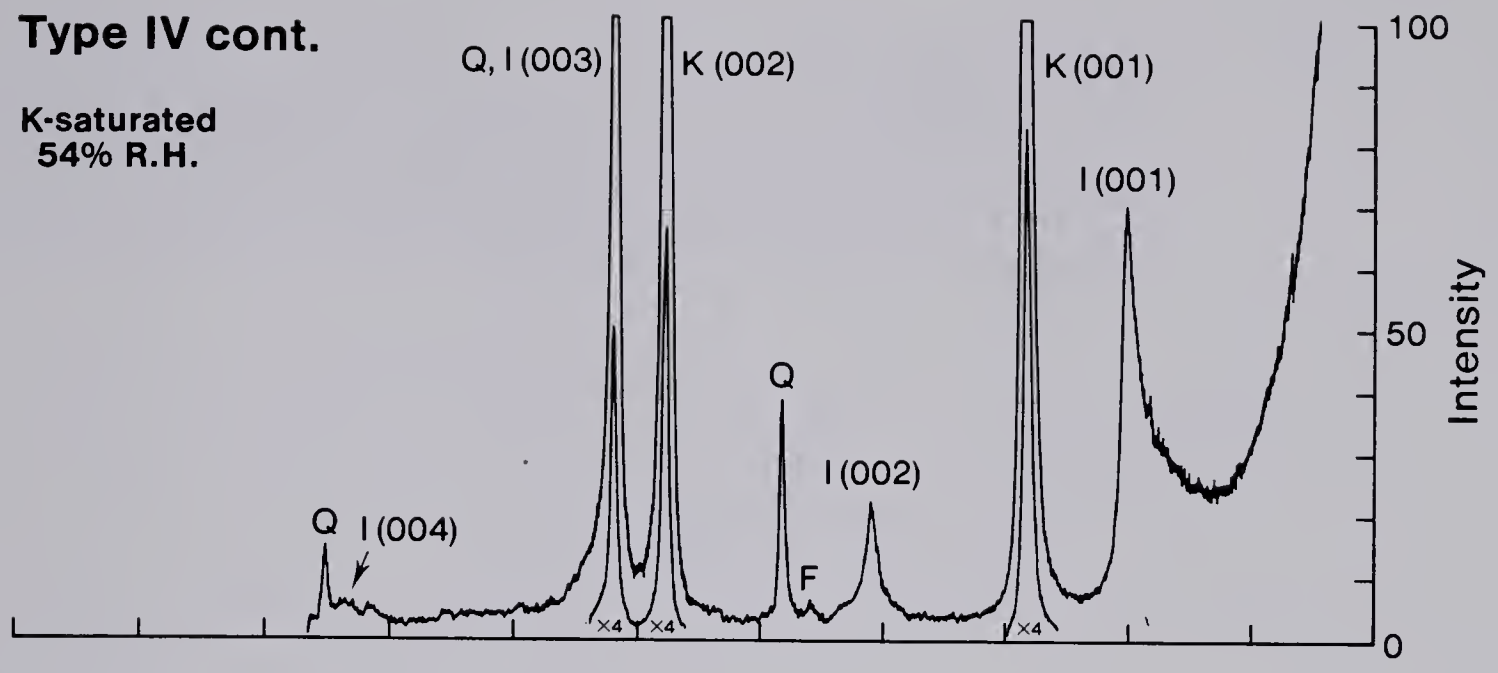
K-saturated
54% R.H.
Q, I (003)
K (002)
K (001)
I (001)
Q
I (002)
Q
I (004)
F
×4
×4
×4
100
50
0
Intensity

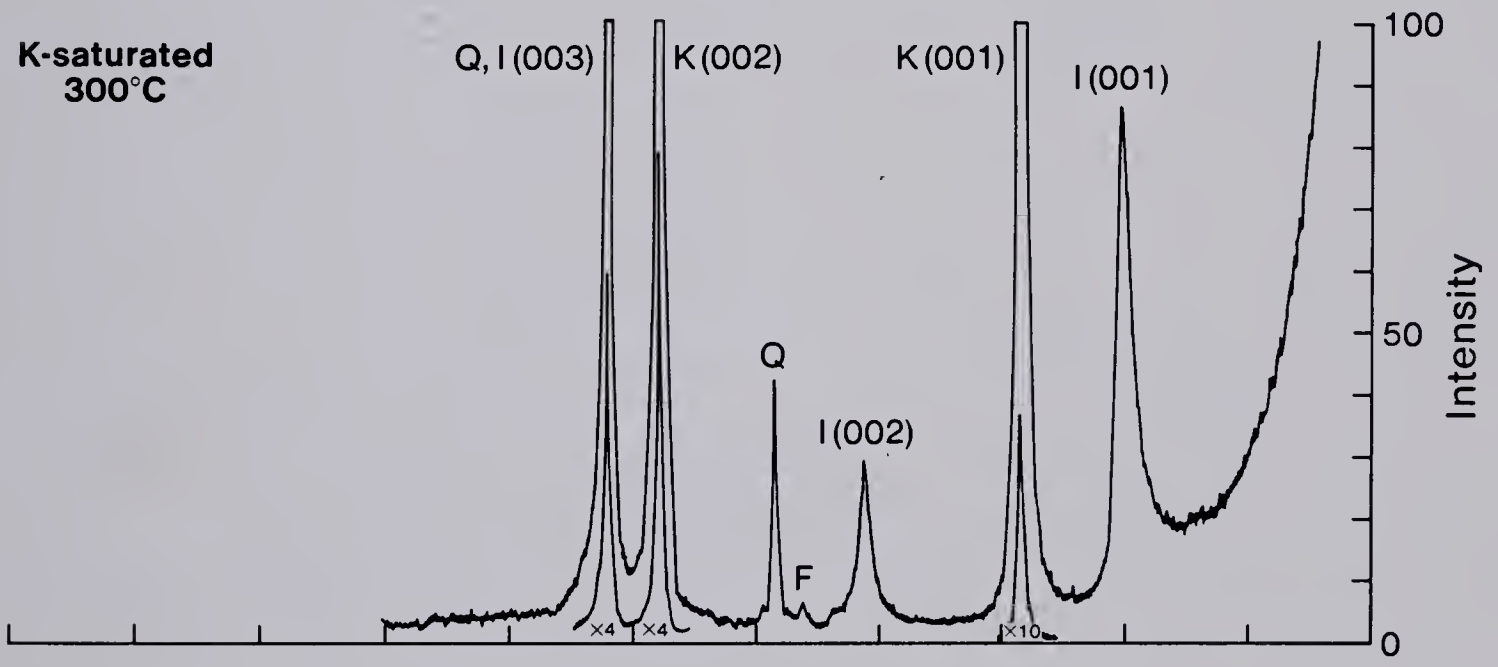
K-saturated
300°C
Q, I (003)
K (002)
K (001)
I (001)
Q
I (002)
F
×4
×4
×10
100
50
0
Intensity

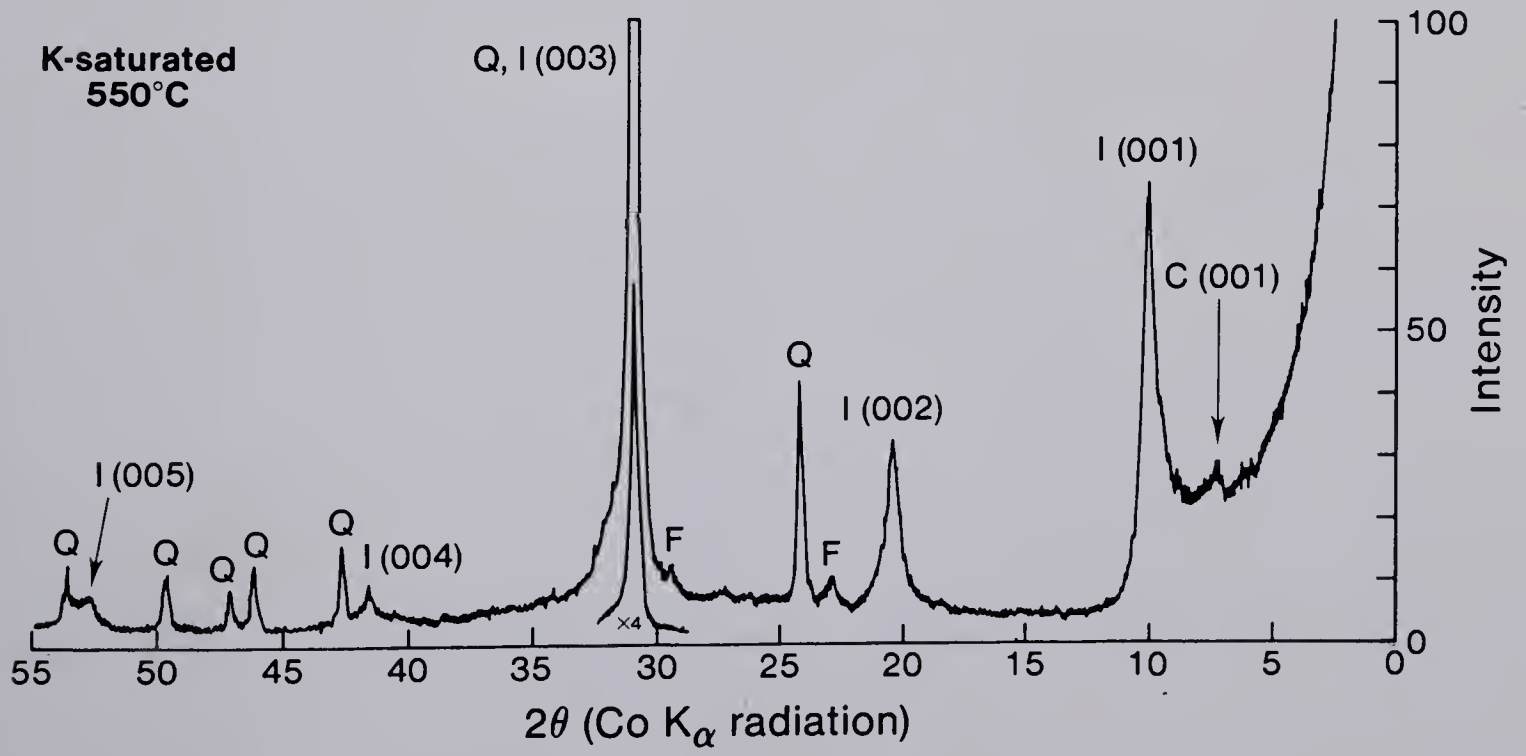
K-saturated
550°C
Q, I (003)
I (001)
C (001)
Q
I (002)
I (005)
Q
Q
Q
Q
I (004)
F
F
×4
100
50
0
Intensity
55
50
45
40
35
30
25
20
15
10
5
0
2θ (Co Kα radiation)

Figure 24 A and B.
X-ray diffractograms representing the <2 micrometre fraction of an oil-saturated sandstone of facies 4, type IV clay assemblage. Smectite content is less than 1 per cent. Smectite (S) is represented by a broad 15A reflection which expands to 17A upon saturation with ethylene glycol. Discrete chlorite occurs in trace amounts. The chlorite (001) peak, C(001), is enhanced upon heating to 550°C (Fig. 24B) and shows as a low intensity, broad peak.

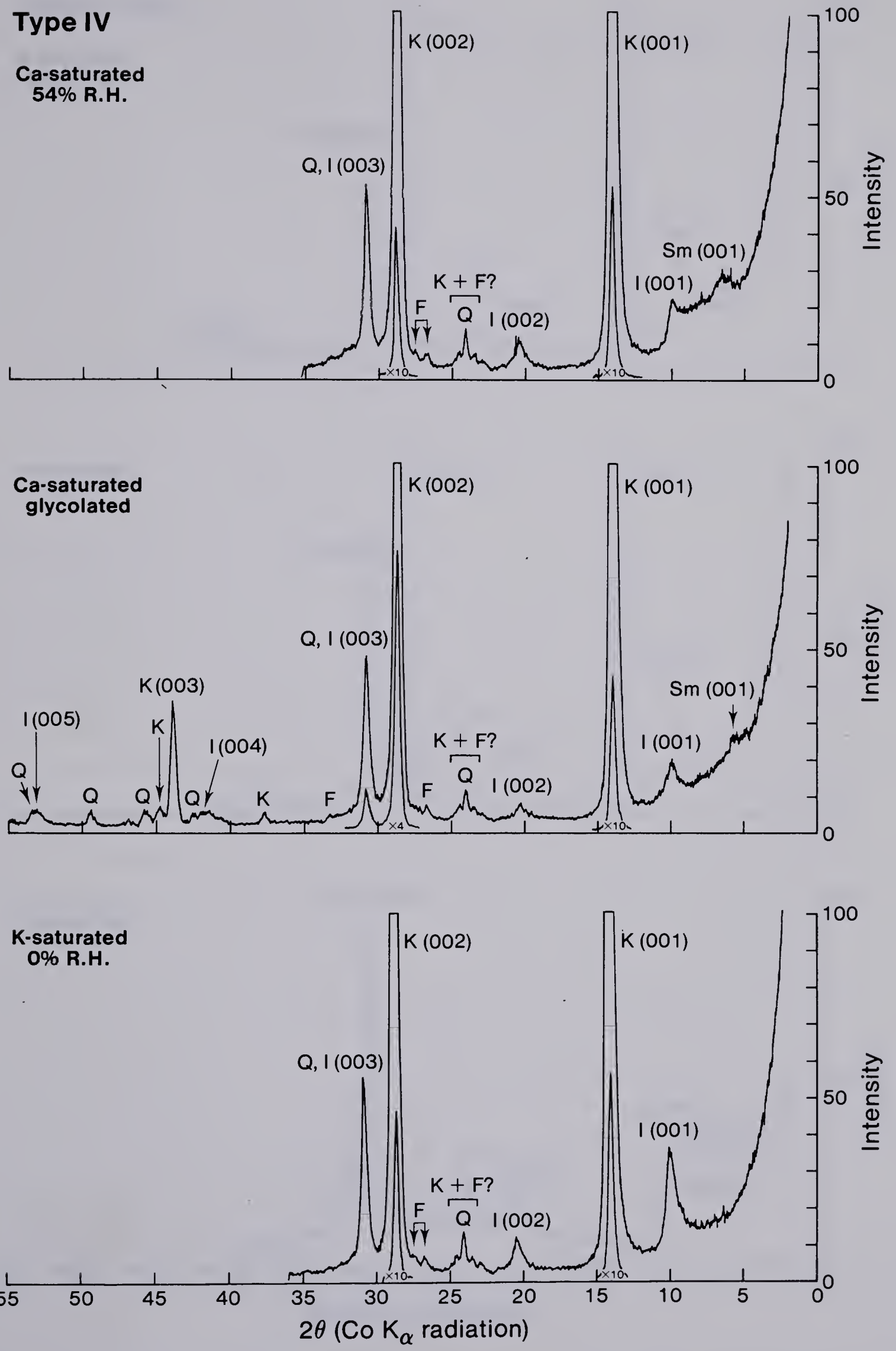
Type IV
Ca-saturated
54% R.H.
K (002)
K (001)
Q, I (003)
K + F?
F
Q
I (002)
Sm (001)
I (001)
×10
×10
100
50
0
Intensity
Ca-saturated
glycolated
K (002)
K (001)
Q, I (003)
K (003)
I (005)
K
I (004)
Q
Q
Q
Q
K
F
F
K + F?
Q
I (002)
Sm (001)
I (001)
×4
×10
100
50
0
Intensity
K-saturated
0% R.H.
K (002)
K (001)
Q, I (003)
K + F?
F
Q
I (002)
I (001)
×10
×10
100
50
0
Intensity
55
50
45
40
35
30
25
20
15
10
5
0
2θ (Co Kα radiation)

Type IV cont.

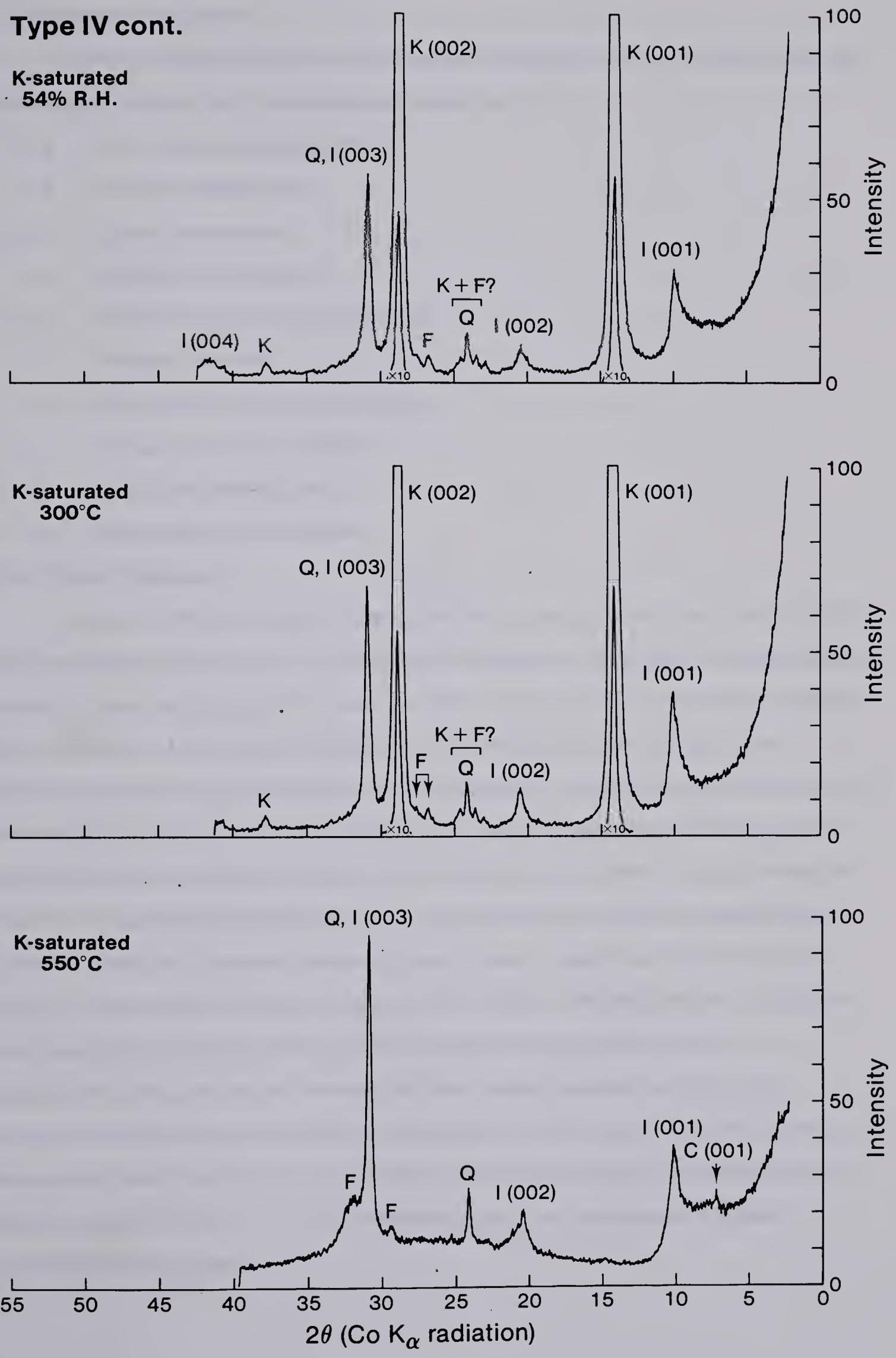
K-saturated
54% R.H.
K (002)
K (001)
Q, I (003)
I (001)
K + F?
Q
I (002)
I (004)
K
F
×10
×10
100
50
0
Intensity
K-saturated
300°C
K (002)
K (001)
Q, I (003)
I (001)
K + F?
F
Q
I (002)
K
×10
×10
100
50
0
Intensity
K-saturated
550°C
Q, I (003)
I (001)
C (001)
F
Q
I (002)
F
100
50
0
Intensity
55
50
45
40
35
30
25
20
15
10
5
0
2θ (Co Kα radiation)

C. Paragenetic Sequence

Textural relationships within the Glauconitic Sandstone of the Suffield heavy oil sand deposit indicate that the paragenetic sequence is:

1. a. First stage calcite cementation
   b. Pyrite crystallization
2. a. Quartz cementation
   b. Kaolinite crystallization
3. a. Second stage calcite cementation
   b. Feldspar leaching
   c. Minor kaolinite/illite crystallization
   d. Growth of calcite crystals
4. a. Smectite/chlorite growth
   b. Hydrocarbon emplacement

First Stage Diagenesis

Calcite-cemented zones are rare within the upper portion (facies 5 through 3) of the Glauconitic Sandstone and their distribution appears to be random. First stage calcite cement occurs in a 3 meter thick interval within facies 4 of one of the cores examined. Early formation of the calcite is indicated by: (1) the loose grain packing of the calcite-cemented sandstone (Plate 8-1); (2) the random distribution of such sandstones in the stratigraphic section; and (3) the absense of further diagenetic modification in the calcite-cemented sandstone (Galloway, 1979). The paucity of grain-to-grain contacts (Plate 8-1) indicates that calcite cementation occurred very soon after sedimentation, before compaction. Silicified carbonate grains, possibly algal fragments, brachiopod spines, or less likely calcispheres, occur in one calcite-cemented sample. The calcium may have come from dissolution of these fragments. Quartz grains in this calcite-cemented sample are more angular than in other samples which are not calcite-cemented. This textural difference suggests that the calcite cement is partially facies controlled, forming in more protected zones of the beach where reworking of grains is minimal. The very low clay content suggests that subsequent diagenetic modification was limited.

Although other evidence indicates that the calcite cement formed at an early stage, its relatively coarse texture (Plate 8-2) is typical of a late-stage cement. Staining techniques indicate chemical variation within the cement. The purer $CaCO_3$ zones may have been created during later stage partial recrystallization of the cement.

Pyrite formation probably occurred early in the paragenetic sequence. Pyrite in the Glauconitic Sandstone occurs in several forms, one of which is the apparent replacement of an organic structure (Plate 5-4). The original framework and porosity associated with the organic material is preserved and suggests that the pyrite replacement occurred early before compaction. Dypvik and Vollset (1979) and Merino (1975) describe pyrite which they consider was formed by bacterial reduction of sulphate from sea water in the uppermost metre of sediment. Pyrite cubes, associated with detrital clays (Plate 5-3) are not abraded, suggesting that they are diagenetic.

Second Stage Diagenesis

The relative timing of quartz overgrowths versus kaolinite precipitation is equivocal. Textural evidence exists for: (1) kaolinite forming after quartz overgrowths (Plate 6-5); (2) kaolinite inhibiting the growth of authigenic quartz (Plate 8-3); and (3) interlocking growth of quartz and kaolinite (Plate 6-6). Regardless, certain textural evidence suggests that both quartz cement and kaolinite formed at a relatively early stage in diagenesis. In the less argillaceous sandstones, the preservation of good porosity indicates that quartz cementation inhibited compaction. In these rocks, quartz overgrowths are well formed, authigenic kaolinite is large (>80 micrometres long), and both kaolinite and quartz are coated by later authigenic phases. The well-developed form of quartz and kaolinite indicates growth in open pore spaces.

Kaolinite and quartz probably precipitated from circulating meteoric waters that were enriched in silica and aluminum; rather than kaolinite, montmorillonite or illite will precipitate unless the waters are sufficiently dilute (Blatt, 1979). The source of the silica- and aluminum-enriched solution is difficult to estimate; it may be derived from weathering or alteration in adjacent areas (Dypvik and Vollset, 1979; and Almon and Davies, 1979).

Third Stage Diagenesis

The third stage of diagenesis involves a second episode of calcite cementation, feldspar leaching and kaolinite formation, and still later precipitation of calcite crystals. The presence of uncorroded feldspars in sandstones cemented with second stage authigenic calcite suggests that the calcite cementation took place before feldspar leaching.

The second stage calcite cement is ubiquitous in the very fine grained sandstones at the base of the Glauconitic Sandstone, immediately above the calcareous "ostracode zone". The calcite may have precipitated from fluids derived from pressure-solution of these underlying calcareous rocks. The cement encloses authigenic kaolinite (Plate 8-4) and therefore crystallized after the kaolinite. Smectite and chlorite are absent in calcite-cemented sandstone and formed after this episode of cementation.

The few feldspar grains present in the more porous units are commonly leached. Some corroded feldspar grains are coated with small kaolinite platelets (Plate 8-5) suggesting that the feldspar has altered to kaolinite. Illite coatings, which are very rarely found on kaolinite booklets (Plate 7-2), may have formed at this stage with K^+ supplied from leached feldspars. Much of the K^+ liberated from feldspar may have been fixed in the detrital, interstratified illite-smectite (Dypvik and Vollset, 1979). Following leaching of the feldspar, calcite crystallized in the newly created, secondary pore space (Plate 8-6).

Fourth Stage Diagenesis

The fourth stage of diagenesis involved the development of minor amounts of smectite and chlorite, and the emplacement of hydrocarbons. The late stage growth of smectite and chlorite is indicated by their habit of bridging or coating earlier authigenic phases (Plate 7-3). The presence of smectite and chlorite in oil-saturated sandstones, in addition to their greater abundance below the oil/water interface, suggests that they began to form before hydrocarbon emplacement, and continued to develop below the oil/water interface. Hydrocarbon emplacement occurred late in the paragenetic sequence; the only difference in diagenesis above and below the oil/water interface for rocks with similar detrital components is the abundance of smectite (Tables 5 and 6). Cations necessary for the development of chlorite and smectite may have been derived from solutions released during the compaction of surrounding shales.

VII. RESERVOIR QUALITY

The reservoir quality of a rock formation refers to a combination of all factors which might affect its petroleum yield. Such factors include the porosity, permeability, continuity, and fluid sensitivity of the formation. Units of varying reservoir quality within the Glauconitic Sandstone can be correlated directly to the sedimentary facies.

A. Facies 4

The top of the best oil saturation, as suggested by the resistivity logs (Figs. 4 and 5), corresponds to the top of facies 4, the relatively clean, laminated zone. The reservoir quality of the Glauconitic Sandstone gradually improves downward from facies 3a, where there is negligible porosity and permeability, to facies 4, which has good porosity (Plate 9-1), permeability and lateral continuity. The sandstones of facies 4 contain 1 to 4 weight percent clay of almost entirely authigenic origin. Clean pores average about 80 micrometres in diameter and in some cases have been reduced in size by quartz overgrowths and small local clusters of authigenic kaolinite (Plate 9-2). Other pores are lined with masses of authigenic clays (Plate 9-3), or are almost totally eliminated by the junction of quartz overgrowths (Plate 9-4). Argillaceous rock fragments are a common constituent of these sandstones. During compaction these soft grains were squeezed around harder grains and this destroyed much of the original intergranular porosity associated with them (Plate 4-4). Permeability is inhibited by clusters of kaolinite which form bridges extending across the pores (Plate 9-5). Pyrite clusters (Plate 5-4), and dolomite and/or siderite grains (Plate 5-2) also reduce porosity and permeability. A minor amount of feldspar corrosion has increased the porosity, but the remnant skeletal framework (Plate 5-1) inhibits permeability.

B. Permeability and Continuity

Vertical and horizontal permeability in facies 4 should be relatively good, aside from the above mentioned microscopic permeability barriers. Core and petrologic examinations give no indication of any significant difference in vertical and horizontal permeability. There are no shale breaks in the oil-saturated zone and laminations in facies 4 (Plate 1-5 & 6) are defined by slight variations in mineralogy rather than by significant grain-size changes. Horizontal permeability may be limited in the upper portions of some wells where the top of facies 4 is situated structurally higher than facies 4 in the adjacent well. For example, in well P2 the upper portion of facies 4, from -115 m to -167 m, is at the same structural horizon as facies 3 in the adjacent well 02 (Fig. 5). However from -167 m downwards to the oil/water interface in well P2, facies 4 is laterally continuous with facies 4 in well 02.

Parts of facies 3d have reservoir properties similar to those of facies 4, but these zones have limited lateral and vertical continuity. Photographs of core slabs in Plate 1-7 demonstrate the lack of continuity in facies 3d; sandstone lenses, with no oil saturation, are common and serve as permeability barriers.

C. Detrital Clay

The main influence on reservoir quality is the abundance of detrital clay. Facies 4 has little or no detrital clay whereas all of facies 3 has detrital clay with quantities increasing upwards. This is related to energy conditions at time of deposition, with facies 3d representing fluctuating energy conditions. Bioturbation has also played a significant role in creating clay-rich zones within facies 3.

D. Irreducible Water Saturation

The argillaceous sandstones of facies 3 have a significant microporosity, created by the abundance of detrital kaolinite. A rock of this type with small pore apertures and high surface area also has high irreducible water saturation (Pittman, 1979), ie., water tightly held because of the physical attraction of the solid for the liquid. In such

sandstones, log calculations may indicate that water saturations are too high for a productive interval. However, the reservoir may be capable of essentially water-free production because the water is predominantly irreducible.

E. Fluid Sensitivity

The main concern related to fluid sensitivity in this reservoir pertains to the dispersion of fine kaolinite. Many of these kaolinite plates are only loosely attached to grain surfaces and could easily be dispersed by moving fluids and become lodged in pore throats. Gray and Rex (1966) report that damage caused by migration of fines can drop a very permeable sandstone to less than 1 percent of its original permeability within a few hours of flow.

Iron-containing minerals are sensitive to acidization. These minerals dissolve, precipitate when conditions change, and cause reservoir damage. Although Fe-chlorite is very rare, pyrite (FeS_2) is present in minor amounts. Therefore, acidization should be avoided.

Effect of the Application of Wet Forward Combustion on the Reservoir

Several workers conducting laboratory experiments under conditions similar to those of steam injection operations indicate that significant amounts of smectite are formed where kaolinite, quartz, and a very small amount of dolomite are present. Data and results are reported in Bayliss and Levinson (1971), Levinson and Vian (1966), Day, McGlothlin, and Huitt (1967), and Perry and Gillot (1979). Smectite poses a special problem due to the swelling of its crystal lattice upon hydration. This expansion can cause a fifty-fold decrease in permeability (Waldorf, 1965). A test on SHOP project samples using a firetube to simulate wet forward combustion conditions (Bennion, Moore and Donnelly, 1979) indicated that the illite-smectite content of the clay fraction increased from 1 to 5 percent , as temperatures were raised from 245°C to 635°C. These data suggest that the formation of smectite over the time duration of the pilot project may create significant problems in reservoir sensitivity.

Another reaction which may occur during the *in situ* recovery of bitumen by, wet thermal methods, is the dissolution and precipitation of SiO_2 (Boon, 1979). Low quartz and amorphous silica may dissolve when temperature and pH are increased and precipitate as the fluid reaches cooler regions. Such fluid–rock interactions can lead to a change in reservoir properties such as reduced porosity and permeability and to an undesirable composition of produced fluids: suspended clays, high dissolved silica and a high degree of hardness (Boon, 1979). Chert percentage in the bitumen–saturated portion of the Glauconitic Sandstone in the SHOP project is about 20 per cent (Table 1). This chert may be particularly susceptible to dissolution under raised temperature and pH conditions.

VIII. CONCLUSIONS

Three factors control the distribution of hydrocarbons and the reservoir quality in the Glauconitic Sandstone within the Suffield area. They are (1) sedimentology, (2) structure, and (3) mineralogy and diagenesis.

A. Sedimentogical Controls

Hydrocarbons are located along a northwest to southeast trending broad arch of thick, vertically continuous sandstone. The sandstone consists of facies representing in ascending order, the shoreface, foreshore, backshore, marsh and lagoonal or continental zones of a progradational beach or barrier island complex. The facies representing the foreshore zone (laminated sandstone of facies 4) was deposited under high energy conditions and has good reservoir properties: high porosity, low clay content, and good lateral and vertical continuity. Fluctuating energy conditions and bioturbation in the backshore zone created a rock with poor reservoir properties in facies 3 (argillaceous or bioturbated sandstone facies). This unit is characterized by low porosity and high clay content with only isolated porous zones. Tidal inlet and channel deposits occurring along the sandstone trend disrupt the continuity of the reservoir.

B. Structural Controls

Basement faults, possibly related to tectonic activity associated with the North Battleford Arch and active during late Mannville time, have caused downfaulting of local blocks of sandstone such that nondepositional facies changes occur. Thus the hydrocarbon trapping mechanism is stratigraphic with some structural effect.

Movement on basement faults during deposition of the Glauconitic Sandstone is most likely responsible for the locally occurring, unusually thick (45m), progradational beach deposits. Areas with the thickest sandstone accumulations were probably located over downfaulting basement blocks. The rate of subsidence equalled the rate of sediment imput such that the shoreline remained in a relatively stable position and facies accumulated vertically.

C. Mineralogical and Diagenetic Controls

The Glauconitic Sandstone is a litharenite, composed of quartz, chert, other sedimentary rock fragments, and trace amounts of feldspar. The dominant clay mineral is kaolinite which occurs in both detrital and authigenic forms. It is the abundance of detrital kaolinite present in the rock which determines the reservoir quality. The bioturbated or structureless facies 3 with abundant detrital clay forms a poor reservoir, whereas the clean, nonargillaceous facies 4 has good reservoir qualities. Porosity and permeability is only slightly reduced in the clean sandstones by diagenetic forms such as kaolinite, quartz overgrowths and deformed rock fragments.

The paragenetic sequence is: (1) first stage calcite cement and pyrite crystallization;(2) quartz cementation and kaolinite growth; (3) second stage calcite cementation, feldspar leaching, minor kaolinite/illite development, and growth of calcite crystals; and (4) smectite/chlorite crystallization and the emplacement of hydrocarbons.

The main concern related to fluid sensitivity is the dispersion of kaolinite. Iron-containing minerals (pyrite and Fe-chlorite) which are sensitive to acidization occur only in trace amounts. When the temperature of the reservoir is raised during the wet combustion process, kaolinite, quartz and dolomite may react to form the swelling clay, smectite. Further reduction in permeability may result from dissolution and reprecipitation of SiO_2 (quartz and particularly chert).

D. Recommendations for Future Work

Areas for further study include regional sedimentology, and diagenesis. Preliminary examination of core from the eastern sandstone belt centred in range 7, townships 19 and 20, suggest that conglomerates with shale interbeds within this belt represent offshore storm deposits. Further study is necessary to negate or substantiate this idea. The Glauconitic Sandstone in the Suffield area is only a small part of the extensive regional Glauconitic Sandstone for which the entire depositional picture is yet to be understood. Stable isotope analyses are needed to develop a further understanding of water/rock interaction during diagenesis. With similar objectives in mind, new cores should be drilled in the SHOP project site after the combustion front has past through the area. Samples from these new cores should be examined in thin section and by SEM to

evaluate any reservoir damage due to water–rock interaction during stimulation.

PLATE 1: Core Photographs for Facies 6 to Facies 3d.

1. Facies 6b. Light grey to light brown very fine to fine-grained sandstone with well-defined laminations.
   Left: Wave-rippled sandstone with a thin shale interbed at the base of the photograph.
   Centre: Ripple troughs and subhorizontal, planar laminations defined by carbonaceous debris.
   Right: Cross-laminated, very fine grained sandstone near the base of the Glauconitic Sandstone.

2. Facies 6b. Calcite-cemented siltstone or very fine grained sandstone.
   Left: Calcite-cemented sandstone with low angle, planar laminations. The circular homogenous patches in the lower right of the photograph are probably burrows.
   Right: Calcite-cemented sandstone with interbeds of carbonaceous shale. The shale has syneresis cracks and the bed is partially bioturbated.

3. Facies 6a. Bioturbated, structureless or indistinctly laminated, fine-grained sandstone.
   Left: Generally structureless sandstone, poorly-defined laminations in lower portion of photograph.
   Right: Bioturbated zone in upper portion of photograph to structureless in the lower portion.

4. Facies 5. Medium-grained sandstone interbedded and interlaminated with fine-grained sandstone.
   Left: Thicker, medium-grained sandstone bed with erosional base. The bed fines upward to fine-grained sandstone.
   Right: Low angle, planar-laminated, medium- and fine-grained sandstone.

5. Facies 4. Horizontal laminated to low angle cross-laminated, fine-grained sandstone. Low angle cross-laminations.

6. Facies 4. Low angle, planar laminations. The black piece of core at the top of the photograph is an uncleaned, oil-saturated portion.

7. Facies 3d. Fine-grained sandstone with variable sedimentary structures and argillaceous zones. This facies is characterized by patches with good oil-saturation interrupted by zones with poor oil-saturation or no saturation.
   Left: Zone with irregular bedding and patchy oil-saturation. The upper part of the slab has been cleaned but the lower portion demonstrates an oil-saturated lense surrounded by a nonsaturated, clay-rich sandstone.
   Left-centre: Slightly coarser sandstone interbeds and lenses. This slab has been cleaned.
   Right-centre: Relatively high angle laminated, nonargillaceous sandstone. Both pieces have been cleaned but they probably had good oil-saturation originally.
   Right: Sandstone breccia. The laminated breccia blocks are angular and randomly oriented. The matrix is a slightly coarser clay-rich sandstone.

Scale: All core in the photographs is 3 inches (7.6 cm.) wide.

1

2

3

4

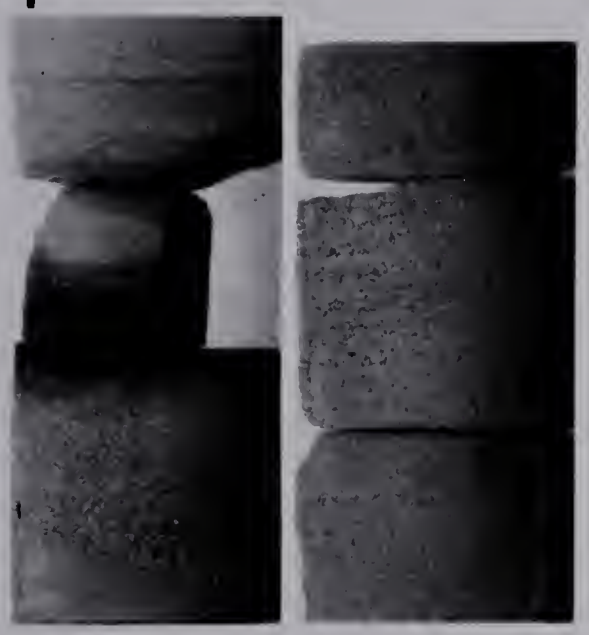

5

6

7

PLATE 2 : Core Photographs for Facies 3c to Facies 1.

1. Facies 3c. Facies 3c is more argillaceous than facies 3d and lacks any regular bedding.
   Left: Indistinctly bedded sandstone with patchy oil saturation.
   Centre: Bioturbated sandstone.
   Right: Structureless, argillaceous sandstone.

2. Facies 3bi. Bioturbated, argillaceous sandstone.
   Left: Bioturbated to structureless sandstone.
   Right: Bioturbated sandstone with clay streaks.

3. Facies 3bii. Cross-laminated sandstone unit overlain by a breccia.
   Left: Structureless, fine-grained sandstone containing coarse-grained pyrite overlain by cross-laminated sandstone.
   Right: Breccia. Disrupted zone with carbonaceous rootlets and irregularly shaped or subrounded blocks. Breccia blocks are finer grained than the matrix.

4. Facies 3biii. Laminated to low angle cross-laminated, argillaceous sandstone. Laminations are defined by coarse sand sized, magnetite grains.

5. Facies 3a. Light-brown, rooted argillaceous sandstone.

6. Facies 2. Carbonaceous sandstone and shale.
   Left: Dark grey sandy shale. The base of the unit is an irregular boundary marked by a colour change from medium or light grey (facies 3) to dark grey (facies 2).
   Right: Poor quality coal overlain by bioturbated, carbonaceous shale.

7. Facies 1. Very fine grained sandstone, siltstone and shale.
   Left: Structureless to laminated, medium grey shale with light grey silt interlaminations and small burrows.
   Right: Interlaminated siltstone and shale, rippled to cross-laminated with isolated burrows, carbonaceous debris along some laminations.

Scale: All core in the photographs is 3 inches (7.6 cm.) wide.

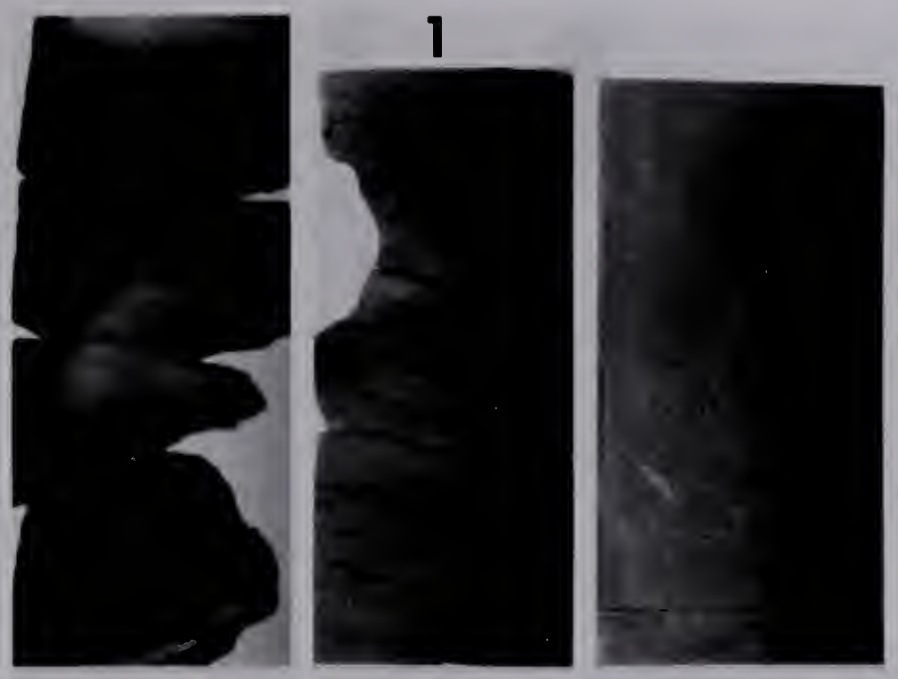
1


2

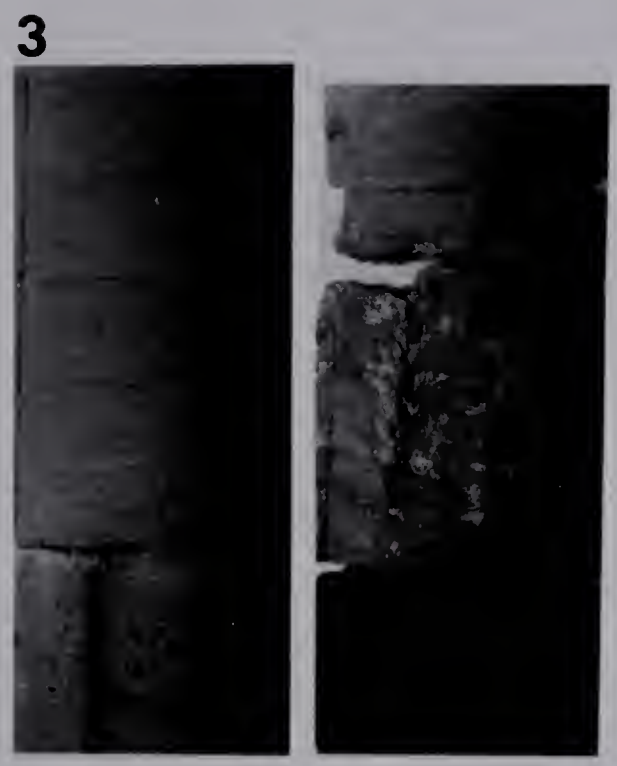
3


4


5

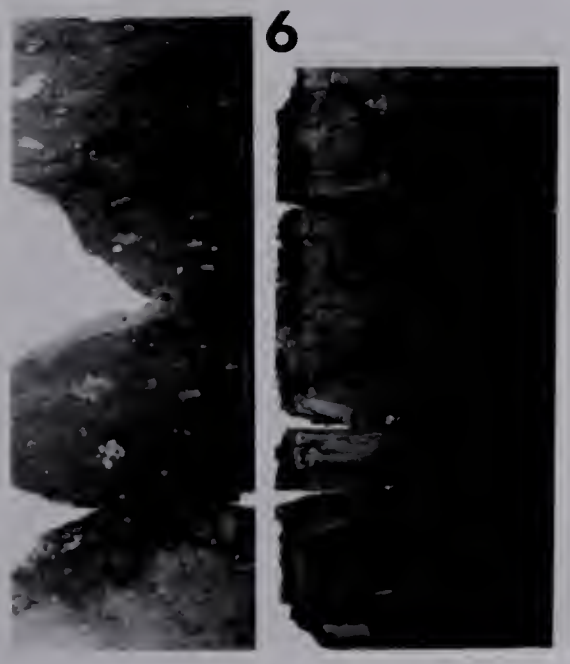
6

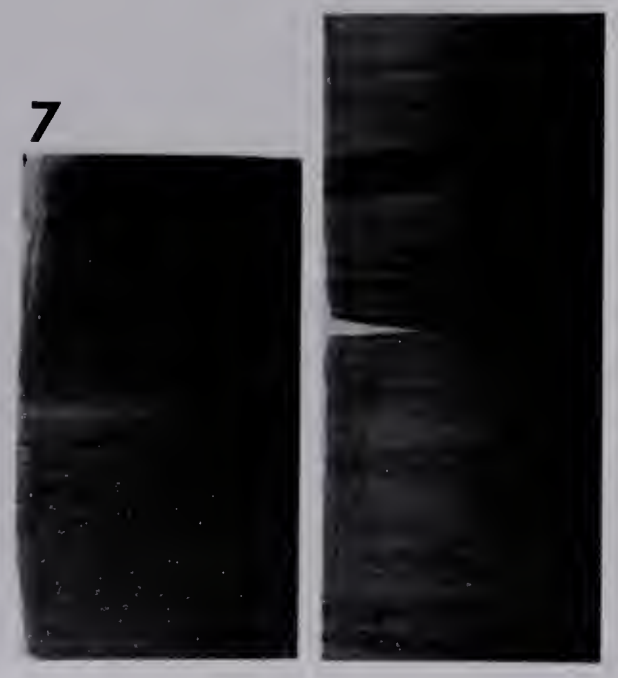
7

PLATE 3: Thin Section Textures for Facies 5 and Facies 3biii.

1. Facies 5. Thin section photomicrograph of a sample from facies 5 showing bimodal grain size with coarser chert grains (Ch) and fine quartz (Q). Chert grains have low sphericity and are more angular than the quartz. Plane polarized light.

2. Facies 3bii. Thin section photomicrograph of a sample from facies 3biii showing the preferential horizontal fabric resulting from compaction flattening of soft rock fragments (RF) and orientation of elongate chert grains (Ch). Feldspars (F) (K-feldspar, and plagioclase) are more abundant than in other facies. Plane polarized light.

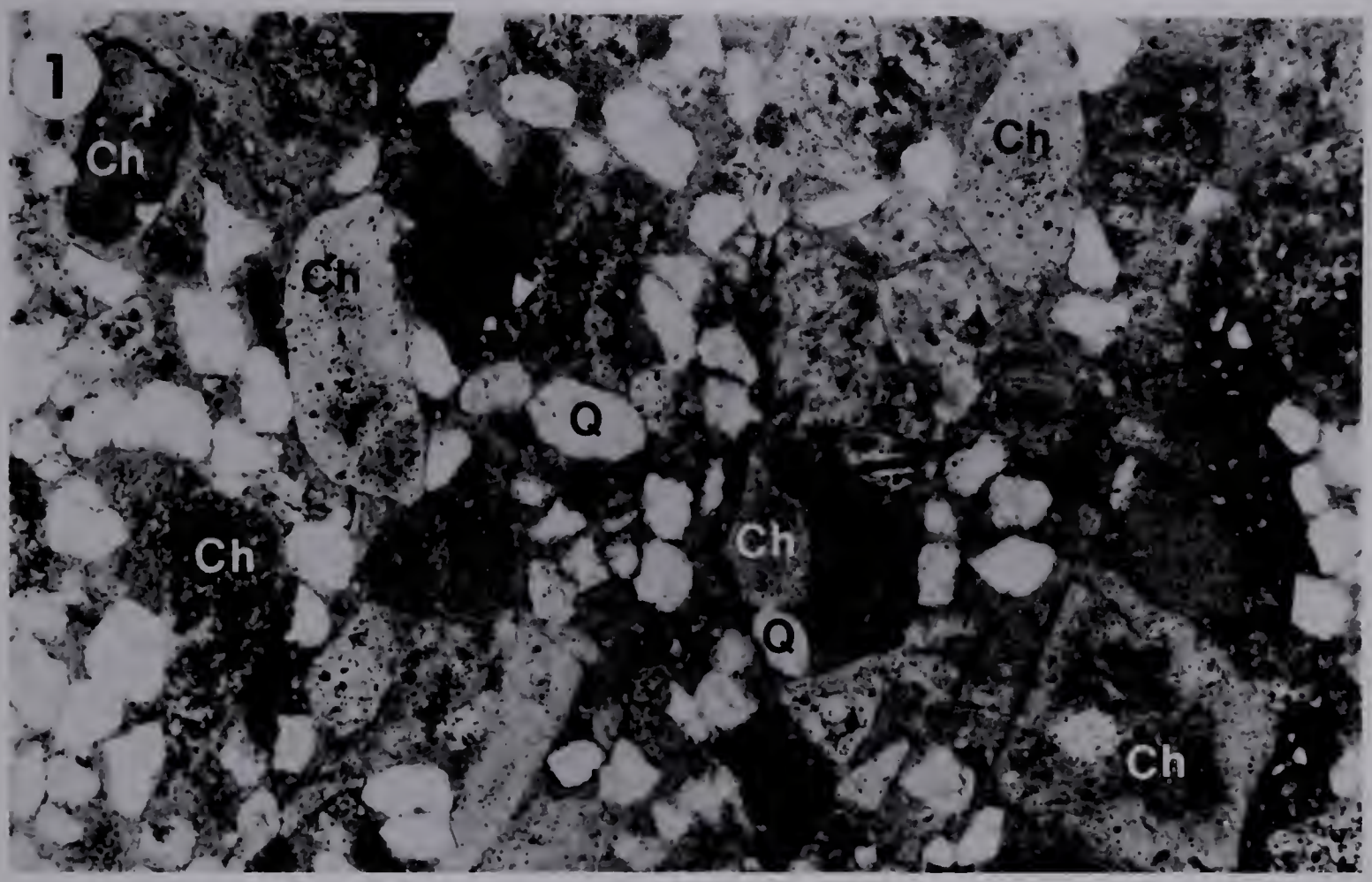
1
Ch
Ch
Ch
Q
Ch
Q
Ch
Ch
300μm

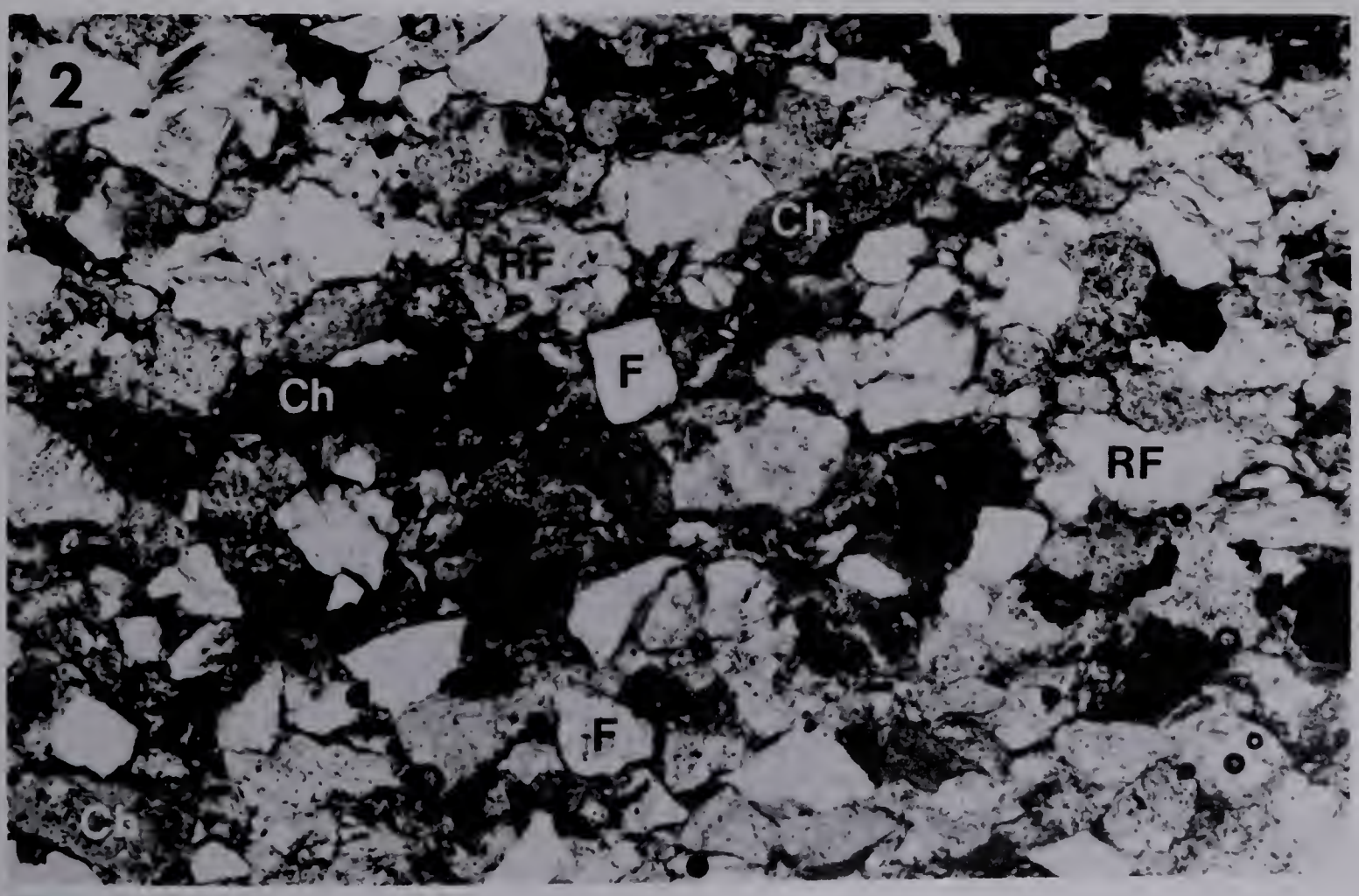
2
Ch
RF
F
Ch
RF
F
Ch
300μm

PLATE 4: Bulk Mineralogy

1. The detrital shape of some quartz grains is defined by a thin line of abundant inclusions trapped at the boundary between detrital and authigenic quartz (short arrow, right side of thin section photomicrograph). Other quartz overgrowths produce an interlocking of quartz grains (long arrows, left side of photomicrograph) such that original detrital shape is not obvious. Plane polarized light. Scale bar is 100 micrometres.

2. Thin section photomicrographs showing:
(a) microcrystalline chert. Plane polarized light.
(b) macrocrystalline chert. Crossed nicols.
(c) chalcedonic chert. Crossed nicols.
Scale bar is 100 micrometres.

3. Thin section photomicrograph showing a deformed siltstone fragment (RF). Plane polarized light. Scale bar is 100 micrometres.

4. Thin section photomicrograph showing a deformed argillaceous rock fragment (RF). Note the lack of intergranular pore space associated with the rock fragment. Plane polarized light. Scale bar is 100 micrometres.


4
RF

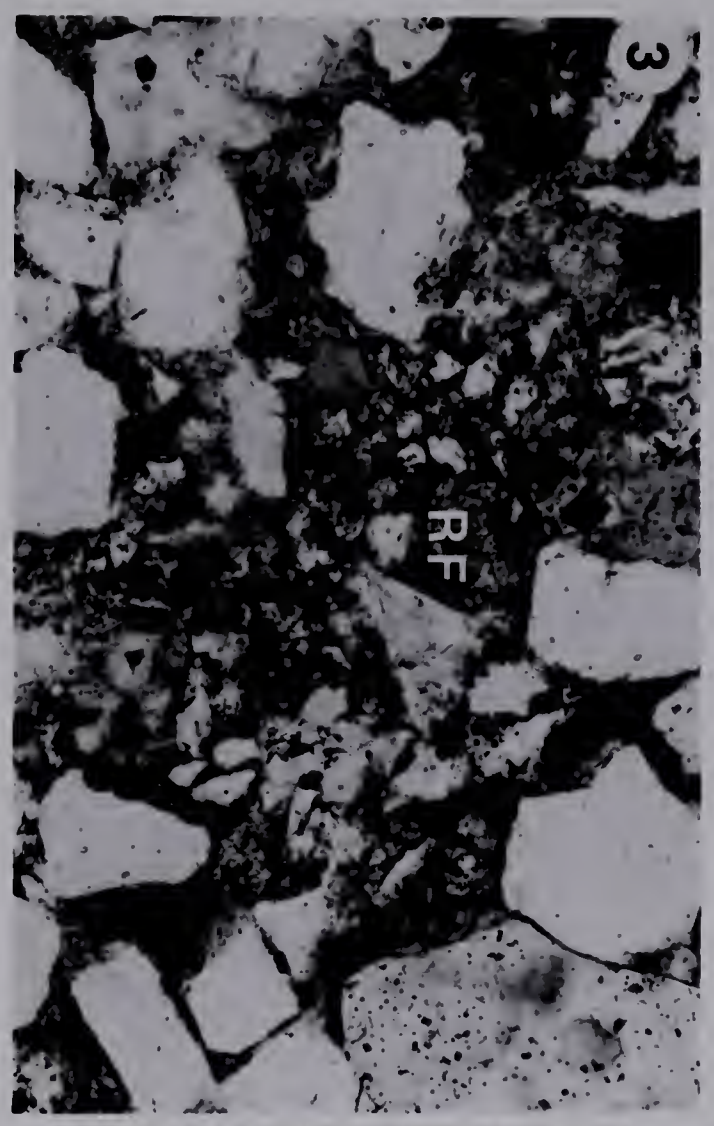
3
RF

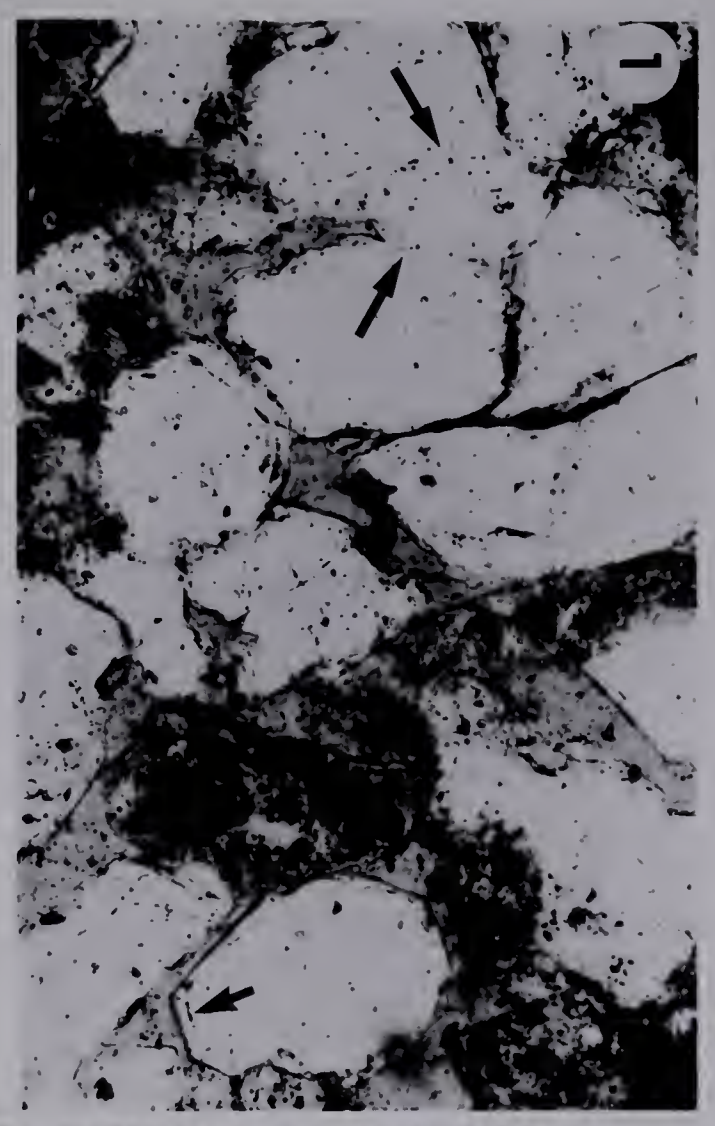
1


c


b

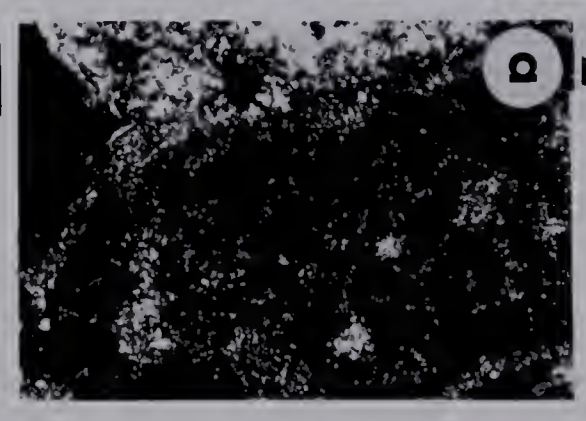
a

PLATE 5: Bulk Mineralogy and Texture of the Argillaceous Sandstone, Facies 3

1. Thin section photomicrograph showing the skeletal framework of a corroded feldspar (F). Note the secondary porosity (P) created by the corrosion of the grain. Plane polarized light.

2. Thin section photomicrograph showing carbonate grains (dolomite or siderite). The black arrow (upper left) points to a median grain sized zone of carbonate which has interlocking contacts with adjacent grains. The interlocking contacts may be either the result of remobilization of a carbonate grain or due to a combination of both quartz and carbonate overgrowths. The white arrows point to a carbonate zone which is a larger than median grain size. Contacts with adjacent grains are interlocking and this carbonate probably represents a very local early diagenetic cement. Plane polarized light.

3. SEM photomicrograph of pyrite (Py) associated with clay on a pore wall.

4. SEM photomicrograph of an organic structure replaced by pyrite (Py), subfacies 3a.

5. SEM photomicrograph of a very argillaceous sample from facies 3. Masses of very fine kaolinite coat the grains and fill the pores.

6. Thin section photomicrograph showing a silt–size quartz and clay matrix surrounding sand–sized grains, quartz (Q), chert (Ch). Plane polarized light.

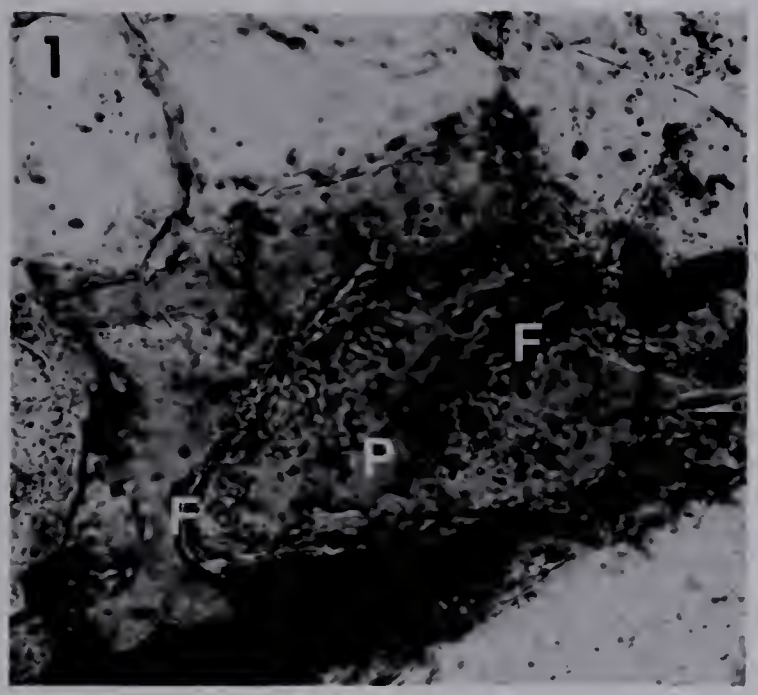

100 µm

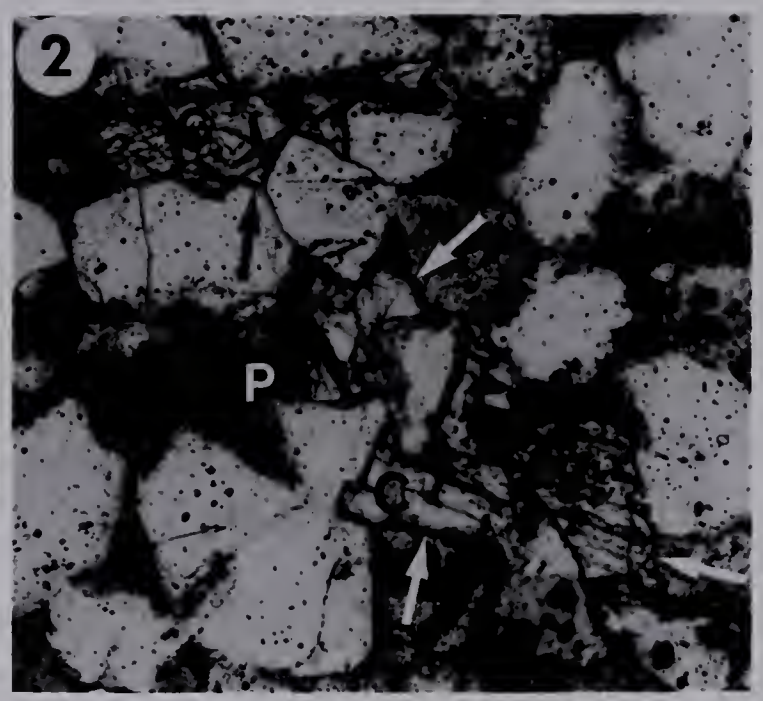

100 µm

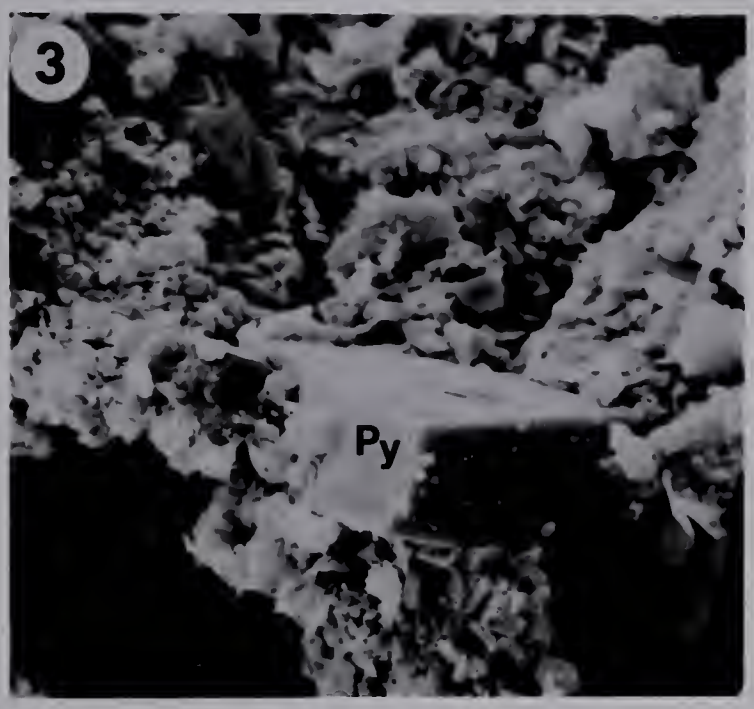

20 µm

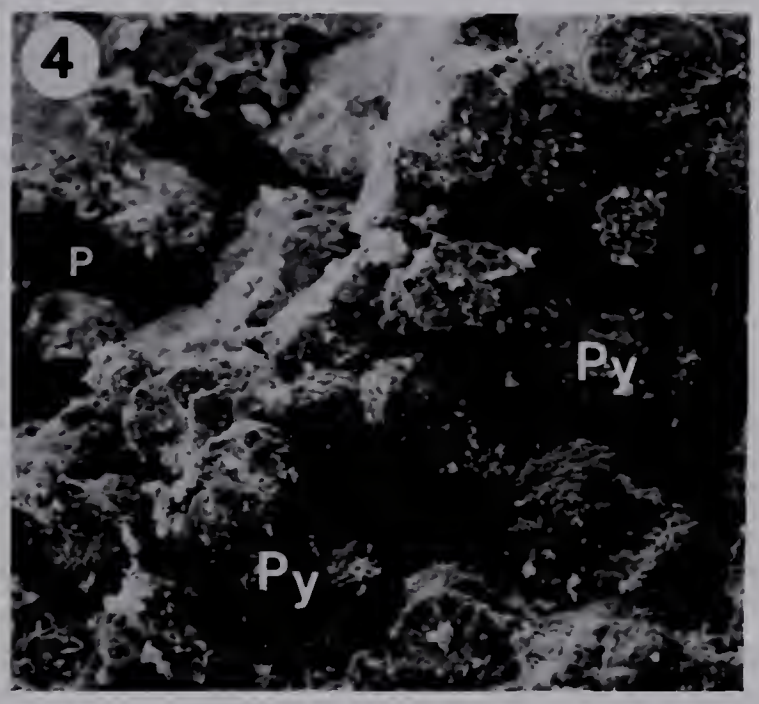

100 µm

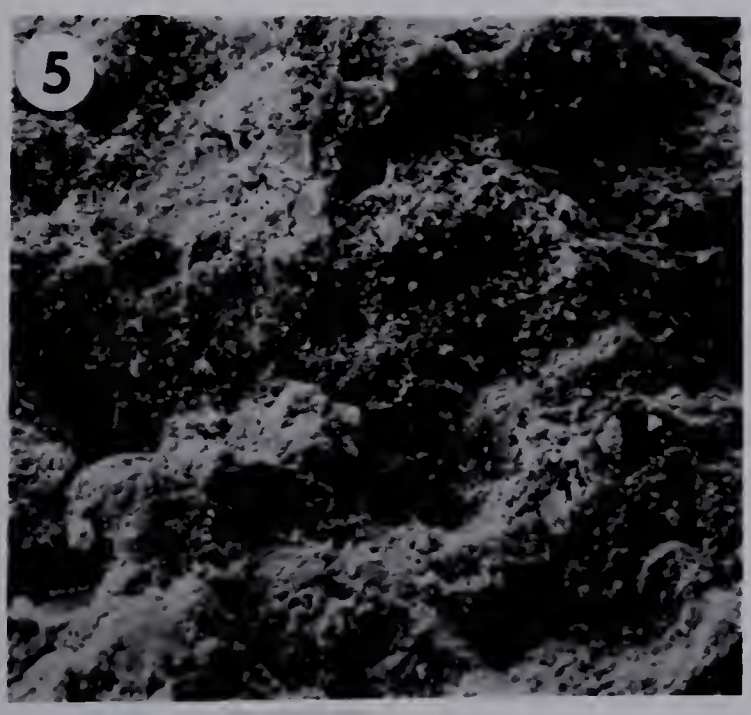

200 µm

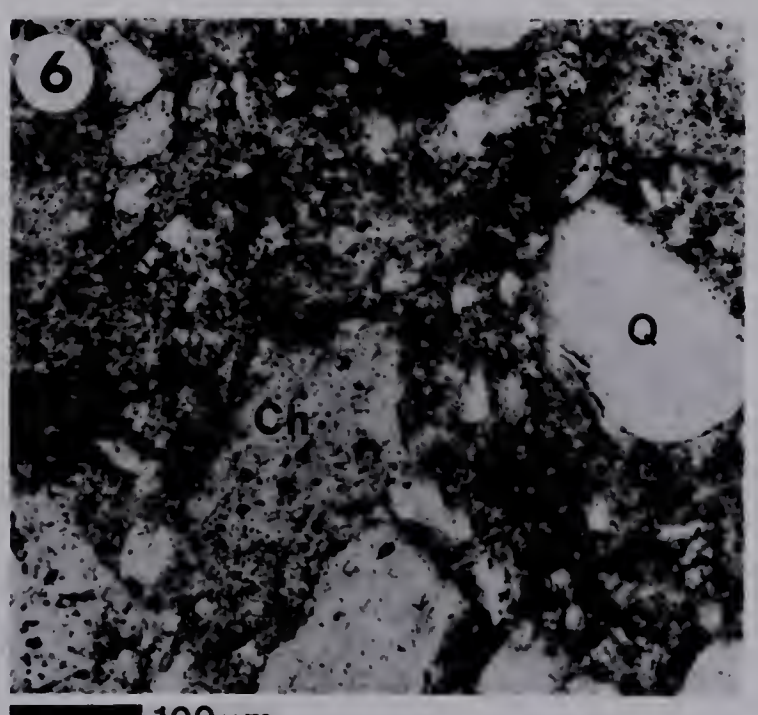

100 µm

PLATE 6: Pore Space Reduction by Kaolinite and Quartz

1. SEM photomicrograph showing a sheet composed of very fine clay attached to a detrital grain and extending into the pore space.

2. SEM photomicrograph showing the majority of pore spce filled by fine detrital kaolinite (dK). Most of the remaining pore space is filled by authigenic kaolinite (aK) and quartz overgrowths (Q).

3. SEM photomicrograph of large, authigenic, vermicular kaolinite (vK) filling much of the pore space. Note the smaller vermicular kaolinite (white arrow) on the surface of the large kaolinite.

4. SEM photomicrograph showing the occlusion of porosity by vermicular kaolinite (vK) and quartz overgrowths (Q). Note the smaller authigenic kaolinite (arrows) sitting on the larger forms.

5. SEM photomicrograph showing a mass of kaolinite booklets (K) sitting on quartz overgrowths (Q) and reducing pore space. This kaolinite–quartz relationship indicates that kaolinite formed after completion of the quartz overgrowth.

6. SEM photomicrograph showing a silt–sized cluster of authigenic quartz (Q) and kaolinite (K) reducing the pore size. This kaolinite–quartz relationship suggests that quartz and kaolinite grew at approximately the same time.

20µm

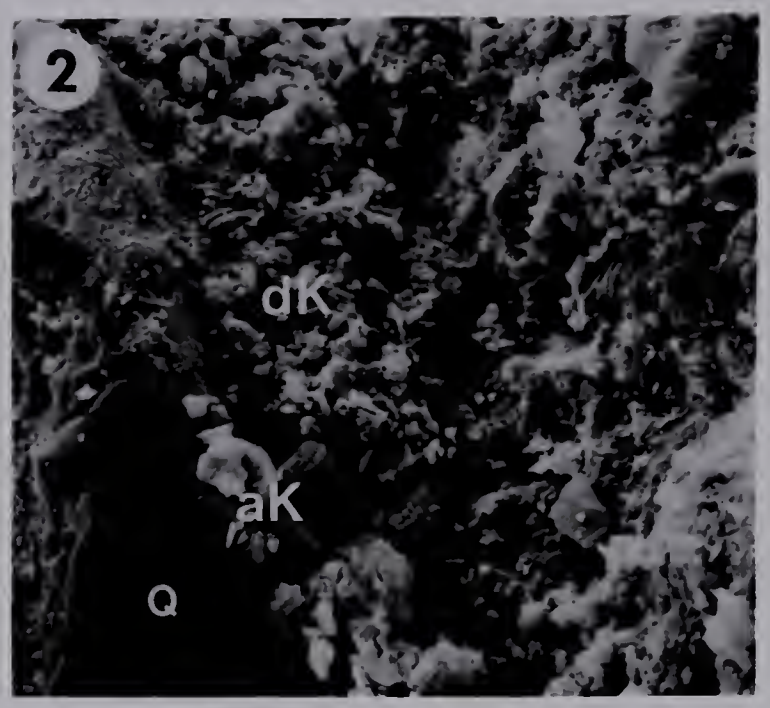

40µm

20µm

40µm

4µm

10µm

PLATE 7: **Morphologies of Illite and Smectite**

1. SEM photomicrograph of a clay ridge on a detrital grain. This clay ridge has an illitic component but may contain very fine detrital kaolinite or a mixed layer illite–smectite.

2. SEM photomicrograph of a very fine grained, delicate clay coating (white arrow) on a kaolinite booklet and extending across a pore space. This authigenic clay coating is probably illite or interstratified illite–smectite..

3. SEM photomicrograph showing a rare occurrence of smectite in a honeycomb–like growth habit (white arrow).

4. SEM photomicrograph of a sample with approximately 5 per cent smectite in the clay fraction. Note the abundance of clay ridges on the detrital grains.

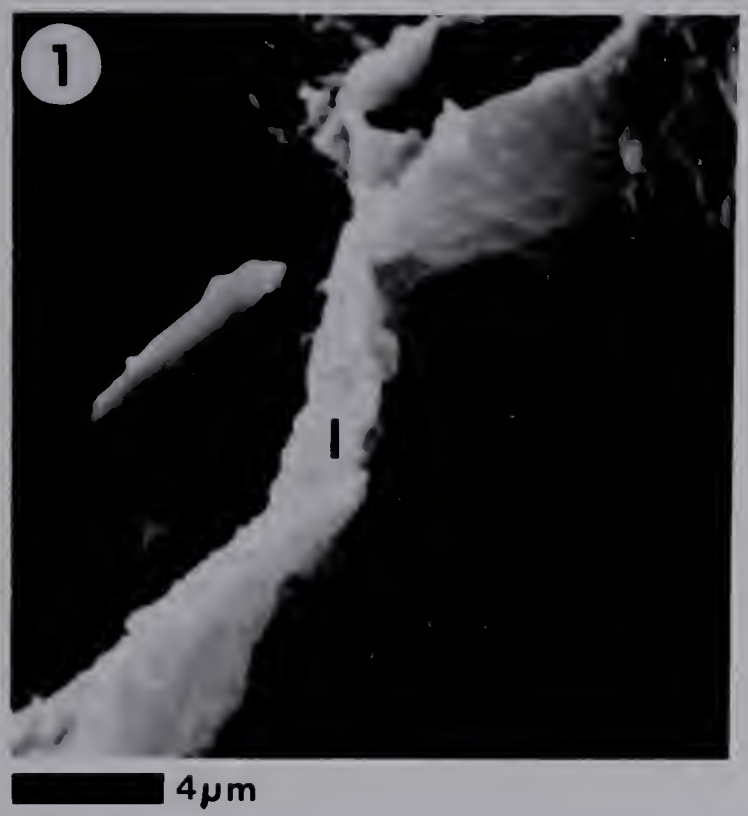
1
I
4μm

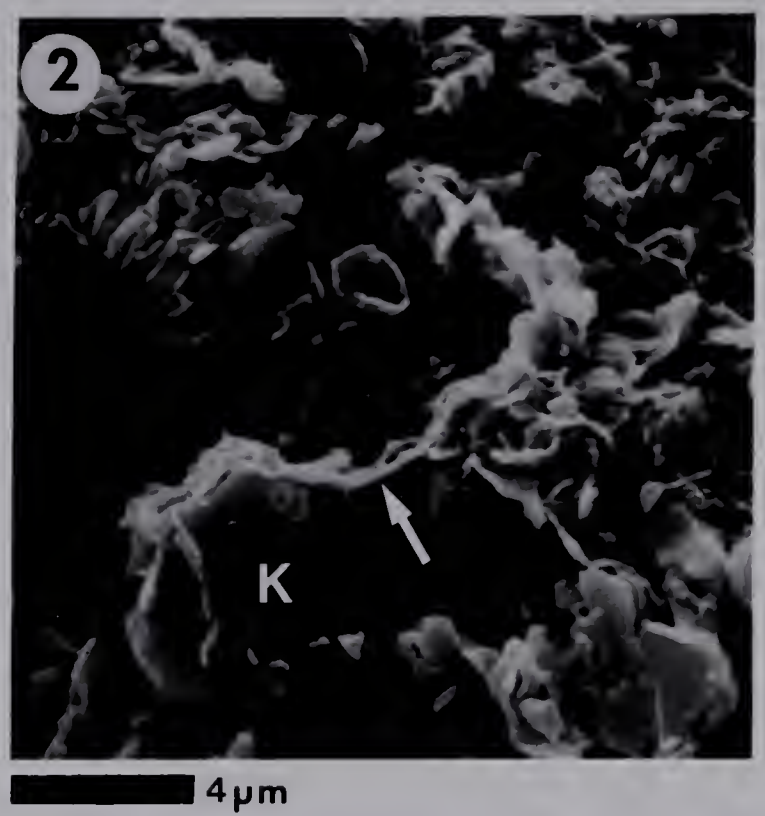
2
K
4μm

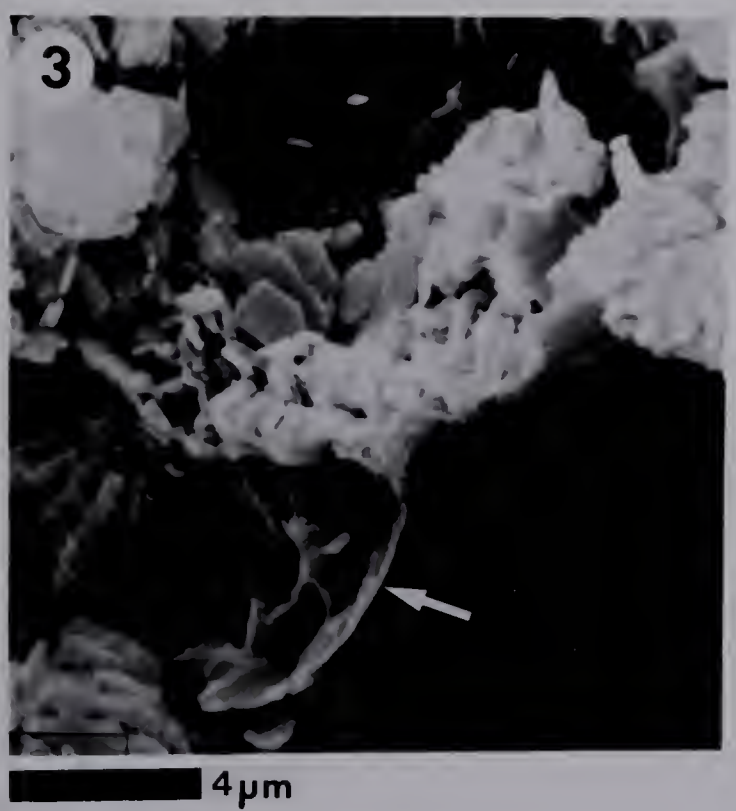
3
4μm

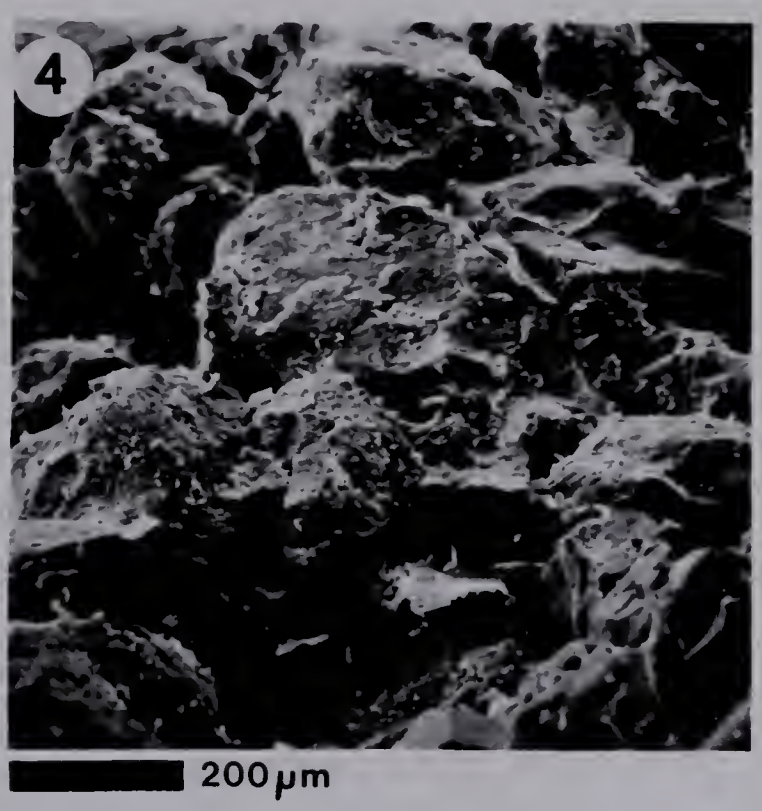
4
200μm

PLATE 8: Paragenetic Sequence

1. Thin section photomicrograph of a calcite-cemented sandstone. Dark material surrounding grains is calcite cement (C). Note the loose grain packing with few grain-to-grain contacts, and the lack of clay rims around grains. This sandstone was probably cemented very soon after sedimentation. Plane polarized light.

2. Thin section photomicrograph showing a close-up of the calcite cement (C). Note the coarse texture of the cement. The dark patches in the cement are zones which have stained a darker pink. These zones have fewer impurities than the lighter pink patches and may represent partial recrystallization of the early calcite cement. Crossed nicols.

3. SEM photomicrograph showing a close association of kaolinite (K) and quartz overgrowths (Q). The arrow points to a zone where the presence of the kaolinite inhibited completion of the quartz overgrowth. The quartz overgrowth probably began forming before the kaolinite grew, but continued after kaolinite formation.

4. SEM photomicrograph showing a kaolinite booklet (K) embedded in calcite cement (C). The kaolinite was present at the time of carbonate cementation.

5. SEM photomicrograph showing kaolinite (K) in the pore space created by feldspar (F) dissolution. This association of kaolinite with the corroded feldspar grain suggests that kaolinite was formed as a result of the feldspar dissolution. An earlier stage kaolinite (black K) grew on the uncorroded feldspar surface.

6. SEM photomicrograph of calcite cubes in the pore space created by dissolution of feldspar. This association indicates that calcite crystals grew after feldspar dissolution.

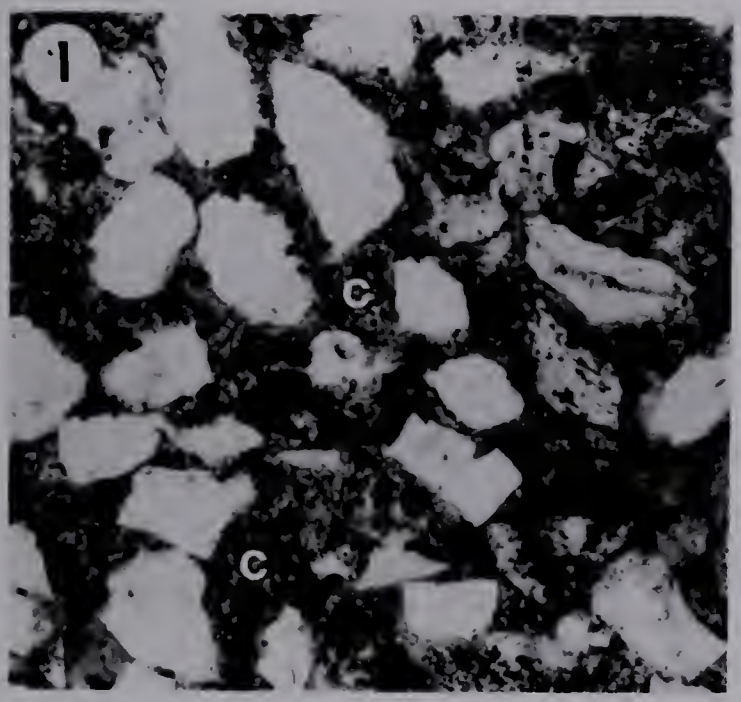

300 µm

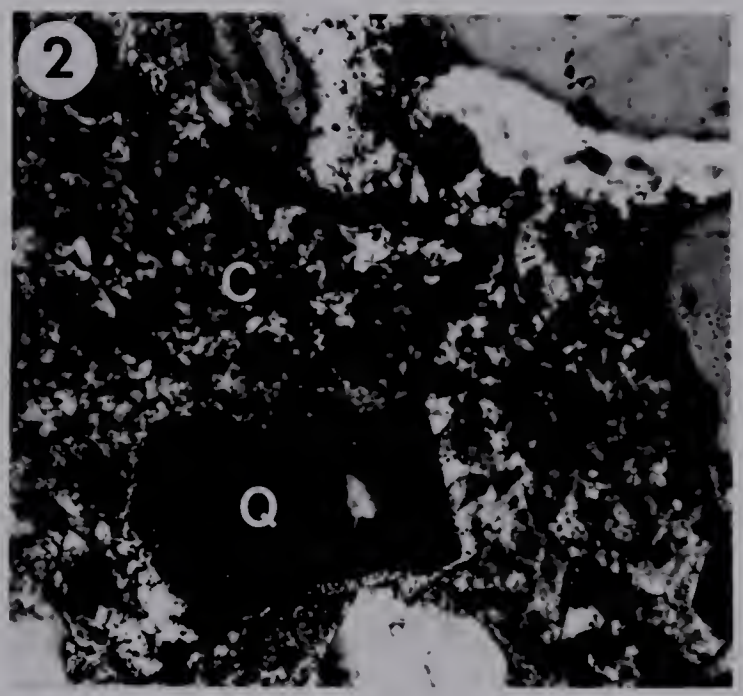

100 µm

4 µm

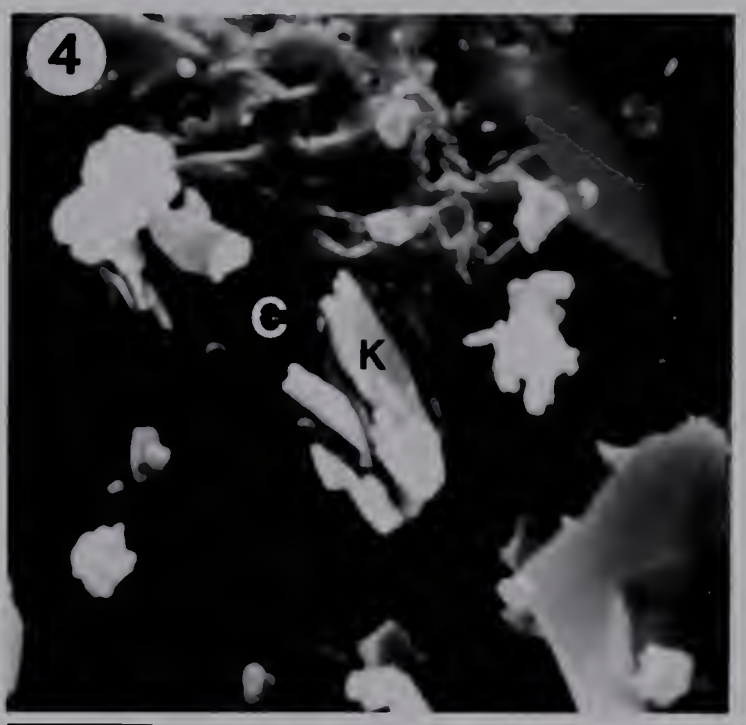

4 µm

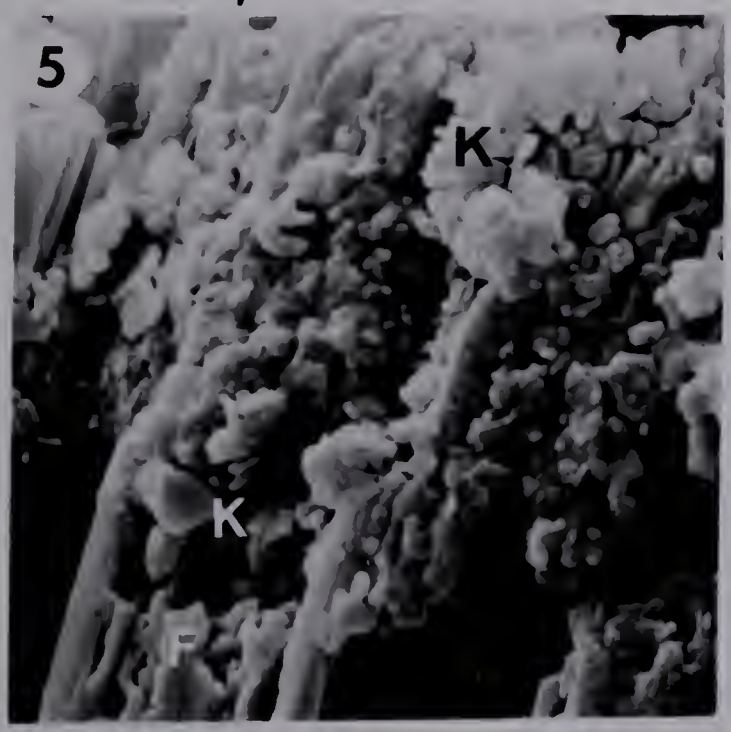

4 µm

4 µm

PLATE 9: **Pore Morphology**

1. SEM photomicrograph of a sample from the laminated facies 4. Note the good porosity, slightly reduced by quartz overgrowths and scattered clusters of authigenic clays.

2. SEM photomicrograph showing a typical clean pore from a sample representing facies 4. The pore space has been reduced in size slightly by local clusters of authigenic kaolinite (aK) and quartz overgrowths (Q).

3. Thin section photomicrograph showing a pore space (P) lined by masses of authigenic kaolinite (aK). Plane polarized light.

4. SEM photomicrograph showing the occlusion of pore space by quartz overgrowths (Q).

5. SEM photomicrographs showing a cluster of kaolinite coating the grain and extending across the pore to form a pore bridge and permeability barrier.

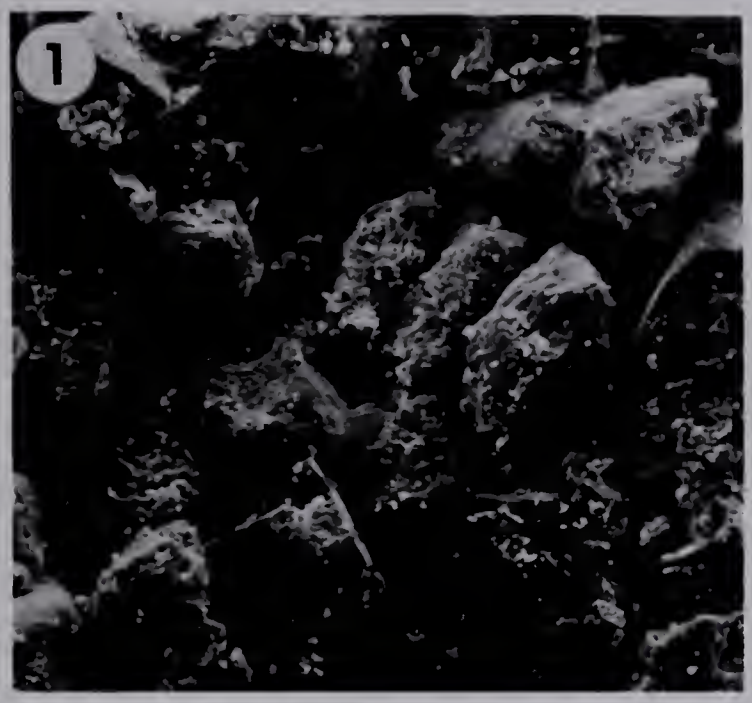
1
200µm

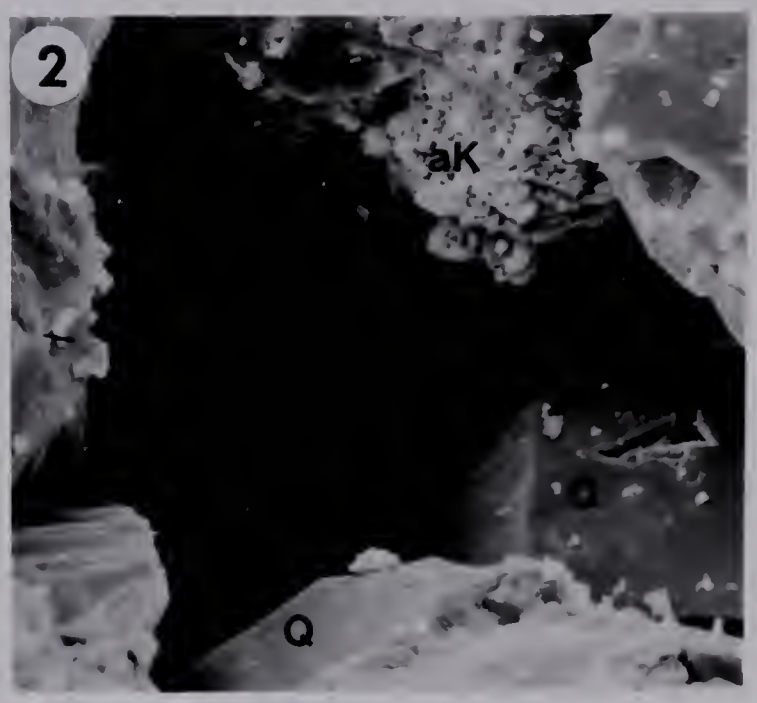
2
aK
Q
Q
40µm

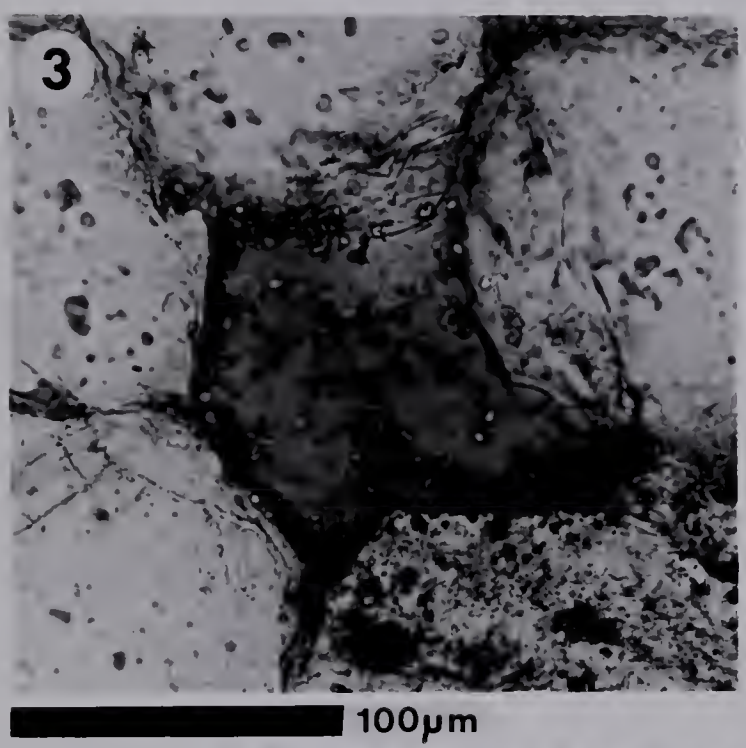
3
100µm


4
Q
40µm

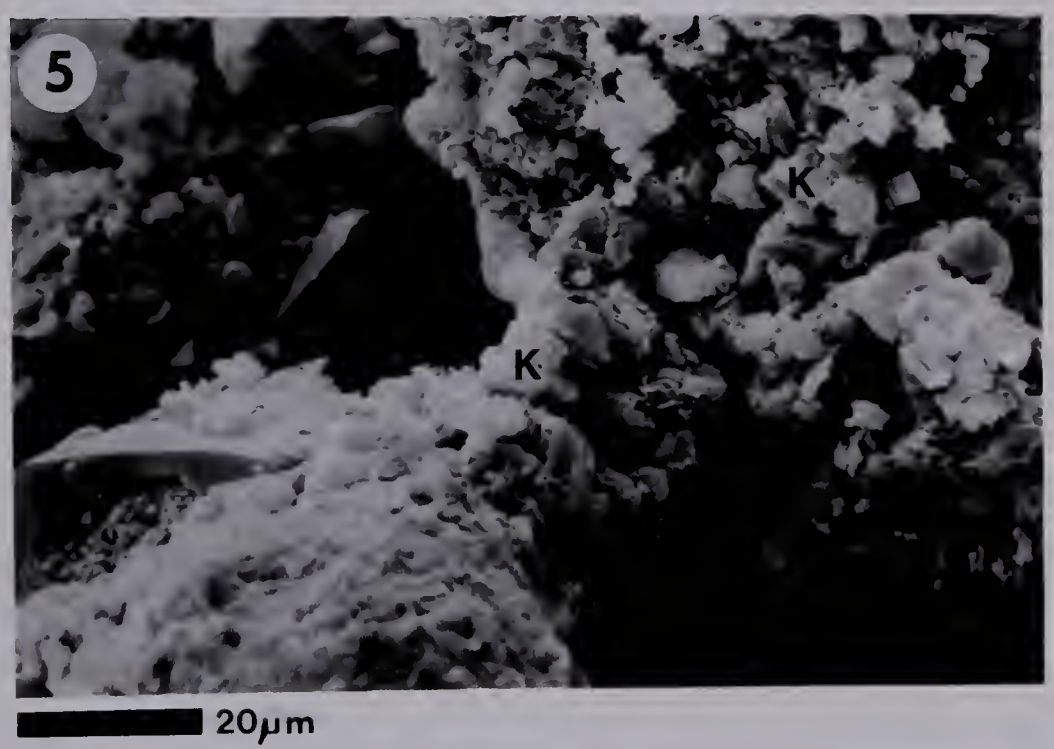
5
K
K
20µm

IX. REFERENCES

AIPEA nomenclature committee (1980): Summary of recommendations of AIPEA nomenclature committee; Clays and Clay Minerals, Vol. 28, No. I, p. 73-78.

Alberta Society of Petroleum Geologists (1960): Lexicon of Geologic Names in the Western Canada Sedimentary Basin and Arctic Archipelago; John D. McAra Limited, Calgary, 380p.

Almon, W.R. and Davies, D.K. (1979): Regional diagenetic trends in the Lower Cretaceous Muddy Sandstone, Powder River Basin in Peter A. Scholle and Paul R. Schluger (eds.) Aspects of Diagenesis; SEPM Special Publication No. 26, p. 379-400.

Barnhisel, R.I. (1977): Chlorites and hydroxy interlayered vermiculite and smectite in J.B. Dixon and S.B. Weed (eds.) Minerals in Soil Environments, Soil Society of America, Madison, Wisconsin, p. 331-356.

Bayliss, P. and Levinson, A.A. (1971): Low temperature synthesis from dolomite or calcite, quartz and kaolinite; Clays and Clay Minerals, Vol. 9, p. 109-114.

Bennion, D.W., Moore, R.G. and Donnelly, J.K. (1979): Alberta Energy Company test number 4, Department of Chemical Engineering, University of Calgary.

Bernard, H.A., Le Blanc, R.J. and Major, C.F. (1962): Recent and Pleistocene geology of southeast Texas: Geology of Gulf Coast and central Texas guidebook; Houston Geological Survey, p. 175-224.

Biscaye, Pierre E. (1965): Mineralogy and sedimentation of recent deep-sea clay in the Atlantic Ocean and adjacent seas and oceans; Geological Society of American Bulletin, Vol. 76, p. 803-832.

Blatt, Harvey (1979): Diagenetic processes in sandstones in Peter A. Scholle and Paul R. Schluger (eds.) Aspects of Diagenesis; SEPM Special Publication No. 26, p. 141-157.

Boon, J.A. (1977): Fluid-rock interactions during steam injection in D.A. Redford and A.G. Winestock (eds.); The Oil Sands of Canada-Venezuela 1977, The Canadian Institute of Mining and Metallurgy, p. 133-138.

Brindley, G.W. (1980): Order-disorder in clay mineral structure in G.W. Brindley and G. Brown (eds.); Crystal Structures of Clay Minerals and their X-ray Identification, Mineralogical Society, London, 495p.

Brown, Rodney S. (1976): Computer analysis of sand and petroleum distribution in the Mannville Group, Turin area, Southern Alberta; University of Alberta M.Sc. thesis, 104p.

Carter, Charles, H. (1978): A regressive barrier and barrier-protected deposit:

Depositional environments and geographic setting of the Late Tertiary Cohansey Sand; Journal of Sedimentary Petrology, Vol. 48, No. 3, p. 933-950.

Conybeare, C.E.B. (1976): Geomorphology of Oil and Gas Fields In Sandstone Bodies; Developments in Petroleum Science, 4; Elsevier Scientific Publishing Company, New York, p. 231-233.

Curray, J.R. and Moore, D.G. (1964): Holocene regressive littoral sand, Costa De Nayarit, Mexico; in L.M.J.U. Van Straaten (ed.) Deltaic and Shallow Marine Deposits, Developments in Sedimentology, I. Elsevier, Amsterdam, p. 76-82.

Day, John J., McGlothlin, B.B., and Huitt, J.L. (1967): Laboratory study of rock softening and means of prevention during steam or hot water injection; Journal of Petroleum Technology; Vol. 19, p. 703-711.

Dixon, James (1977): The Lower Cretaceous Atkinson Point Formation on the Tuktoyaktuk Peninsula, N.W.T. A coastal fan-delta to marine sequence; Bulletin of Canadian Petroleum Geology; Vol. 27, No. 2, 163-182.

Dypvik, H. and J. Vollset (1979): Petrology and diagenesis of Jurassic sandstones from Norwegian Danish Basin, North Sea; American Association of Petroleum Geologists Bulletin, Vol. 63, No. 2, p. 182-193.

Elliott, T. (1979): Clastic shorelines in H.G. Reading (ed.); Sedimentary Environments and Facies, Elsevier, New York, p. 143-177.

Fanning, D.S. and Keramidas, V.Z. (1977): Micas in J.B. Dixon and S.B. Weed (eds.); Minerals in Soil Environments, Soil Science Society of America, Madison, Wisconsin, p. 195-258.

Folk, R.I. (1968): Petrology of sedimentary rocks; Hemphillis Austin, Texas, 170p.

Galloway, William, E. (1979): Diagenetic control on reservoir quality in arc-derived sandstones: Implications for petroleum exploration in Peter A. Scholle and Paul R. Schluger (eds.) Aspects of Diagenesis; SEPM Special Publication No. 26, p. 251-262.

Glaister, R.P. (1959): Lower Cretaceous of Southern Alberta and adjoining areas; Bulletin of the American Association of Petroleum Geologists, Vol. 43, No. 3, p. 590-640.

Gray, D.H. and Rex, R.W. (1966): Formation damage in sandstones caused by clay dispersion and migration; 14th National Conference on Clays and Clay Minerals, p. 355-366.

Grim, R.E. and Johns, W.D. (1954): Clay mineral investigation of sediments in the northern Gulf of Mexico; Clays and Clay Minerals, National Academic Science - National Research Council Publication 327, p. 81-103.

Harmes, J.C., Southard, J.B., Spearing, D.R. and Walker, R.G. (1975): Depositional environments as interpreted from primary sedimentary structures and stratification sequences; SEPM Short Course No. 2, Dallas, 161p.

Hayes, B.J.R. (1982): Upper Jurassic and Lower Cretaceous stratigraphy of Southern Alberta and North-central Montana. University of Alberta Ph.D. thesis, 234p.

Hayes, M.O. and Kana, T.W. (1976): Terrigenous Clastic Depositional Environments, Some Modern Examples: American Association of Petroleum Geologists Field Course, University of South Carolina, Technical Report No. 11-CRD, 315p.

Herbaly, Elmer, L (1974): Petroleum geology of Sweetgrass Arch, Alberta; The American Association of Petroleum Geologists Bulletin, Vol. 58, No. 11, p. 2227-2244.

Hermanson, S.W., Hopkins, J.C. and Lawton, D.C. (1982): Upper Mannville "Glauconitic" channels, Little Bow area, Alberta: Geologic models for seismic exploration: Abstract in Book of Abstracts, AAPG Annual Convention, June 27-30, p. 62.

Holmes, I.G. and Rivard, Y.A. (1976): A marine barrier island bar, Jenner Field, Southeastern Alberta; 4th Core Conference, Alberta Society of Petroleum Geologists, Calgary, p. 44-61.

Hoyt, J.H. and Weimer, R.J. (1963): Comparison of modern and ancient beaches, central Georgia coast; American Association of Petroleum Geologists Bulletin, Vol. 47, p. 529-531.

Jackson, M.L. (1979): Soil Chemical Analysis - Advanced Course 2nd Edition, 11th printing. Published by author, Madison, Wisconsin, 895p.

Kraft, J.C. (1971): Sedimentary facies patterns and geologic history of a Holocene marine transgression; Geological Society of America Bulletin, Vol. 82, p. 2131-2158.

Krumbein, W.C. and Sloss, L.L. (1963): Stratigraphy and Sedimentation, Second Edition; W.H. Freeman and Company, San Francisco, 660p.

Le Blanc, R.J. and Hodgson, W.D. (1959): Origin and development of the Texas shoreline; Transactions of the Gulf-Coast Geological Society, Vol. 9, p. 197-220.

Levinson, A.A. and Vian, R.W. (1966): The hydrothermal synthesis of montmorillonite group minerals from kaolinite, quartz, and various carbonates; The American Mineralogist, Vol. 51, p. 495-498.

Loranger, D.M. (1951): Useful Blairmore microfossil zone in central and southern Alberta, Canada; American Association of Petroleum Geologists Bulletin, Vol. 35, No. 11, p. 2348-2367.

McCubbin, D.G. (1982): Barrier-island and strand-plain facies; in P.A. Scholle and D. Spearing (eds.); Sandstone Depositional Environments, American Association

of Petroleum Geologists, Tulsa, p. 247-279.

Merino, Enrique (1975): Diagenesis in Tertiary sandstones from Kettleman North Dome, California. I. Diagenetic mineralogy; Journal of Sedimentary Petrology, Vol. 45, No. 1, p. 320-336.

Perry, C. and Gillott, J.E. (1979): The formation and behaviour of montorillonite during the use of wet forward combustion in the Alberta oil sand deposits; Bulletin of Canadian Petroleum Geology, Vol. 27, No. 3, p. 314-325.

Pittman, Edward D. (1979): Porosity, diagenesis and productive capability of sandstone reservoirs;in Peter A. Schoole and Paul R. Schluger (eds.) Aspects of Diagenesis; SEPM Special Publication No.26, p. 159-173.

Reinson, G.E. (1980): Facies Model 6. Barrier island systems; in Walker, R.G. (ed.), Facies Models, p. 57-74.

Rich, C.I. (1968): Hydroxy interlayers in expansible layer silicates; Clays and Clay Minerals, vol. 16, p. 15-30.

Rudkin, R.A. (1964): Chapter 11 Lower Cretaceous; in R.G. McCrossan and R.P. Glaister (eds.); Geological History of Western Canada, The Alberta Society of Petroleum Geologists, Calgary, p. 156-168.

Scholle, P.A. (1979): A Color Illustrated Guide to Constituents, Textures, Cements, and Porosities of Sandstones and Associated Rocks, American Association of Petroleum Geologists, Tulsa, 201p.

Shelton, J.W. (1964): Authigenic kaolinite in sandstone; Journal of Sedimentary Petrology, V. 34, p. 102-111.

Shepard, F.P. (1960): Gulf Coast barriers; in F.P. Shepard, F.B. Phleger and Tj. H. van Andel (eds.) Recent Sediments, Northwest Gulf of Mexico, American Association of Petroleum Geologists, Tulsa, p. 197-220.

Shepard, F.P. (1973): Beaches and shore processes in Submarine Geology, Third Edition, Harper & Row, Publishers, New York, p. 123-161.

Thompson, Graham, R. and Hower, John (1975): The mineralogy of glauconite; Clays and Clay Minerals, Vol. 23, p. 289-300.

Tovell, W.M. (1958): The development of the Sweetgrass Arch, southern Alberta, Proceedings of the Geological Association Canada, Vol. 10, p. 19-30.

Tye, Robert S. (1981): Geomorphic evolution and stratigraphic framework of Price and Capers Inlets, South Carolina, University of South Carolina M.Sc. Thesis, 96p.

Waldorf, D.M. (1965): Effect of steam on permeabilities of water-sensitive formations; Journal of Petroleum Technology, p. 1219-1222.

Wilson, M.D. and Pittman, E.D. (1977): Authigenic clays in sandstones: recognition and influence on reservoir properties and paleoenvironmental analysis; Journal of Sedimentary Petrology, Vol. 47, No. 1, p. 3-31.

Workman, L.E. (1958): Glauconitic Sandstone in Southern Alberta; Journal of Alberta Society of Petroleum Geologists, Vol. 6, p. 237-245.

X. APPENDICES

Appendix A: Core Logs for Wells from the SHOP Project (see attached pocket)

Appendix B: Analytical Methods for Detailed XRD Analyses

Samples were gently crushed by hand and treated with a 3 per cent bleach solution (sodium hypochlorite) at 50°C for three days to remove any organic phases. Excess hypochlorite solution was then removed by repeated washings (high speed centrifugation). The mineral material was then dispersed in distilled water using an ultrasonic probe and allowed to settle in columns for the appropriate period of time[9] to extract the particles with an equivalent spherical diameter of <2 micrometres. The settling procedure was repeated three times for each sample and the <2 micrometre material collected after each step combined. The <2 micrometre material was treated with the 3 per cent sodium hypochlorite solution again at 50°C for two days in order to destroy residual organic materials and then repeatedly washed. The sample was split into fractions and separate portions saturated with K^+ and Ca^{2+}. [10] Once saturated, the <2 micrometre material was thoroughly washed, freeze-dried, and then precipitated by suction onto a porcelain disc. The <2 micrometre Ca- and K-discs were analyzed on the X-ray diffractometer using the following analytical conditions:

1. Co K-alpha radiation (obtained by means of a graphite monochromater);
2. 1 degree divergent slit;
3. 1 degree two theta/minute at 600 mm/h;
4. Time constant = 2;
5. 50KV, 20mA;

The following X-ray patterns were obtained for the <2 micrometre samples:

1. Ca-disc at 54% relative humidity, 2-35 degrees two theta;
2. Ca-disc glycolated, 2-55 degrees two theta;
3. K-disc at 0% relative humidity, 2-35 degrees two theta;
4. K-disc at 54% relative humidity, 2-35 degrees two theta;
5. K-disc at 300°C, 2-35 degrees two theta;
6. K-disc at 550°C, 2-35 degrees two theta.

In all cases humidity conditions were controlled both during sample equilibrium and during

---

[9] Settling time was calculated by means of Stokes' law for streamline or viscous flow about a falling spherical body combined with the differential specific gravity and the gravitational constant (Jackson, 1979).

[10] The (001) spacings and intensities of smectite and vermiculite are decreased by potassium saturation and increased by calcium saturation (Jackson, 1979). Thus, XRD analyses of both Ca^{2+} and K^+ portions are valuable for the identification of these minerals.

the analysis of the sample on the diffractometer. The glycolated Ca–disc was prepared by placing the Ca–saturated disc in an enclosed ethylene glycol environment. The disc was heated in this environment at 65°C for 14 hours and then left for one day to allow the ethylene glycol to fully penetrate into the clay structures.

Relative percentages of kaolinite, illite and smectite were estimated using the weighted peak–area method described in Biscaye (1965). The peaks and weighting factors used were: the area of the 17A glycolated peak for smectite; four time (4X) the 10A peak area (glycolated trace) for illite; and twice (2X) the 7A peak area for kaolinite. Since kaolinite and chlorite have a common 7A peak, the 3.5A peaks for these minerals are used to determine the relative proportion of kaolinite and chlorite. The kaolinite peak at 3.58A and the chlorite at 3.54A form a couplet which can sometimes be resolved (Biscaye, 1975). In the clay samples from the Glauconitic Sandstone there is generally no indication of a couplet at 3.5A. Thus, the 7A peak is calculated as 100 per cent kaolinite.

NAME AEC et al P2 SUFFIELD

Alberta
RESEARCH COUNCIL
OGICAL SURVEY

aturation

apart
ions
detached
nail
detached

s around

ECOVERY)

DEPTH – TOPS SAMPLES	GRAIN SIZE	LITHOLOGY	SEDIMENTARY STRUCTURES	ORGANIC MATTER	BEDDING THICKNESS	CEMENT/ACC. MINERALS	DESCRIPTION	INDURATION	SATURATION	CORE/CDRE DEPTH (RECOVERY)
										1 / 908.00–917.00 (9.00/9.00)
										2 / 917.00–925.00 (7.50/8.00)
										3 / 925.00–930.00 (5.50/5.00)

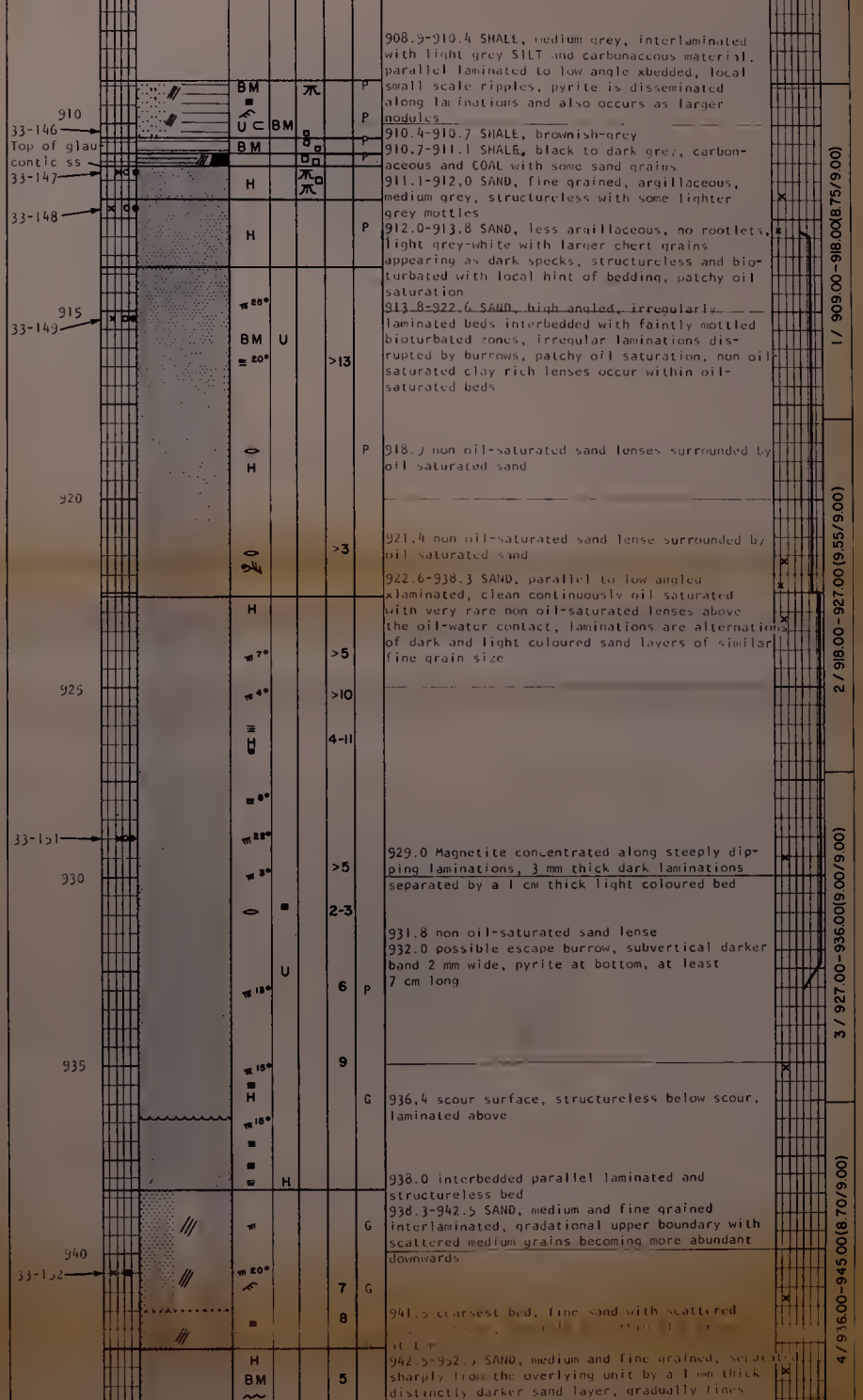
908.3-910.4 SHALE, medium grey, interlaminated with light grey SILT and carbonaceous material, parallel laminated to low angle xbedded, local small scale ripples, pyrite is disseminated along laminations and also occurs as larger nodules
910
33-146
Top of glauconitic ss
33-147
910.4-910.7 SHALE, brownish-grey
910.7-911.1 SHALE, black to dark grey, carbonaceous and COAL with some sand grains
911.1-912.0 SAND, fine grained, argillaceous, medium grey, structureless with some lighter grey mottles
33-148
912.0-913.8 SAND, less argillaceous, no rootlets, light grey-white with larger chert grains appearing as dark specks, structureless and bioturbated with local hint of bedding, patchy oil saturation
915
33-149
913.8-922.6 SAND, high angled, irregularly laminated beds interbedded with faintly mottled bioturbated zones, irregular laminations disrupted by burrows, patchy oil saturation, non oil-saturated clay rich lenses occur within oil-saturated beds
918.3 non oil-saturated sand lenses surrounded by oil saturated sand
920
921.4 non oil-saturated sand lense surrounded by oil saturated sand
922.6-938.3 SAND, parallel to low angled xlaminated, clean continuously oil saturated with very rare non oil-saturated lenses above the oil-water contact, laminations are alternations of dark and light coloured sand layers of similar fine grain size
925
33-151
929.0 Magnetite concentrated along steeply dipping laminations, 3 mm thick dark laminations
930
separated by a 1 cm thick light coloured bed
931.8 non oil-saturated sand lense
932.0 possible escape burrow, subvertical darker band 2 mm wide, pyrite at bottom, at least 7 cm long
935
936.4 scour surface, structureless below scour, laminated above
938.0 interbedded parallel laminated and structureless bed
938.3-942.5 SAND, medium and fine grained interlaminated, gradational upper boundary with scattered medium grains becoming more abundant
940
33-152
downwards
941.5 coarsest bed, fine sand with scattered
942.5-952.5 SAND, medium and fine grained, separated sharply from the overlying unit by a 1 mm thick distinctly darker sand layer, gradually fines
1 / 909.00-918.00(8.75/9.00)
2 / 918.00-927.00(9.55/9.00)
3 / 927.00-936.00(9.00/9.00)
4 / 936.00-945.00(8.70/9.00)

34-156 Top of glauconitic ss
910
34-157
34-158
915
34-159
920
925
34-160
930
935
940
34-161
34-162

909.2-910.0 SHALE, sandy, dark grey, carbonaceous

910.0-911.0 SAND, very argillaceous, medium-light grey, structureless

911.0-922.6 SAND, less argillaceous than above, structureless to indistinctly high angled laminated, scattered clay-rich patches produce irregular patchy oil saturation

911.8-912.4 BRECCIA, fine grained laminated blocks similar to overlying and underlying sand, outlined by slightly coarser clay-rich sand fracture fill and matrix

913.5 Burrow at least 11.5 cm long, .4-1 cm wide, filled with similar sized lighter coloured sand, cuts through angled parallel laminations

919.0 medium grained sand lamination

922.6-937.3 SAND, fine grained, planar laminated to low angle xbedded, no obvious grain size change between laminations

932.5 Interbedded parallel laminated and structureless bed

937.3-941.7 SAND, medium and fine grained interlaminated, interbedded with fine grained sand, low angle to horizontal laminated, coarser beds vary from .5 cm thick to structureless 8 cm thick beds

941.2 poorly sorted coarse-fine sand interbedded with fine grained sand

941.7-954.3 SAND, fine grained, fining downward to very fine grained

Small quality broken slabs

Large proportion of the core has been cleaned

1 / 909.00-917.25 (7.70/8.25)

2 / 917.25-926.25 (7.25/9.00)

3 / 926.25-935.25 (7.85/9.00)

4 / 935.25-944.25 (9.00/9.00)

9.00)

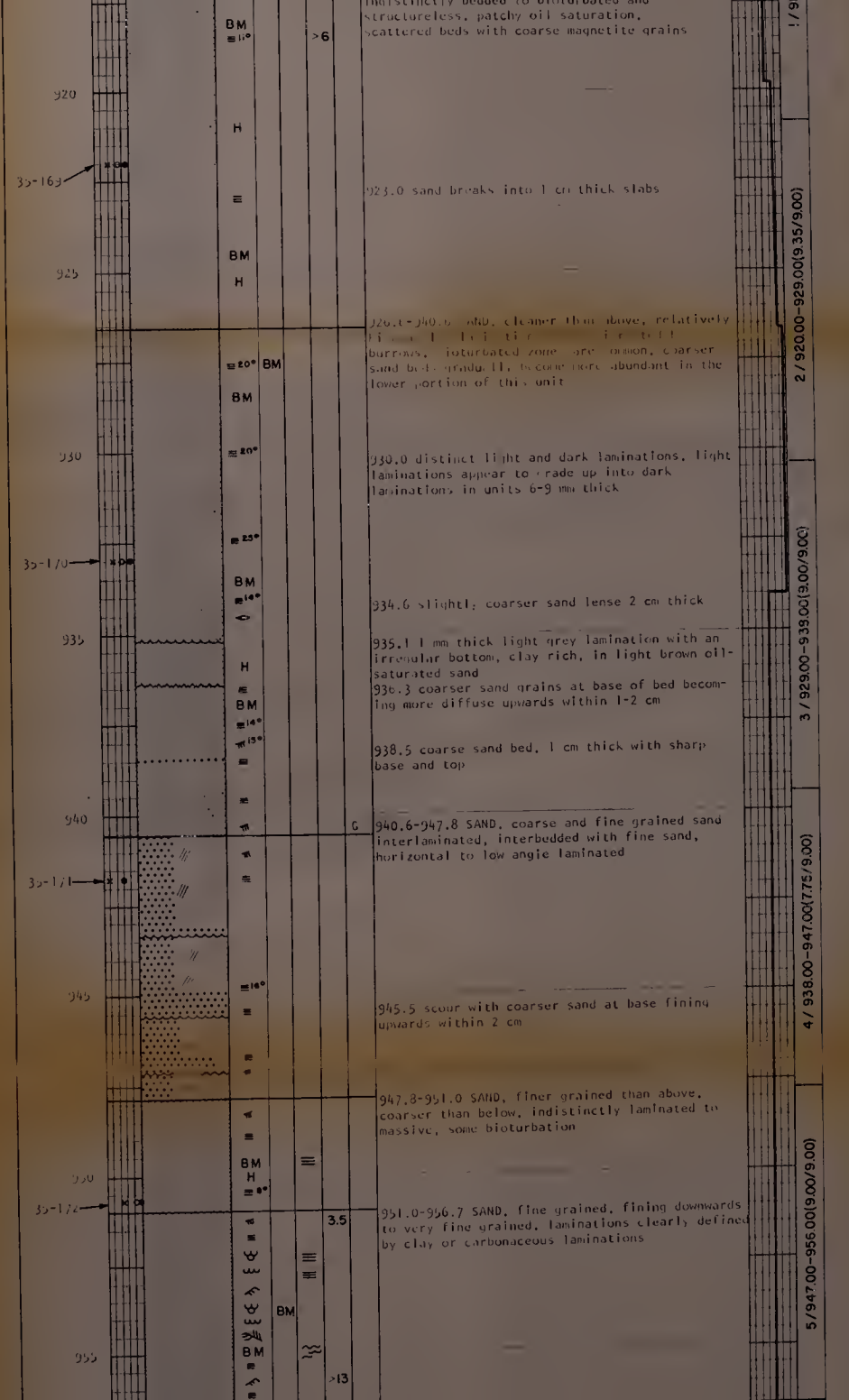
BM
>6
920
H
35-169
923.0 sand breaks into 1 cm thick slabs
925
BM
H
926.1-940.6 SAND, cleaner than above, relatively
burrows, bioturbated zone are common, coarser
sand beds gradually become more abundant in the
lower portion of this unit
BM
930
930.0 distinct light and dark laminations, light
laminations appear to grade up into dark
laminations in units 6-9 mm thick
35-170
BM
934.6 slightly coarser sand lense 2 cm thick
935
935.1 1 mm thick light grey lamination with an
irregular bottom, clay rich, in light brown oil-
saturated sand
936.3 coarser sand grains at base of bed becom-
ing more diffuse upwards within 1-2 cm
H
BM
938.5 coarse sand bed, 1 cm thick with sharp
base and top
940
C
940.6-947.8 SAND, coarse and fine grained sand
interlaminated, interbedded with fine sand,
horizontal to low angle laminated
35-171
945
945.5 scour with coarser sand at base fining
upwards within 2 cm
947.8-951.0 SAND, finer grained than above,
coarser than below, indistinctly laminated to
massive, some bioturbation
950
BM
H
35-172
3.5
951.0-956.7 SAND, fine grained, fining downwards
to very fine grained, laminations clearly defined
by clay or carbonaceous laminations
BM
955
BM
>13
1 / 9
2 / 920.00-929.00(9.35/9.00)
3 / 929.00-938.00(9.00/9.00)
4 / 938.00-947.00(7.75/9.00)
5 / 947.00-956.00(9.00/9.00)

DEPTH – TOPS SAMPLES	GRAIN SIZE	LITHOLOGY	SEDIMENTARY STRUCTURES (main / acc.)	ORGANIC MATTER	BEDDING THICKNESS	CEMENT/ACC MINERA	DESCRIPTION	INDURATION	SATURATION	CORE/CORE DEPTH (RECO

DESCRIPTION

NOTE. A complete detailed log of this core is impossible. Large portions of the core removed for analyses render the core incomplete. No structures can be seen in the rubbly or uncleaned oil saturated zones.

905

Top of glauconitic sandstone

906.0-910.0 SHALE, medium grey, interlaminated with light grey SILT. Lower portion of unit is well laminated and rippled, upper portion is structureless to laminated with carbonaceous rootlets disturbing laminations.

909.8 SHALE, sandy, carbonaceous, brown-black, with carbonaceous chips

910

37-166

910.0-921.1 SAND, very argillaceous, fine-grained with scattered medium grains. Top l n is light grey-white and has subvertical grooves probably created by roots. Below this the sand is slightly lighter in colour. Light grey clay is churned in with the sand. The sand gradually becomes less argillaceous downwards. Laminations occur at a relatively high angle 915.8 hint of lamination

915

37-167

920

9_1.1-_1.0 SAND, fine grained, fairly high angled laminations with some bioturbation

925

37-168

930

Sedimentary structures: BM, H, U, NV, 15°, RUBBLE, 20°

Core/core depth:

1 / 907.00-916.00(8.00/9.00)

2 / 916.00-924.00(8.00/8.00)

3 / 924.00-931.00(6.75/7.00)

BEDDING CONTACTS

— Flat

◡ Erosional

Rootlets

Discontinuous laminae

ooo Carbonaceous grains

3 Moderately hard

4 Hard

...using a fingernail; grains can be detached with a knife

sample breaks ... most grains

P - Pyrite, G - Glauconite, C - Carbonate Cement

NOTE All depths have been adjusted so that lithology log depths correspond to geophysical log depths

DEPTH – TOPS SAMPLES	DESCRIPTION	CORE/CORE DEPTH + RECOVERY
895	895.5-897.6 SAND, medium grey, fine grained, low angle xbedded to parallel laminated, very thin shale interlaminations, bioturbated zones where shale is churned with sand, shale clasts near base of unit, 2x3 cm in size rimmed by pyrite, occur in disrupted shale horizon	1 / 896.00-905.00(8.95/9.00)
	897.6-898.6 SAND, very fine grained, interlaminated with SILT and SHALE, carbonaceous debris define ripples	
Top of Glauconitic Sandstone	898.6-899.3 SHALE, medium grey, parallel laminated to massive, broken into thin slabs	
900	899.3-899.8 SAND, dark grey, and carbonaceous SHALE, churned together, small light brown sand chips	
38-189	899.8-900.2 SAND, light brown-light grey, porous clay-rich	
	900.2-902.0 SAND, very argillaceous, light grey-white, dark chert grains create speckled appearance, bioturbated, slightly darker clay streak churned in with sand	
38-190, 905	902.0-907.2 SAND, less clay rich than above, light brown oil stain, structureless to bioturbated with scattered hints of lamination	
	906.3 heavier oil saturation begins below a bioturbated bed 3" thick with slightly darker clay churned in	2 / 905.00-914.00(8.60/9.00)
38-191	907.2-910.3 SAND, laminations are better preserved than above but bioturbation is still common, laminations often wavy and disturbed	
910	910.3-930.0 SAND, fine grained, low angle laminations, one bioturbated sand interval but no shale involved, in uncleaned core slabs the laminations can still be seen as alternations of light and heavy oil saturation	
915		3 / 914.00-923.00(8.70/9.00)
38-192, 920	[illegible] possible burrow	
		[illegible]0/8.00)

Breccia
Coal
Calcareous

BEDDING CONTACTS

Flat
Erosional

ORGANIC MATTER

Carbonaceous fragments
Carbonaceous laminae
Rootlets
Discontinuous laminae
Carbonaceous grains

INDURATION

1 Unconsolidated – grains falling apart in dry conditions
2 Friable – grains can be detached using a fingernail
3 Moderately hard – grains can be detached with a knife
4 Hard – sample breaks around most grains

P - Pyrite, G. - Glauconite, C - Carbonate Cement

NOTE All depths have been adjusted so that lithologic log depths correspond to geophysical log depths.

DEPTH – TOPS SAMPLES	GRAIN SIZE (>1.000–1.000 / 1.000–0.500 / 0.500–0.250 / 0.250–0.125 / 0.125–0.062 mm)	LITHOLOGY	SEDIMENTARY STRUCTURES (main / acc)	ORGANIC MATTER	BEDDING THICKNESS	CEMENT/ACC MINERALS	DESCRIPTION	INDURATION (1 2 3 4)	SATURATION (oil / gas / wat)	CORE/CORE DEPTH (RECOVERY)
905										
36-174			BM			P	907.1-907.3 SAND, very fine grained, carbonaceous laminations defining ripples 907.3-908.6 SHALE, medium grey, parallel laminated to structureless, pyrite laminations and nodules			
			BM			P				
			BM			P	908.6-909.7 SILT, churned with shale, interbedded with SHALE beds, carbonaceous debris defines laminations and occurs as chips in the shale			
910			BM			P				
36-175			U			P	909.7-910.3 SAND very fine grained, low angle xlaminated to rippled			
Top of glauconitic sandstone			BM			P	910.3-910.8 SHALE, medium grey, with thin white silt interlaminations, very small scale ripples and burrows			
36-176										
36-204			BM			P	910.8-911.0 SAND, dark grey, very carbonaceous 911.0-912.3 SAND, fine grained, argillaceous, light brown, upper 15 cm is light grey with carbonaceous chips			1 / 907.00-916.00(8.80/9.00)
			BM				912.3-914.4 SAND, medium grey, bioturbated and churned in with SHALE, rootlets still present			
915			BM							
36-177			BM				914.4-917.5 SAND, less clay-rich than above, burrow mottled with little shale, becoming faintly and indistinctly laminated towards the base, lightly oil-saturated 917.4 hint of bedding			
			BM				917.5-930.4 SAND, fine grained, heavier oil-saturation, planar parallel laminated to low angle xbedded, local indistinct, disturbed or irregular laminations, upper 2.5 m is bioturbated as above but is heavier oil saturated			2 / 916.00-925.00(8.70/9.00)
			U							
920										
			U	U		P				
925										3/925.00-930.50(5.65/5.50)
36-178										
			H			P				
930										

Conglomerate
Sandstone, c-vc, m, vf f
Siltstone
Shale
Breccia
Coal
Calcareous

BEDDING CONTACTS
— Flat
‿ Erosional

Oscillation ripples
Discontinuous laminae
Flaser bedding

ORGANIC MATTER
Carbonaceous fragments
Carbonaceous laminae
Rootlets
Discontinuous laminae
Carbonaceous grains

NV Structures not visible due to oil saturation
Rip-up clasts
Penecontemporaneous faults

INDURATION
1 Unconsolidated – grains falling apart in dry conditions
2 Friable – grains can be detached using a fingernail
3 Moderately hard – grains can be detached with a knife
4 Hard – sample breaks around most grains

P - Pyrite, G - Glauconite, C - Carbonate Cement

NOTE All depths have been adjusted so that lithologic log depths correspond to geophysical log depths.

DEPTH – TOPS SAMPLES	GRAIN SIZE	LITHOLOGY	SEDIMENTARY STRUCTURES (main / acc.)	ORGANIC MATTER	BEDDING THICKNESS	CEMENT/ACC MINERALS	DESCRIPTION	INDURATION	SATURATION	CORE/CORE DEPTH (RECOVERY)
905			U	⊥	≡	1-1.5	C	906.7-907.5 SAND, fine to very fine grained, carbonate cemented, climbing ripples outlined by carbonaceous debris, slumped blocks near top, bioturbated calcareous shale interbeds near top			1 / 907.00-916.00(8.85/9.00)
						P	907.5-907.9 SAND, as above but non-calcareous			
			U ≡ U			P	907.9-909.5 SHALE, medium grey, burrowed to bioturbated to finely laminated, pyrite concretions 1.5-8 cm thick			
910			≡ U	H	≡	30		909.5-912.1 SILT, interlaminated with carbonaceous debris outlining ripples, small burrows, interbedded with SHALE, medium grey, massive with some faint laminations and rootlets			
Top of Glauconitic Sandstone			≡			P	912.1-912.4 SHALE, medium grey			
						P	912.4-912.7 COAL			
39-193			BM		⊼	P, G	912.7-913.2 SAND, very fine to fine grained, clay-rich, light grey, bioturbated with clay churned in			
39-194			BM			P, G	913.2-915.4 SAND, medium grained with clay abundant as matrix and clay aggregates, ~~slight greenish colour, indistinctly xlaminated~~ to bioturbated, disseminated, coarse grained pyrite, thin shale at base of unit			
915				≡		P	913.2-913.5 medium grained and fine grained clay-rich sand breccia			
39-195			BM H BM				915.4-919.4 SAND, clay-rich, light grey, bioturbated, gradually becomes less clay-rich downwards, clay-filled fracture network is common, heavily oil saturated bed at top of unit appears misplaced			
39-196							919.4-926.0 SAND, less clay-rich than above, still bioturbated			2 / 916.00-925.00(8.80/9.00)
920			H				920.9-922.5 lenses of slightly coarser sand 1-2 cm thick causing variation in oil-saturation			
39-197			≡ BM							
925			H H							3 / 925.00-931.50(6.50/6.50)
39-198			≡14° ≡ ≡		5	P	926.0-931.0 SAND, fine-grained, low angle parallel laminated to xbedded			

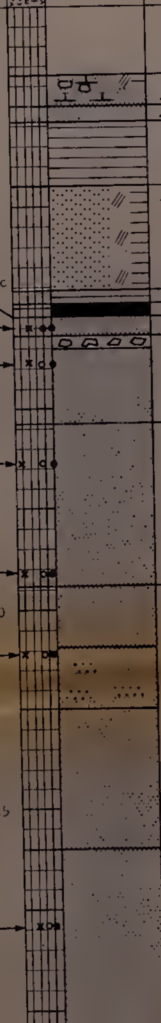

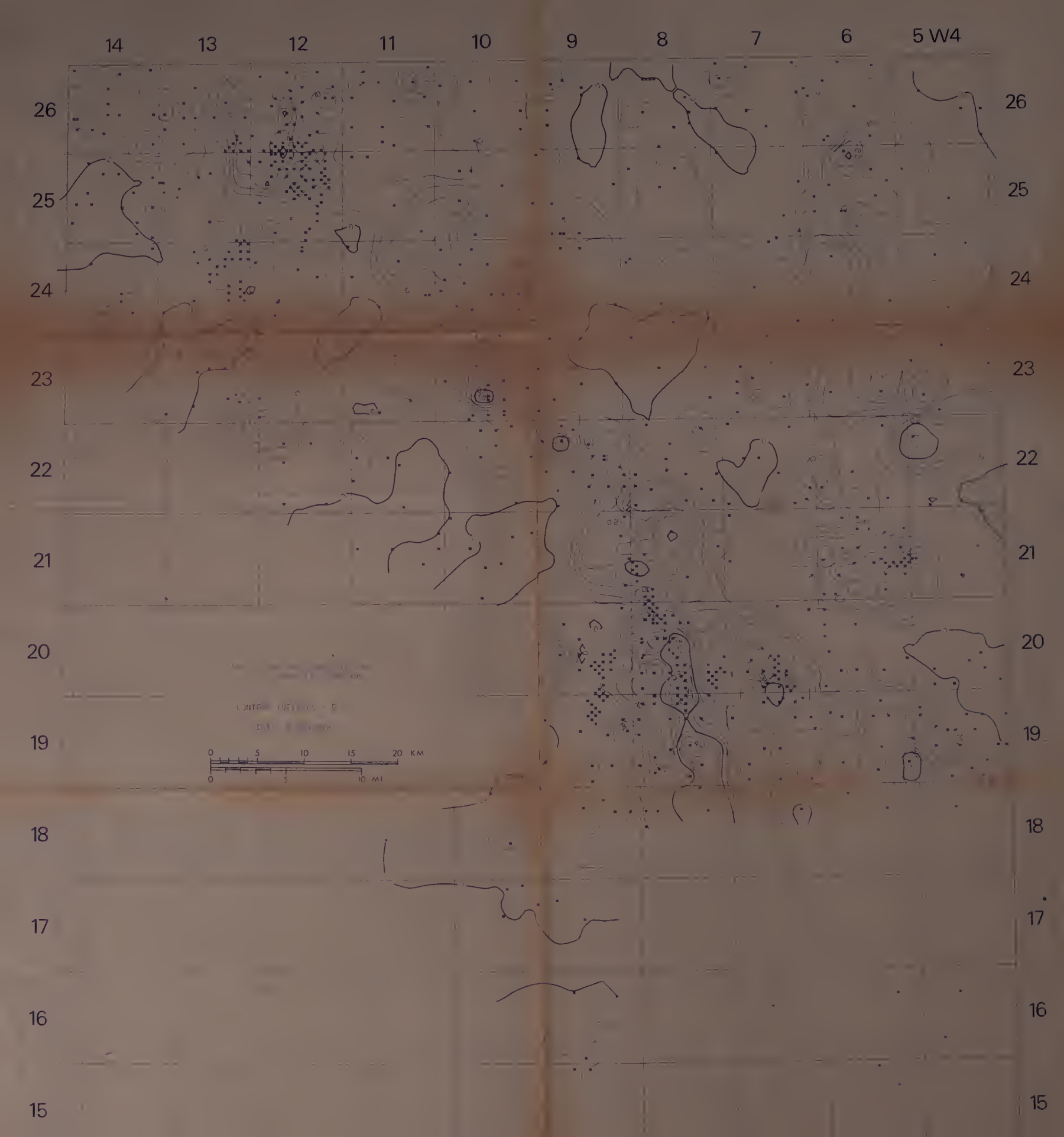
14
13
12
11
10
9
8
7
6
5 W4
26
25
24
23
22
21
20
19
18
17
16
15
0 5 10 15 20 KM
0 5 10 MI